Peel Tests for Quantifying Adhesion and Toughness: A Review

Michael D. Bartlett,[1,2*] Scott W. Case,[2,3] Anthony J. Kinloch,[4] and David A. Dillard[2,5]

[1]Department of Mechanical Engineering, Soft Materials and Structures Lab, Virginia Tech, Blacksburg, VA 24061, USA.
[2]Macromolecules Innovation Institute, Virginia Tech, Blacksburg, VA 24061, USA.
[3]Via Department of Civil & Environmental Engineering, Virginia Tech, Blacksburg, VA 24061, USA.
[4]Department of Mechanical Engineering, Imperial College London, Exhibition Road, London SW7 2AZ, UK
[5]Department of Biomedical Engineering and Mechanics, Virginia Tech, Blacksburg, VA 24061, USA.
*To whom correspondence should be addressed: mbartlett@vt.edu

Cite this article: Bartlett, M.D., *et al.* Peel Tests for Quantifying Adhesion and Toughness: A Review. *Progress in Materials Science* (2023): 101086.

This version of the article has been accepted for publication. The Version of Record is available online at: https://doi.org/10.1016/j.pmatsci.2023.101086

Abstract

The peeling apart of layered materials is common in nature and has been used by humans in myriad applications since prehistoric times. Over the past century, a wide range of peel tests has been proposed, standardized, and used to characterize important properties of materials, adhesives, and interfaces. Understanding the relative merits and limitations of these tests, and meaningful ways to analyze the results, is essential for current and emerging applications – from tough, high strength aerospace structures and 3D printing to soft hydrogels and wearable devices. Here, we review the historical development of peel tests and then convey a categorization scheme that is applicable to various peel configurations. Four categories are presented, depending on whether peeling is elastic or inelastic, and if debonding is self-similar or not, to capture nearly all types of peel experiments from reversible interfaces to extremely tough permanent joints. Analysis methods and peel metrics are reviewed and discussed, along with recommendations for interpretation. We further consider the effects of geometric and material properties, viscoelastic effects, and structure-property relationships. We show that these topics are highly relevant for emerging areas like biological and bio-inspired mechanisms to control peeling as well as structured systems through kirigami and architectural geometries.

Keywords: Peel; Adhesion; Toughness; Fracture energy, Gels; Bio-inspired

Contents

Nomenclature	
A	Area of peeling or peeled area (m^2)
a	Crack length (length of peeled area) (m)
$\dot{a}$	Crack velocity (m/s)
a_t	WLF time-temperature shift factor (–)
a_p	Projected crack length (m)
Δa	Change in crack length (m)
B	Bonding term for PSAs (–)
C	Compliance (m/N)
C_m	Machine and load-train compliance (m/N)
D	Debonding term for PSAs (–)
E	Adherend (also termed substrate)/peel arm modulus of elasticity (Pa)
E_s	Adherend/peel arm modulus of elasticity in a stiff region (Pa)
E_c	Adherend/peel arm modulus of elasticity in a compliant region (Pa)
F	Applied force or load (N)
F_c	Critical force for peeling (N)
$F_{c,s}$	Critical force for peeling in the stiff region of a heterogeneous adhesive (N)
$F_{c,c}$	Critical force for peeling in the compliant region of a heterogeneous adhesive (N)
F_c/w	Peel force per unit width for separation, or called the measured peel energy (often called the 'peel strength' in Standards) (N/m or J/m^2)
F_{ca}	Stick-slip arrest force (N)
F_{ci}	Stick-slip initiation force (N)
F_{max}	Maximum adhesive force (N)
F_{min}	Minimum adhesive force (N)
F_{peak}	Peak adhesive force prior to 'plateau' (N)
G	Applied or available energy release rate (J/m^2)
G_I	Mode I energy release rate (J/m^2)
G_{II}	Mode II energy release rate (J/m^2)
G_c	Fracture energy or critical energy release rate (J/m^2)
G_D	Mechanical energy dissipation during fracture at crack tip (J/m^2)
G_0	Intrinsic fracture energy (J/m^2)

G_c^{eb}	Fracture energy for a peel test with a thin peel arm which can deform elastically in the axial direction but is completely flexible in bending (J/m^2)
$G_c^{\infty E}$	Fracture energy for a peel test with a thin peel arm which is infinitely-stiff in the axial direction but is completely flexible in bending (J/m^2)
G_{db}	Energy dissipated per unit area of crack growth during bending of the peel arm (J/m^2)
$G^{'}$	Storage shear modulus (Pa)
$G^{''}$	Loss shear modulus (Pa)
h	Thickness of adhesive layer (m)
I	Second moment of area of a peel arm cross section (m^4)
I_s	Second moment of area in a stiff region (m^4)
I_c	Second moment of area in a compliant region (m^4)
K	Stress intensity factor (MPa $m^{1/2}$)
K_c	Fracture toughness or critical stress intensity factor (MPa $m^{1/2}$)
K_I	Mode I stress intensity factor (MPa $m^{1/2}$)
K_{II}	Mode II stress intensity factor (MPa $m^{1/2}$)
M	Moment (Nm)
M_0	Fully-plastic bending moment limit (Nm)
t	Thickness of adherend/peel arm (m)
$\tan\,\delta$	Loss tangent in a viscoelastic material (–)
U_{db}	Energy dissipated during bending of the peel arm (J)
U_{dt}	Energy dissipated during tensile deformation of the peel arm (J)
U_{ext}	External work (J)
U_k	Kinetic energy term (J)
U_E	Stored (elastic) strain-energy in the peel arm (J)
V	Test speed (m/s)
W	External work (J)
W_{adh}	Thermodynamic work of adhesion (J/m^2)
W_e	Essential work of fracture (J/m^2)
w	Width (peel arm and bond, unless otherwise noted) (m)
δ	Specimen displacement (m)
Δ	Total displacement (specimen plus machine displacement (m)

ε	Strain (–)
κ	Curvature (1/m)
κ_e	Curvature at elastic limit (1/m)
θ	Applied peel angle (°)
θ_o	Local angle at the contact point in a peel test (°)
ψ	Phase angle for mode-mixity (°)
ψ_v	Dissipative fracture term at crack tip (–)
σ	Stress (Pa)
σ_c	Critical value of maximum principal stress (Pa)
σ_{max}	Critical stress/traction in a CZM (Pa)
σ_y	Adherend/peel arm yield stress (Pa)
ω	Angular frequency (1/s)

Acronyms	
AA	Acrylic acid
AM	Additive Manufacturing
BA	Butyl acrylate
BoEF	Beam on Elastic Foundation
CF	Correction factor
CFRP	Carbon-fiber reinforced-plastic
CLS	Cracked Lap Shear
CNT	Carbon nanotube
CRS	Cold-rolled steel
CZM	Cohesive Zone Model
DCB	Double Cantilever Beam
EA	Ethyl acrylate
EGZ	Electrogalvanized steel
EHA	2-ethylhexyl acrylate
EPFM	Elastic-Plastic Fracture Mechanics
EPZ	Embedded Process Zone
EWF	Essential work of fracture
FEA	Finite Element Analysis
FFF	Fused Filament Fabrication
HDPE	High density polyethylene
HDG	Hot dipped galvanized steel
IC Peel	Imperial College Peel
IWP	Impact Wedge Peel
JKR	Johnson-Kendall-Roberts
LEFM	Linear-Elastic-Fracture-Mechanics
MA	Methyl acrylate
MMA	Methyl methacrylate
MW	Molecular weight
MWCNT	Multi-walled CNT
NCA	Notched Coating Adhesion
PAAm	Polyacrylamide
PAMPS	Poly(2-acrylamido, 2-methyl, 1-propanesulfonic acid)

PDMS	Poly(dimethylsiloxane)
PE	Polyethylene
PET	Poly(ethylene terephthalate)
PMMA	Poly(methyl methacrylate)
PSA	Pressure sensitive adhesive
PSTC	Pressure Sensitive Tape Council
SS	Stainless steel
SWCNT	Single-walled CNT
TDCB	Tapered Double Cantilever Beam
UPD	Universal Peel Diagram

1 Introduction

Peeling apart of materials is a common technique to characterize material properties and is relevant in a multitude of applications ranging from skin adhesion to aerospace composites. Also, peeling is commonly observed in nature from animal locomotion to plant growth.[1–8] These ubiquitous applications have led to a variety of techniques to characterize peel properties of layered materials, adhesives, interfaces, and bulk materials.[9–13] This includes cohesive failure (i.e. fracture through one material, such as within an adhesive interlayer or in a peel arm) and interfacial adhesion failure (i.e. fracture at the interface between two materials) where a peeling analysis and the resulting equations allow for the measurement of the fracture energy of bulk materials and adhesive interfaces. Perhaps the most appealing aspect of the peel test is the relative simplicity of conducting such experiments, where a material is peeled to separate an interface, fracture a material, or evaluate a bonded joint. This simplicity has led to its widespread adoption in fields ranging from the analysis of soft tissues in biology to extremely tough, bonded joints in transportation vehicles.[14–19] This broad applicability to materials ranging from soft to stiff with measured peel energies spanning six decades – ranging from tens of mJ/m^2 to tens of kJ/m^2 – is also a significant challenge with peel tests. Running a peel test on different material systems and configurations can lead to significant differences in the appropriate analysis and interpretation.[20–24] The specific aspects of the test interpretation can be complex, challenging novice users and even experts in the field, and a framework to connect the vast variety of peeling scenarios is lacking. This complexity has led to significant challenges across the fields that use peeling, where poor measurement methods and interpretations can lead to incorrectly reported or misleading material properties, utilization of inappropriate methods to evaluate materials, and confusion in the analysis and interpretation of results. This is especially relevant as peeling is often one of the first methods used to characterize novel materials, from tough, high strength aerospace and automotive materials, 3D printed systems, and bio-inspired materials to hydrogels, soft robotics, and pressure sensitive adhesives (Figure 1).[25–29] Further, by manipulating the peeling conditions, materials, or geometry, adhesion can be tuned or enhanced, which is essential for applications in manufacturing, healthcare, robotics, and consumer applications.[25,30–39] Peel tests are also widely used for quality control tests and as a screening tool to select materials. Such applications may result in questionable outcomes if modes of failure and appropriate analyses methods are different. Therefore, the conditions under which an experiment is run must be well described and the appropriate analysis needs to be applied to extract meaningful material and adhesion properties.

Peeling takes a wide array of forms. In the most basic sense, a peel test can consist of 1) a laminate comprising of two (or more) layers peeled apart, often at the interface or 2) an adhesively bonded joint in which two substrates are joined by an adhesive layer and then peeled apart, or 3) peeling of a single, adhesive material from a substrate or itself. Commonly, the bonded material is referred to as a substrate or an adherend. The geometry of the general peel case can be seen in Figure 2a, where a material of width w is bonded to a substrate and a load is applied to the bonded material (which is relatively flexible and is often referred to as a peel arm) at an angle θ relative to substrate. When the force F reaches a critical force, F_c, the material debonds from the substrate. Often, a peak force

Figure 1: Peeling examples in synthetic and biological systems. Applications and systems that utilize peeling to characterize, create, survive, and leverage adhesion. Switchable adhesives image is reprinted with permission from Ref. 25. Copyright 2021, RSC. Wearable electronics image is reprinted with permission from Ref. 26. Copyright 2011, AAAS. Soft robotics image is courtesy of Yichao Tang.[27] Adhesives image is from Jo Szczepanska on Unsplash. Layered materials image is from Eduardo Goody on Unsplash. Composites image is reprinted with permission from Ref. 28. Copyright 2015, RSC. Gels image is reprinted with permission from Ref. 29. Copyright 2016, Springer Nature.

may be observed before the steady peeling at the critical force is reached. This commonly arises due to 1) the lack of a defined crack and 2) the lack of a self-similar geometry, as the peeling configuration and process are still evolving at this point. We take self-similar

to mean that the solution is independent of the debond length, which is also referred to as steady-state debonding in some literature, e.g. Ref. 40. This critical peeling force depends on many factors, including the thicknesses and constitutive properties of the materials involved, whether plasticity or other dissipative processes are occurring in the materials, the adhesive properties of the interface including the types of inter-atomic and inter-molecular bonds present between the materials, the angle θ at which the material is being peeled, and the test conditions such as peel rate, temperature, and environment.[5,21,41–53] Where possible, the explicit relationships among these properties will be established further in this review. Often the goal of the experiment is to either measure 1) the fundamental property of the interface integrity, typically called the fracture energy, G_c*, which captures the materials' resistance to separation as a crack or debond propagates, or 2) measure the peel resistance according to a test standard typically defined as the force of separation per specimen width. In a common idealization, debonding along a material/substrate interface is termed interfacial (or adhesion) failure; debond propagation within the adhesive layer or substrate(s) is termed cohesive failure (within the relevant material). Several common peel scenarios are used to measure these properties, including the 180° peel, and the T-peel, as shown in Figure 2b-d. However, although these geometries are commonly used to undertake peel testing, and appear to be relatively simple test methods, the relevant analyses needed to obtain meaningful fracture energy values depend on several properties of the materials involved, the interfacial integrity, the geometry of the test, and various test parameters. Table 3 serves as a reference to some of the more common and relevant testing standards which have been developed to capture these different characteristics. The interaction between the different material systems and geometries makes the peeling problem very interesting, and even though the general geometries and loading conditions may be the same, the appropriate analysis method to apply for a material set can vary significantly, especially when changes in fracture energy, energy dissipation in the peel arm, and specimen dimensions, and their interactions, alter the resulting behavior.

In this review, we aim to provide a framework to describe the peeling behaviors of diverse materials and interfaces and provide relevant analysis approaches to understand synthetic and natural peel scenarios. In Section 2, we will introduce peeling as a form of fracture test and discuss some of the common misconceptions of peeling, introduce relevant frameworks to analyze peel problems, and discuss the relevant ranges of adhesion energy. In Section 3, we introduce a categorization scheme that specifies whether peeling involves elastic or inelastic deformation of the peeling arm(s), and if the debonding occurs in a self-similar manner or not, identifying four distinct categories to capture nearly all types of peel experiments spanning from reversible interfaces to extremely tough permanent joints where the peel energy can reach thousands of Joules per square meter. Section 4 focuses on additional peel geometries and Section 5 considers the effects of geometric and material properties including viscoelastic rate and temperature effects. We then discuss methods used to control peeling and the influence of microstructure on adhesion properties in biological systems (Section 6) as well as provide a discussion around examples of peeling in diverse synthetic and engineered materials (Section 7). The aim of the review is to inform readers of various backgrounds

*This quantity is sometimes referred to as the interfacial fracture toughness (Γ). In this discussion, we reserve "fracture toughness" for K_c.[54]

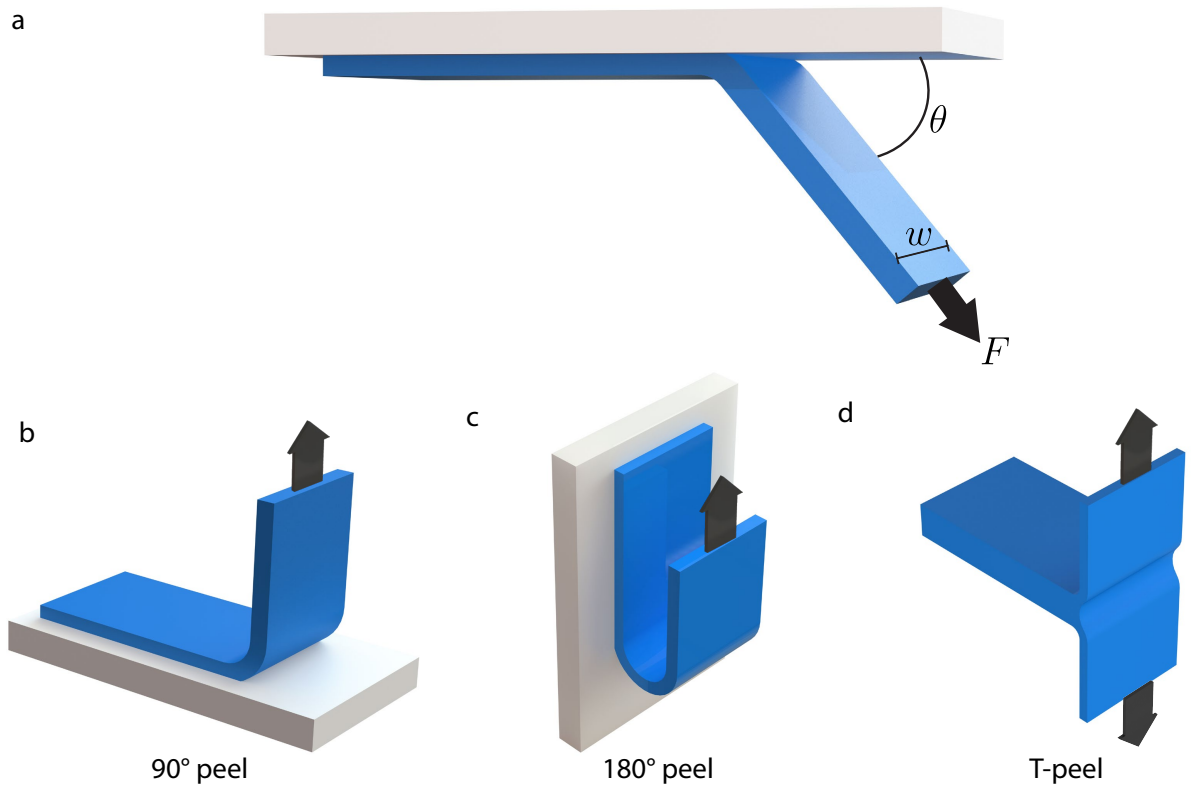

Figure 2: Examples of peel tests. a) Schematic of a general peeling test, where θ is the peel angle, F is the applied force, and w is the width. Schematic of b) 90° peel, c) 180° peel and d) T-peel test. Source: ©M.D. Bartlett et al., CC BY-SA 4.0. Available at http://hdl.handle.net/10919/113716.

about peeling to measure material and bonded system properties, provide guidance on test method selection and how to appropriately analyze and interpret results, provide discussion of mechanisms to control peeling, and finish with conclusions and future opportunities in peeling of materials.

Table 1: Common peel test methods and standards. Source: Schematics ©M.D. Bartlett et al., CC BY-SA 4.0. Available at http://hdl.handle.net/10919/113716.

Summary of peel designations and relevant standards		
Schematic	Test	Representative Standards
	0° peel	ASTM D3654: static shear adhesion of PSA tapes (creep rupture) ASTM D6463: time to failure under sustained shear PSTC-7: "holding power" of PSA tapes PSTC-17: shear adhesion failure temperature (SAFT)
	90° peel	ASTM D6862: peel resistance of adhesives ISO 8510-1: flexible-bonded-to-rigid assemblies ISO 813: rubber adhesion to rigid substrate ASTM D6252: pressure-sensitive label stocks BS-EN-1895: paper and board, packaging, and disposable sanitary products ASTM B533: "peel strength" of metal electroplated plastics ASTM D3330 (method F): pressure-sensitive tape
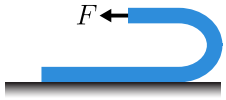	180° peel	ASTM D903: peel of stripping strength of adhesive bonds ISO 8510-2: flexible to rigid bonded assemblies ASTM D3330 (method A): pressure-sensitive tape ASTM C794: adhesion-in-peel of elastomeric joint sealants
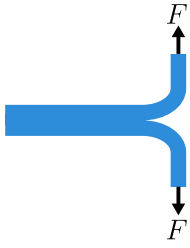	T-peel	ASTM D1876: peel resistance of adhesives ISO 11339: flexible-to-flexible bonded assemblies ASTM D2918: durability of adhesive joints stressed in peel BS-EN-1895: paper and board, packaging, and disposable sanitary products ASTM F2256: tissue adhesive characterization
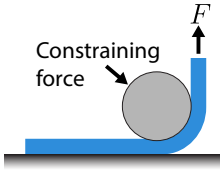	Mandrel peel	Not a standardized peel test

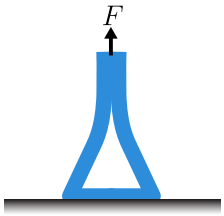	Loop tack	ASTM D6195: adhesive loop tack strength testing
	Trouser tear	ASTM D624: standard test method for tear strength of conventional vulcanized rubber and thermoplastic elastomers
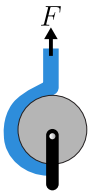	German wheel	DIN 53357: testing of plastic sheets; Adhesion test
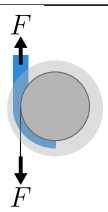	Climbing drum	ASTM D1781: for flexible to rigid adhesion ASTM D429: rubber to metal adhesion ASTM D2558: shoe sole adhesion
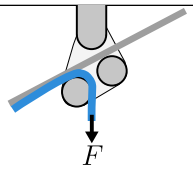	Floating roller	ASTM D3167: peel resistance of (structural) adhesive bonds ISO 4578: peel resistance of (structural) adhesive bonds ISO 14676: wet-peel for aluminum surface treatments ISO 22631: Peel of floor and wall covering adhesives
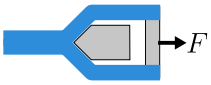	Impact wedge	ISO-11343: impact wedge peel (IWP) method

2 Introduction to peeling as a form of fracture test

The debonding of a peel joint can be seen as a cracking process where a crack initiates and then propagates as the joined materials separate. This debonding can therefore be evaluated as a fracture mechanics problem. The analysis of such tests leads to a fracture energy G_c (also known as the critical energy release rate) expressed as an energy per unit area, so in metric units such as J/m^2 or equivalently as a force per unit width metric such as N/m, as is common in peel test reporting. The fracture energy approach was proposed in Griffith's seminal paper in the field.[9]

In this section, we introduce peeling and discuss its attributes, including some of the most common misconceptions and advantages of using peel tests as tools to evaluate adhesion – the mechanical integrity of material interfaces – and/or the cohesive properties of the materials forming the peel test, depending upon the resulting locus of failure. Included will be the types of data generated with peel experiments, a brief history of peeling, and analysis of peeling as a fracture problem.

2.1 Peeling: The good, the bad, the misleading

To demonstrate the need to understand the appropriate analysis method and associated metric in a peeling scenario, we can examine the simple peeling of two identical strips from one another in two different test configurations (Figure 3). Consider the case of separating two layers, using 90° peeling first with one adherend secured to a rigid base, then switching to a T-peel configuration after removal of both layers from the rigid base. Interestingly, the force required to peel apart the layers in these two scenarios is quite different, even though the material interface being separated is the same, as illustrated in Figure 3. The force measured (for example with a handheld spring scale with a PSA tape or PDMS in a simple classroom demonstration) using the 90° configuration bonded to a supporting, rigid substrate is approximately double that needed when the tapes are loaded in a T-peel configuration, as the force must move through twice the distance per unit area of the debonding in the T-peel configuration. This observation supports the idea that these identical tapes require a given amount of energy, rather than force, to separate a prescribed area, suggesting that it is more meaningful to discuss peel energies rather than the "peel strengths" often reported in peel standards. Further potential confusion with metrics and nomenclature can be seen if one considers the ASTM-D1876 T-peel test standard,[12] where the "T-peel strength" is defined as F/w, which is exactly the same formula as the "resistance-to-peel strength" for the ASTM-D6862 90° peel test standard.[55] Clearly, the analysis of these joints reveals much more than the separating force alone, and should be considered when discussing, analyzing, and comparing peel scenarios. Also, as noted above the term F/w is not a strength term which has units of stress (i.e. force/area) but is an energy per area term with units of J/m^2 (or N/m).[†] So, it should be noted that testing standards are often misleading on the appropriate nomenclature for peel metrics.

In contrast to other adhesive bond fracture tests, such as the popular double cantilever beam (DCB) specimen, peel tests often result in large deformations due to the adherend (or peel arm) flexibility and, in many cases, inelastic yielding occurs as they are tested. This plastic deformation can result in considerable energy dissipation, even several orders of magnitude larger than the energy required for debonding. The "apparent" peel resistance or "practical adhesion" associated with the force measured by the load frame thus can significantly exaggerate or overestimate the energy required to debond or separate the adhesive layer. Therefore, rather than being an adhesive property, peel energies can be highly system dependent.

[†]Adhesion strength is often used to describe the forces or resistance to separation in peel experiments, especially when heterogeneous, patterned, or bio-inspired designs may lead to extrinsic factors for adhesion enhancement.

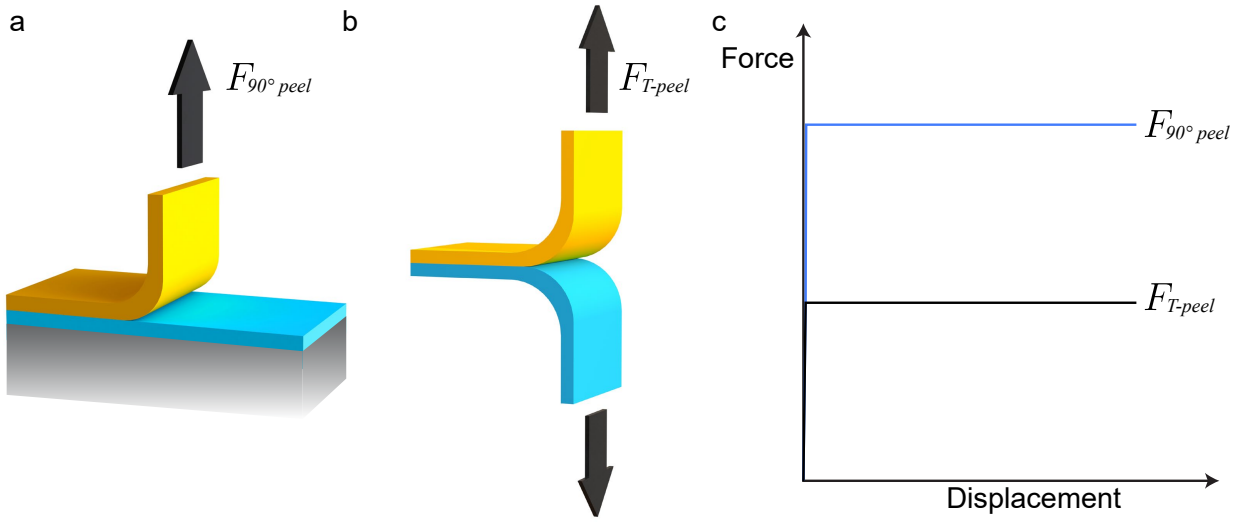

Figure 3: Illustration of peeling apart two layers of a pressure sensitive adhesive tape. a) An adhesive material bonded to a rigid substrate with the top layer peeled part way in a 90° configuration and b) the remaining specimen is removed from the supporting rigid substrate and tested in a T-peel configuration. c) The force observed in the 90° case is approximately double that observed in the T-peel configuration even though the debond propagates along the same adhesive to backing interface. Source: ©M.D. Bartlett et al., CC BY-SA 4.0. Available at http://hdl.handle.net/10919/113716.

These effects can also be demonstrated by a simple experiment based upon the observations of Gent et al.[41,56] In this experiment, a thin film of polyethylene (PE) is bonded to a thin film of poly(ethylene terephthalate) (PET) to form a bilayer laminate by compression molding using heated pressure-plates. A starter crack for the subsequent peel tests is formed by inserting a thin release film of poly(tetrafluoroethylene) between the two layers, at one end of the bilayer laminate, before the molding operation is undertaken. Two types of 90° peel tests are then performed. In the first type of test, the PET layer is firmly bonded to a metal supporting plate and the 90° peel test is conducted by pulling on the PE layer which forms the peel arm and which is bent through an applied peel angle $\theta = 90°$. Assuming that the bilayer has been adequately bonded during the compression moulding operation, then it is found that a relatively high peel energy is needed to separate the bilayer. Indeed, the stress that is generated in the PE peel arm during this process is often such that the PE arm plastically yields and may then fracture completely, leaving the bilayer interface intact. In the second type of test, the peel test is "reversed," i.e. the PE layer is firmly bonded to a metal supporting plate and the 90° peel test is undertaken by pulling on the PET layer which forms the peel arm and which is bent through an applied peel angle $\theta = 90°$. It is found that the peel energy needed to completely separate the bilayer interface is relatively low and that the bilayer interface fully separates with no visible plastic deformation of the PET peel arm occurring. Clearly, the thermodynamic work of adhesion, W_{adh}, which has a value of about 75 mJ/m^2, is exactly the same in both types of peel test, since the bilayer laminate was formed via a single compression molding operation.[57] Therefore, these observations of the very different behavior and values of the peel energies seen from the inverted peel tests are

not due to any differences in the intrinsic adhesion of the bilayer. They are, of course, due to the ability of the given peel arm to undergo dissipative viscoelastic and plastic deformation at the level of stresses generated in the peel test. Thus, a relatively high extent of plastic deformation is observed in the PE arm test, which has a relatively low yield stress, with an associated high value of measured peel energy, compared to that for when the peel arm is the PET layer, which has a relatively high value of yield stress.

Because peel test results are so system dependent, altering the adherend materials or even their thicknesses can greatly affect the measured results. This dependence on system parameters has led to comments that peel tests "allow one to cheat" and that "you can get any number you want" from such tests. Peel tests are clearly a form of fracture tests, but extraneous energy dissipation and other complications associated with these geometries require careful consideration. Unfortunately, test specimen preparation, testing, and the results obtained are sometimes treated as commodity items – sent off for someone else to perform – with little oversight or interpretation, which can lead to inaccurate conclusions of material and adhesive properties. Nomenclature can also be challenging. Conceptually and physically, strength and fracture energy approaches are quite different and the critical values of strength, such as a yield or ultimate strength, and fracture energy are obviously very different quantities. At times, however these nomenclatures are not consistently used.

2.2 Range of typical peel force versus displacement curves

Within our framework of considering peel tests as fracture tests, we note that traditionally, fracture characterization has focused on two stages: initiation and propagation. Both stages are usually present when conducting peel tests, though capturing and reporting the propagation process is often the intent. The resulting force versus displacement traces display a variety of forms depending on the materials, test conditions, and geometry. Figure 4 schematically illustrates a variety of common examples as might be observed when conducting displacement-control experiments at constant crosshead rates (displacement-control and force-control experiments can give rise to differnet behaviors, see Section 5.5.5 and Figure 27). Perhaps the most common for practical adhesive bonds is shown in Figure 4a, where an initial peak is observed, followed by a relatively stable plateau associated with steady-state peeling. The initial peak often involves the initiation process and can arise from several reasons, including the lack of a sharp starter crack; misalignment, adhesive spew and other local details;[58] viscoelastic/plastic blunting of the initial bond terminus region and crack tip at the elevated peak load; and evolving adherend deformation and possible plasticity before self-similar behavior has been achieved, as will be discussed in Section 3.[‡] Figure 4b does not show a prominent peak, and can be observed with PSA testing and with some elastomers, such as certain formulations of PDMS. If adhesion is weak and the adherends are sufficiently stiff, self-similar debonding may not be achieved, so the geometry is continuing to evolve with increasingly longer moment arms, resulting in behavior such as seen in Figure 4c. Stick-slip behavior is very common in peel tests of PSAs and some other systems (Figure 4d), where the crack arrests at an arrest force (F_{ca}) and re-initiates at an initiation force (F_{ca}) in a

[‡]Though the peak force is often discounted, in principle this initiation data could be used to estimate maximum tractions for the cohesive zone method (CZM) approach.[44,59]

meta-stable manner. Although several factors, including load-train compliance, influence stick-slip behavior, the primary cause is associated with crack tip blunting in viscoelastic-plastic systems (stick) followed by sudden crack advance in a more brittle manner (slip), as will be addressed in more detail in Section 5.5. Heterogeneous peel arms can also generate periodic peaks in the peel curve, where the peak force can be described with an F_{max} and the minimum as F_{min}, seen in Figure 4e,f, where different curve shapes can be attributed to the type or structure of the heterogeneity, as will be addressed in more detail in Section 7.7.

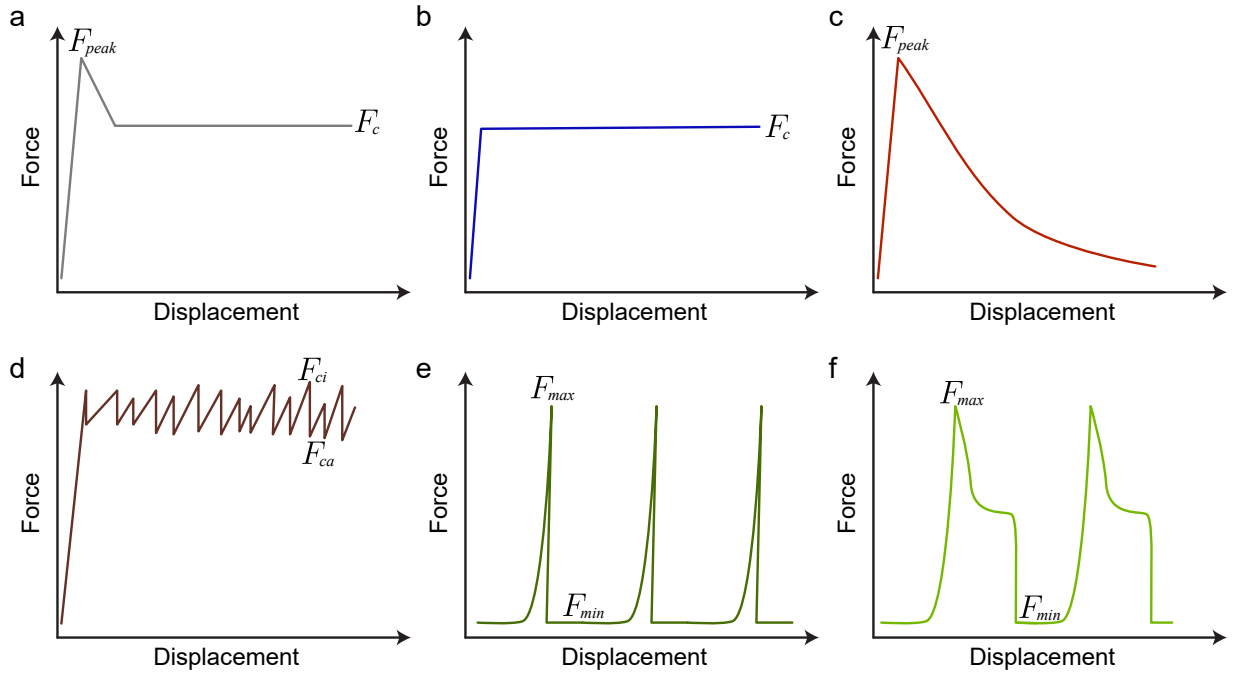

Figure 4: Peel curve examples. a) Peel curve with a peak force F_{peak} at the beginning of the test before reaching a steady-state peel force F_c. b) Peel curve that immediately reaches a steady-state peel force F_c. c) Peel curve that does not reach a steady-state peel force F_c. d) Peel curve showing stick-slip behavior with initiation force F_{ci} and arrest force F_{ca}. e,f) Peel curves for a heterogeneous adhesive where the geometry or material properties vary along the peel length, where F_{max} and F_{min} are the maximum and minimum forces during peeling. Source:

2.3 Brief history of peeling

The analysis of peel through a fracture mechanics framework appeared in 1944 when Rivlin discussed rate-dependent peeling. He undertook his tests by suspending a mass from a flexible adherend and peeling at a fixed angle,[60] in an apparatus that was similar to that described earlier by de Bruyne and later used by Lindley.[61] He argued that this provided a means to measure the "effective work of adhesion" as a function of the applied force (mg, where m is the mass of the weight and g is the acceleration due to gravity) and peel angle using:

$$\frac{mg}{w}\,(1 + cos\ \theta) \tag{2.1}$$

Bikerman,[62] responding to claims of a theoretical "force of adhesion," and by considering a "proper" adhesive bond that contained no weak interfacial region, obtained a "work of stripping" based on an overarching assumption that failure occurred at a critical opening displacement at break. His analysis, based on a beam on elastic foundation (BoEF),[11,63] led him to conclude that the peel test had "no molecular significance" and that "the peeling force and the work of stripping are determined by the bulk mechanical properties of the adhesive film and the geometry of the joint and thus give no information on the molecular adhesion between the adherend and the glue." While such views may not have been welcomed by all, this latter claim remains largely true for many peel tests, in that the measured peel resistance often is controlled by the properties of the materials forming the peel test and the test geometry. Although his analysis was quite simplistic (i.e. linear-elastic behavior and a constant strain at break), more sophisticated analyses continue to bear this out for many practical bonding problems. Interfacial failures suggest that the bond is insufficient to access the full dissipation capabilities of the joint system, so would not be a "proper" bond in Bikerman's terminology. Exceptions, of course, also occur where the interfacial chemistry and work of adhesion values become very important, such as the intrinsic fracture energy as measured by Gent at vanishingly small reduced rates of peeling (i.e. at low rates/high test temperatures so that the viscoelastic dissipation goes to zero, see Section 2.5) and for the case of JKR measurements that operate in this realm.[41,64]

In 1953 Spies published a thorough analysis of what is effectively a 90° peel test using a freely rotating peeling wheel (see Figure 5b).[5§] In Spies' analysis, the bonded portion of the adherend was idealized as a BoEF, the initial curvature of the adherend from being bonded to the wheel was neglected, and the peeled portion of the adherend was idealized as an elastica. Kaelble provided a further treatment in 1960 that remained general with respect to peel angle. His analysis provided the cleavage, shear, and combined stresses in the bond during peeling and showed that shear stresses are dominant at relatively low peel angles and cleavage stresses dominate at high peel angles.[66]

2.4 Peeling as a fracture problem

Because peel tests are inherently fracture tests, it is helpful to examine these tests in the framework of fracture mechanics where one can quantitatively ascertain a resistance to crack growth of a given interface, or material if failure is cohesive. In a monolithic material under certain conditions, the resistance to fracture may be considered a "material property" that can be useful in ranking materials or for design purposes. This approach has also proven very useful in more complex situations including multi-material and layered systems and for rate- and temperature-dependent (e.g. polymeric) materials, though geometric parameters, loading configuration, and test conditions can also affect the resistance to crack growth, rendering it a system property under prescribed conditions.

[§]He acknowledged this as a new test method and attributed to Aero Research, Ltd., though it is now known as a German wheel[65] and German Standard DIN 53357 (though now withdrawn).

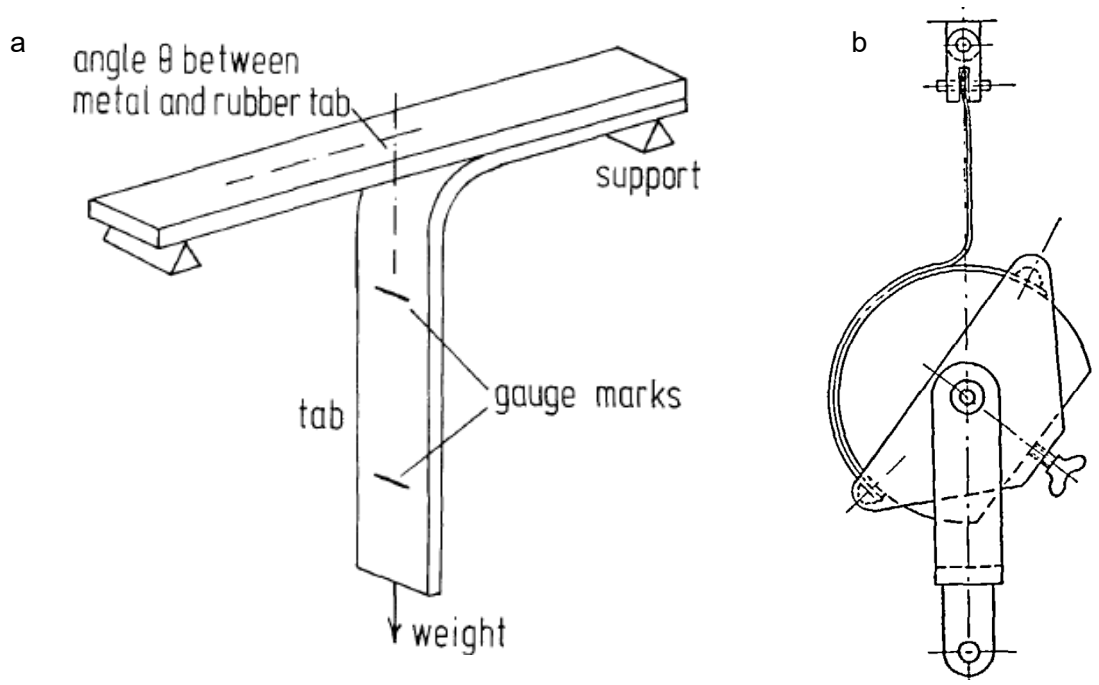

Figure 5: Peel tests used in classical papers. a) 90° peel geometry used by Lindley[61] and described by Rivlin.[60] Figure copyright Journal of the Institution of the Rubber Industry, used under the fair use provision of U.S. copyright law (section 107). b) The German wheel geometry used by Spies.[5] Reprinted with permission from Ref. 5. Copyright 1953, Emerald Publishing.

2.4.1 Griffith's approach to fracture

The essence of fracture mechanics was outlined in the seminal work Griffith presented in 1920[9] which was motivated by his interest in understanding the role of surface finish roughness in reducing the fatigue life of metallic parts that were nominally subjected to "sensibly elastic" stress states. This reasoning led him to conclude that flaw-like defects on the surface were increasing the local stress state. Building on Inglis' analysis for stresses at crack tips,[67] he considered the amount of energy that would be available to drive an increase in surface energy by the growth of a crack in a cracked plate of large extent.

Griffith reasoned that according to the "theorem of minimum energy", "the potential energy of the whole system," including that of the applied "specified surface forces" and "potential surface energy" of crack faces, would be a minimum at equilibrium. This led to his two-fold criteria that cracks would propagate if 1) the stresses at the crack tip were sufficient to break atomic bonds (a condition often met due to the nature of the stress field surrounding relatively sharp flaws) and 2) that the reduction in the system's potential energy with incremental crack growth is sufficient to overcome the fracture energy (G_c) of the material. For arbitrary loading levels in non-dissipative systems, this second criterion is now commonly expressed as:[68]

$$dW = dU_E + G_c \cdot dA \tag{2.2}$$

in terms of increments of external work input to the loaded object, W (which goes to zero for fixed displacement boundary conditions), internal elastic energy, U_E, and crack area, A. One can also introduce the complementary energy, which is defined as $U_C = W - U_E$. Herein, we are interested in increments of complementary energy input that drive increments of crack propagation, and will revisit this as an application to PSAs in Section 7.2.5. In terms of complementary energy, Equation 2.2 is rewritten here, including for arbitrary, sub-critical applied loading, where G is the applied or available energy release rate, as:

$$dU_C = dW - dU_E = G \cdot dA \tag{2.3}$$

Though Griffith did not mention complementary energy by name, his analysis effectively uses increments of complementary energy as the driving potential for crack growth. He further noted that the magnitude of the strain energy is half that of the work for "a body having linear-strain relations", so did not explicitly consider nonlinear behavior (or relevant to us, nonlinear force-displacement, often seen in peeling). When the available energy release rate, G, reaches the system's critical value, G_c,[¶], as will be discussed further in the review. Griffith's second criterion for fracture is satisfied and crack propagation will proceed. This approach has been applied extensively, including applications to peel tests in order to understand and interpret the experimentally measured peeling energies.[‖]

2.4.2 Basic fracture mechanics analysis of peel

As initially demonstrated by Griffith for cracking of a plate, analyzing the energies associated with peeling is a powerful method to understand peel scenarios. Upon examination of Equation 2.2 we see three components drive fracture/debonding. Therefore, generally, the total energy (U_T) of the non-dissipative system is composed of three primary components (here ignoring kinetic energy for the quasi-static focus herein.) There are: 1) Work potential energy (U_P), 2) Elastic potential energy (U_E), and 3) Fracture/surface energy (U_S). We can write the total energy of the system as:

$$U_T = U_P + U_E + U_S \tag{2.4}$$

To determine how the system evolves as a crack moves a distance dA, we define equilibrium such that:

$$dU_T/dA = 0 \tag{2.5}$$

We can see the similarities in Equation 2.2 to Equation 2.5 where $dU_P = -dW$ and represents the change in the work potential energy of the load, dU_E represents the change in the strain energy in the system,[**] and $G_c \cdot dA$ and dU_S represent the change in surface energy as the crack moves. (Note that we use G_c as the material fracture property not G, and for generality, we will use G_c for the fracture energy in the following analysis.)

[¶]All equations assume G_c to be a constant, an idealization that is not often the case in viscoelastic systems

[‖]When we speak of forces and displacements, we mean generalized forces and displacements that are work conjugates of one another, so would include pressure-volume, moment-angle of rotation, etc.

[**]We are using the fracture mechanics nomenclature where work done on the system is positive, the negative of the classic thermodynamic definition.

Depending on the loading conditions some energies are typically assumed to be negligible during peeling. While we will fully analyze peeling forces and energies in Section 3, we believe it is important to first discuss the contributions of the different energies during peeling. We also note that dU_P is not always the negative of dU_E; specifically this is not the case in peeling. To place this in context we will consider a few representative geometries.

For the case of 90° self-similar peeling of an inextensible film, Rivlin showed that the potential energy of the applied force drives the crack,[60] where:

$$dU_T = dU_P + G_c dA \tag{2.6}$$

(The change in elastic energy is $dU_E = 0$ as the film is inextensible and the elastic bend energy does not change as the crack progresses in a self-similar fashion.) Therefore, the change in potential energy of the applied load drives the crack for the common 90° peel test geometry. Upon application of equilibrium through Equation 2.5, we get the well known relationship that under 90° peeling $F_c = G_c w$, where w is the peeling material width.

However, as the peel angle decreases the energy contributing to the crack growth process changes. Significantly, at lower peel angles the material stretching becomes significant, especially for thin films. At this point, the results begin to deviate from Rivlin's prediction, which only considered U_P. The force now moves further as the peel arm extends an amount δ. For this case we find that we must consider:

$$dU_T = dU_E + dU_P + G_c dA \tag{2.7}$$

At near 0° peel angles, the elastic energy of the system begins to dominate as the material extends elastically. The assumption of inextensibility becomes inappropriate as the angle approaches zero and extension becomes the dominant contributor (as seen in Section 3.1.1, the 1-cos θ term in the external work approaches zero near 0° peel angles, which requires much higher forces to induce debonding, thus extension becomes the dominant contributor). Under these conditions:

$$dU_T = dU_E + G_c dA \tag{2.8}$$

The elastic energy now becomes dominant for driving the crack.

Alternatively, we can analyze peeling by considering the energy release rate, G. Note the intentional omission of "strain" here (i.e. not "strain energy release rate"), as strain energy is not always a driver for peeling. In this approach, we calculate G as the peeling material is loaded, when $G = G_c$ we reach equilibrium and the crack propagates. It is important to note that G_c is often the property to be measured, and thus a value of G will exist during loading, but it is at the critical point where cracks evolve and adhesive properties are measured.

Irwin and Kies write the energy release rate G for a system obeying a linear-elastic force versus displacement relationship as:[69,70]

$$G = \frac{1}{2} F^2 \frac{dC}{dA} \tag{2.9}$$

where dC represents the increment in compliance with the increment in crack area dA. For cases where the load versus displacement relation is nonlinear elastic in the form of $P = \left(\frac{\delta}{C}\right)^n$,

the Irwin-Kies relationship can be generalized. Here, we define the compliance $C = \delta/F^{1/n}$, where δ is again the change in the position of the load, n is a constant depending on the loading geometry, and F is the applied force. This results in:[71]

$$G = \frac{n}{n+1} F^{\frac{n+1}{n}} \frac{dC}{dA} \tag{2.10}$$

This generalized Irwin-Kies relationship can be applied in a variety of peeling modes. The linear case of Equation 2.9 is recovered when $n = 1$ (Figure 6a). Another common situation, out-of-plane stretching, results in a cubic form ($n = 3$) for the load-displacement behavior (Figure 6b). Peel tests with negligible change in stored energy of stretching or bending can be understood as the limiting case ($n \to \infty$), where the applied force spikes as the peel arm becomes taut for self-similar debonding (Figure 6c). All three of these cases appear frequently for peel test idealizations, both individually and in combinations. Further discussion and examples can be found in Appendix A.

Lastly, the stress intensity factor, K, quantifies the severity of the stress field in the vicinity of a crack tip. Although widely used in engineering practice, especially with monolithic materials, this stress analysis approach has also been used to study fracture in bonded systems. Generally, energy methods are preferred in peeling geometries for ease of use and because the K-dominant field may be confounded in multi-material layered systems. Nonetheless, K can provide information on the directionality of the stresses near the crack tip which has been utilized for crack path selection, but the use of K has limitations for peeling analysis and the crack direction often does not significantly impact the analysis used for peel tests.

2.5 From thermodynamic adhesion to practical adhesion

The measured peel energy, F_c/w, can vary over a wide range of values. This parameter is dependent on peel test geometry, material properties including the interfacial chemistry, dissipation in adhesive layers, inelastic processes like plasticity in adherends, and the thicknesses of the layers (see in detail Section 3.2).[21,56,57] It is also dependent on environmental and testing conditions such as temperature, testing rate, and the current or prior exposure to moisture or chemicals (see in detail Section 5.4). Therefore, peel test metrics, as defined in the common standards, do not always result in a "material property" or a "fundamental property." However, when the results are analyzed in a correct fracture mechanics framework, we may derive the fracture energy, G_c, which is a material system property and a measure of toughness accepted by the scientific community. These aspects are discussed in detail below. However, let us first consider the fundamental question of how such valid values of G_c are related to the types of inter-atomic and -molecular forces which may act across an interface.

From the first law of thermodynamics the fracture energy may be equated to the sum of the different energy terms involved. Thus, assuming that kinetic terms are negligible, i.e. the experiments are conducted at relatively low crack velocities, then:

$$G_c = G_0 + G_D \tag{2.11}$$

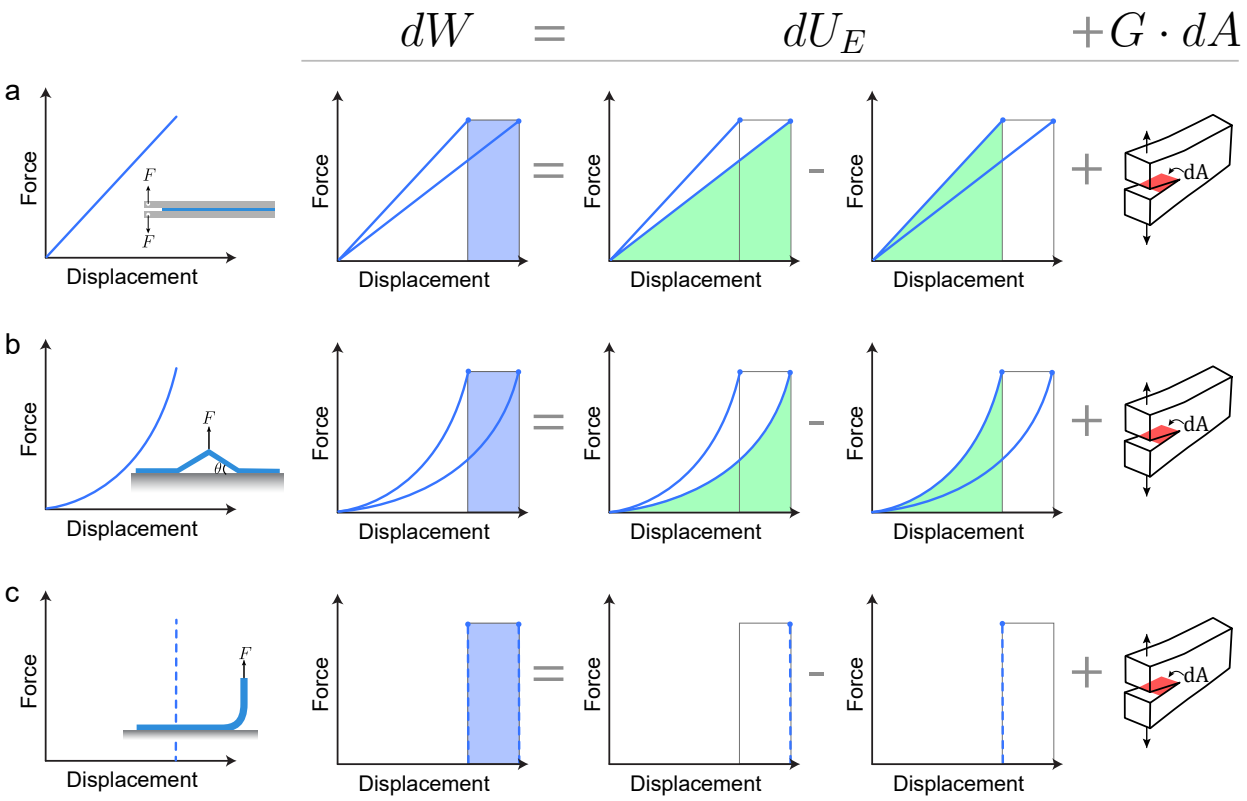

Figure 6: Fracture mechanics analysis schematics. Illustration of applications of the energy balance principle to fracture analysis. The input work of a fixed force moving through a small or virtual distance is equal to the increase in stored energy and energy required to induce fracture, in non-dissipative systems. This equality, captured by the generalized Irwin-Kies relationship, is here shown for: a) Systems with a linear (work-conjugate) load-displacement relationship, such as an idealized DCB specimen, obey the original Irwin-Kies equation (i.e. $n = 1$); b) Systems exhibiting nonlinear load-displacement behavior, such as pull-off or blow-off tests, where out of plane stretching results in cubic relationship, $n = 3$. c) Idealized peel tests (inextensible and no bending resistance) result in $n \to \infty$. Note that there is no stored energy nor change in this quantity, so all work input is directed to fracture. Source: ©M.D. Bartlett et al., CC BY-SA 4.0. Available at http://hdl.handle.net/10919/113716.

where G_0 is the 'intrinsic' fracture energy, which is the energy required to propagate a crack through unit area of interface, or cohesively through the adhesive or substrate, in the absence of viscoelastic, plastic, etc. energy losses. The term G_D is the energy dissipated through viscoelastic, plastic, or viscoplastic dissipative processes within the adhesive surrounding the propagating crack tip per unit area of growth. The intrinsic fracture energy, G_0, should be virtually rate-temperature independent, since its value depends upon the type and strength of inter-atomic and -molecular bonding forces at the interface, or in the adhesive or substrate depending upon the locus of failure. The energy G_D dissipated viscoelastically, plastically, etc. is often the dominant term and is, of course, typically dependent upon the test rate and

temperature. We can re-write this equation in the form:[72,73]

$$G_c = G_0(1 + \psi_v(\dot{a}, T, etc.)) \tag{2.12}$$

where ψ_v is a dissipative term that depends on crack velocity, $\dot{a}$, temperature, T, etc.. When comparing Equation 2.11 and Equation 2.12 we see that the energy G_D and ψ_v are intimately connected, but not identical. Now, the idea that the energy dissipated viscoelastically, G_D, is a function of G_0 makes logical sense. The stronger the intrinsic adhesion forces acting at the interface (for example) are, the more strain (and stress) will be needed to break the interfacial atomic and molecular bonds. Thus, a high G_0 gives access to greater energy dissipation capabilities within the system.[51,74,75] Hence, more energy will also then be dissipated viscoelastically, plastically, etc. at the crack tip due to the increased local strain (stress) field. As a lower bound, the term G_0 may be thought of as the thermodynamic work of adhesion, W_{adh}, if secondary bond breakage and interfacial failure occurs. However, G_0 can be higher than W_{adh}, for example, if failure occurs via the rupture of primary interfacial molecular (e.g. covalent) bonds or within the bulk adhesive. In this last case, for example, the relatively high Lake and Thomas value (they reported values on the order of $\sim$ 50 J/m^2, considerably larger than the $\sim$ 2 J/m^2 associated with breaking C-C bonds across the fracture plane) for the intrinsic cohesive fracture of an elastomer can be attributed to the deformation of the rubber's network during fracture as the mechanical tension in the network chains release as the crack progresses.[76] Essentially, the stored elastic energy in a network chain is lost when a chain breaks, leading to their conclusion that G_0 should be proportional to the square root of the molecular length between crosslinks.[76]

However, while these equations may be of general validity, it is often difficult to determine the values of G_0 and ψ_v. A major reason is the need to establish test conditions when the term ψ_v tends to zero, such that the value of G_c now determined is equivalent to G_0. For example, a glassy epoxy adhesive will always undergo plastic deformation at the crack tip before any rupture of the interface occurs. Thus, the value of ψ_v, and hence G_D, never tends to zero under any test conditions while the adhesive is in a glassy state. (G_0 is an equilibrium property, so is measured at the slowest region of rubbery behavior). Indeed, for most peel tests of commercial interest, while the concepts expressed in Equations 2.11 and Equation 2.12 are valid, the value of the fracture energy, G_c, cannot experimentally be broken down into its separate terms. Hence, the value of G_0 cannot usually be determined.

Nevertheless, the validity of Equations 2.11 and Equation 2.12 have been established from peel tests conducted on a simple rubbery, crosslinked, adhesive adhering to rigid polymeric substrates.[72,73] Here the energy dissipation was solely viscoelastic in nature and the term ψ_v tended to zero at very low crack velocities and high test temperatures, see more details in Section 5.4. Under these test conditions the term G_c was shown to be equivalent to G_0. A second approach, again using rubbery polymers as the adhesive, is the use of the JKR test method,[64] where again the test can be performed (i.e. at low crack velocity and small sizes) to enable the viscoelastic energy dissipation to vanish as the interfacial crack grows, and hence the term ψ_v tends to zero, and G_c is equivalent to G_0.

Therefore, at vanishingly small reduced rates for equilibrium behaviour in the rubbery region, where dissipation vanishes, G_c approaches the thermodynamic work of adhesion, W_{adh}. For example, a feature of the 90° peel test using optically smooth rubber (cast silicone

rubber on poly(methyl methacrylate) (PMMA)) is that it obeys the thermodynamic theory suggested first by Griffith and later employed by Rivlin.[9,60] First, it is reversible, since the peeled rubber can heal back in place onto the smooth PMMA surface; second, the peel energy at very slow peeling velocities (e.g. 1 nm/s) is low (0.1 N/m) and fits the van der Waals fracture energy around 0.1 J m^{-2}; third, the force depends only on the strip width:

$$\frac{F_{c,\theta=90^\circ}}{w} = W_{adh} \tag{2.13}$$

However, the adhesion force rises with increasing crack speed and contact dwell-time, decreasing temperature, and inelastic behavior or other variables.[77] The conclusion is that the peeling adhesion energy can obey the thermodynamic theory, where the energy of debonding is equal to the energy of bond formation. But for many practical engineering applications, the energy associated with debonding is many orders of magnitude larger than the thermodynamic work of adhesion. Thus, at the low end of the fracture energy range, G_c can approach the thermodynamic work of adhesion, $W_{adh} \approx 0.1$ J/m^2, while at the high end of the range G_c can be measured beyond several kJ/m^2 in the case where tough engineering adhesives are employed. Such tough joints are often used as structural adhesives for applications in construction, aerospace, and automotive industries. These materials are often bonded to the adherends with van der Waals and hydrogen bonds which are sufficiently strong to induce cohesive failure within the adhesive; covalent bonds can also be utilized, especially when a good environmental resistance is required of the joint. In the middle of the range are typically soft materials such as elastomers, pressure sensitive adhesives (PSAs), and tough hydrogels that range from approximately $1 < G_c < 1000$ J/m^2. In this $1 < G_c < 1000$ J/m^2 range, these materials may still be bonded at the interface with van der Waals interactions, but the fracture energy is greater than W_{adh}. This occurs as dissipative processes near the crack tip (i.e. viscoelastic dissipation) substantially increase the energy required to debond the materials by 4 - 5 orders of magnitude, as illustrated in Figure 7. A relevant example of adhesion in this intermediate regime is the behavior of adhesive systems found in nature. Wall-climbing geckos use reversible van der Waals peeling to stick to, then release from, vertical surfaces.[3,78] Millions of fine hairs covering gecko toe-pads are sufficient to support a 100 g lizard, however, the gecko can easily unpeel the toe and climb the surface. Therefore this intermediate regime is useful for packaging, consumer adhesives, and many other applications that are not directly load bearing from an engineering viewpoint. As demonstrated by the gecko, this regime is also useful for temporary adhesives, which has given rise to research in bio-inspired adhesives, which can act as switchable adhesives which can have high adhesion strength yet be switched to a low adhesive state, and other reversible adhesive systems.

Spanning many orders of magnitude, the general range of G_c values with representative regimes is displayed in Figure 7. Characterization methods spanning multiple decades are a challenge, and suggest that different peeling scenarios will often require a different analysis depending on the materials and conditions of the test. In Section 3, we now introduce categories for different types of peeling conditions, providing a means to select the appropriate equations for analysis.

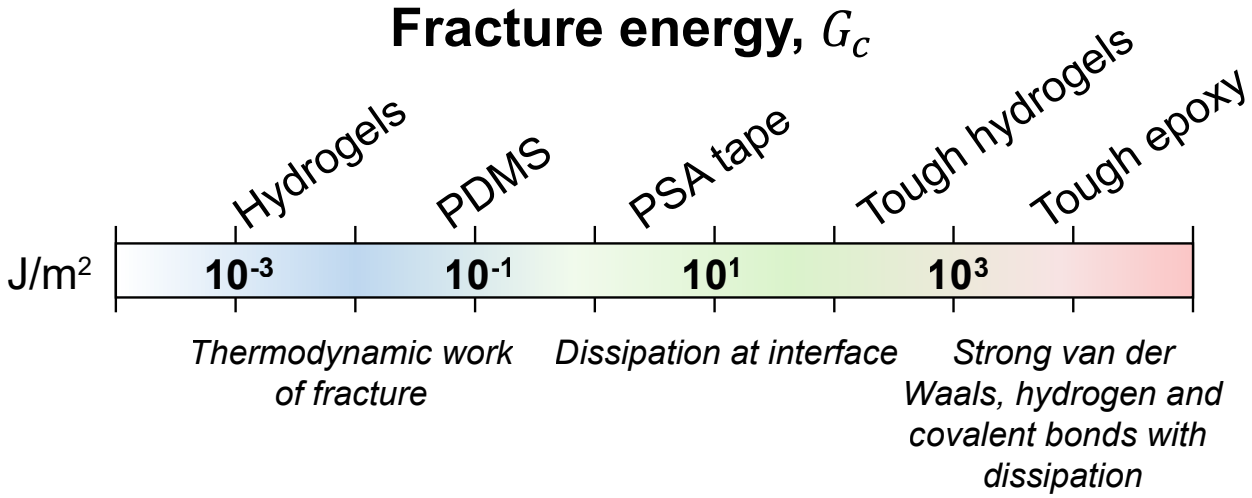

Figure 7: General range of fracture energies. Materials and interfaces display a wide range of fracture energies spanning several orders of magnitude depending on the materials and interfacial chemistry. The ranges displayed are meant to be a general guide, where the selection of substrate (i.e. metal, polymer, ceramic) or interface treatment process may influence G_c for any given type of material. Depending on whether the material fails in the bulk or at an interface, may also influence the G_c value. Several other factors that influence G_c values are discussed in Section 2.5.

3 Analyzing peel test behavior

Peel tests may nominally be grouped into one of four categories, depending on whether peeling is elastic or inelastic, and if the debonding is self-similar or not. Nearly all types of peel experiments from reversible interfaces to extremely tough permanent bonds will conceivably fall into one (or more as debonding proceeds) of these categories. Herein, inelastic is used to denote peel arms that experience strains and deformations sufficiently large that they do not return to their original configuration upon removal of the stress; plastic deformation is a common example of inelastic behavior commonly cited in peel experiments. We take self-similar to mean that the solution is independent of debond length, which is also referred to as steady-state debonding in some literature.[40] This idealization has been widely used, including in seemingly all the original analyses of both elastic and inelastic peel behavior for stable debond propagation. Additionally, this categorization has greater dependence on specimen dimensions, material properties, and measured adhesion energy, than the specific test configuration being used. The categories are as follow:

1. Category I: Elastic arms and self-similar
2. Category II: Inelastic arms and self-similar
3. Category III: Inelastic arms and not self-similar
4. Category IV: Elastic arms and not self-similar

Although Category I and II behaviors are most commonly observed in laboratory peel tests, Category III and IV behaviors do arise in various configurations. To clarify why these categories are more dependent on materials, geometry, and adhesive characteristics, we can consider the specific example of a T-peel experiment. If an adhesive/adherend combination is used which gives rise to weak intrinsic adhesion (i.e. relatively weak inter-atomic and -molecular forces are generated across the interface) and/or the adhesive and peel arm materials possess a relatively high yield stress, then we expect the behavior to fall into Category I. However, as the intrinsic adhesion increases and/or the adhesive and peel arm materials possess lower yield stresses, the larger forces and bending moments needed to fracture the peel test induce plastic deformation in the adhesive and/or adherends. Indeed, very high energy dissipation can be associated with adherend yielding so that the behavior then belongs in Category II if self-similar debonding occurs. Even for tests that ultimately exhibit Category I or II behaviors, the initial debonding typically does not proceed in a self-similar fashion. If the debonding is not self-similar throughout, we expect the peeling to at least initially fall into Category III and IV, depending on whether the peel arms behave in an inelastic or elastic manner, respectively. In this section we will review and provide analysis and evaluation of the different categories.

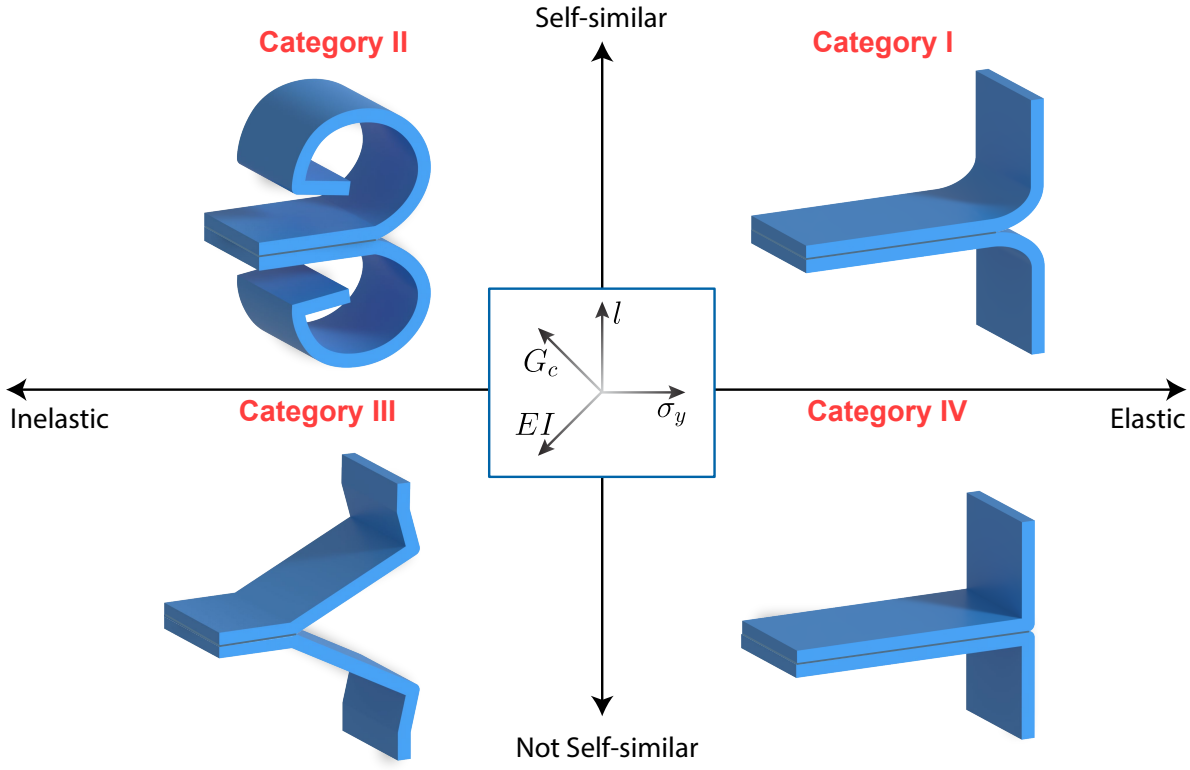

Figure 8: Peel categories. Schematic representations of the four different peel categories depending on their elastic or inelastic behavior (x-axis) and their self-similar or not self-similar (y-axis) behavior. T-peel specimens are shown for illustration purposes, but the categorization applies to other configurations as well. Source:

3.1 A review of Category I: Elastic self-similar debonding

3.1.1 Elementary analysis of peeling

For the case of an elastic peeling material as shown in Figure 9a, consider, as Lindley[61] did for self-similar debonding (i.e. where the debond process zone "is independent of the amount of peeling which has taken place"), an unstressed material[‡] of width w, thickness t, and modulus E. Allow an increment of length a to be peeled from a substrate at an angle θ, as shown in Figure 9b, by an external force, F. The debonded portion of the peel arm will elastically strain by an amount ε and the increment in stored elastic energy U_E within length a is:

$$U_E = wta \int_0^{\varepsilon} \sigma d\varepsilon \tag{3.1}$$

in general or $U_E = 1/2Fa\varepsilon$ for the case of linear-elastic behavior, resulting in:

$$U_E = \frac{F^2 a}{2Ewt} \tag{3.2}$$

Note that because we are considering self-similar debonding of an elastic peel arm, we have neglected the elastic bending energy of the tape as it remains constant during peeling for a homogeneous strip and we need not consider plastic dissipation within the elastic peel arms of Category I peeling.

Debonding a distance a at some arbitrary load, F, this external force would move through a distance $\delta = a[(1 - \cos\theta) + \varepsilon]$ with the external work done by this force, W:

$$W = Fa\,(1 - cos\ \theta + \varepsilon) \tag{3.3}$$

or for the linear-elastic case:

$$W = Fa\left(1 - cos\ \theta + \frac{F}{Ewt}\right) \tag{3.4}$$

We define the available energy release rate:

$$G = \frac{\partial W}{\partial A} - \frac{\partial U_E}{\partial A} \tag{3.5}$$

As in Griffith's seminal work, partial derivatives are often used in this expression to eliminate changes in work and strain energy that could result from other factors such as thermal expansion. Recognizing that for the case of peeling, and assuming that the bond width is also w (here and throughout the paper unless otherwise noted) $\frac{\partial}{\partial A} = \frac{da}{dA}\frac{\partial}{\partial a} = \frac{1}{w}\frac{\partial}{\partial a}$, the

[‡]The stored energy relationship and resulting equations must be altered if residual stresses are present (e.g. see Kendall[79])

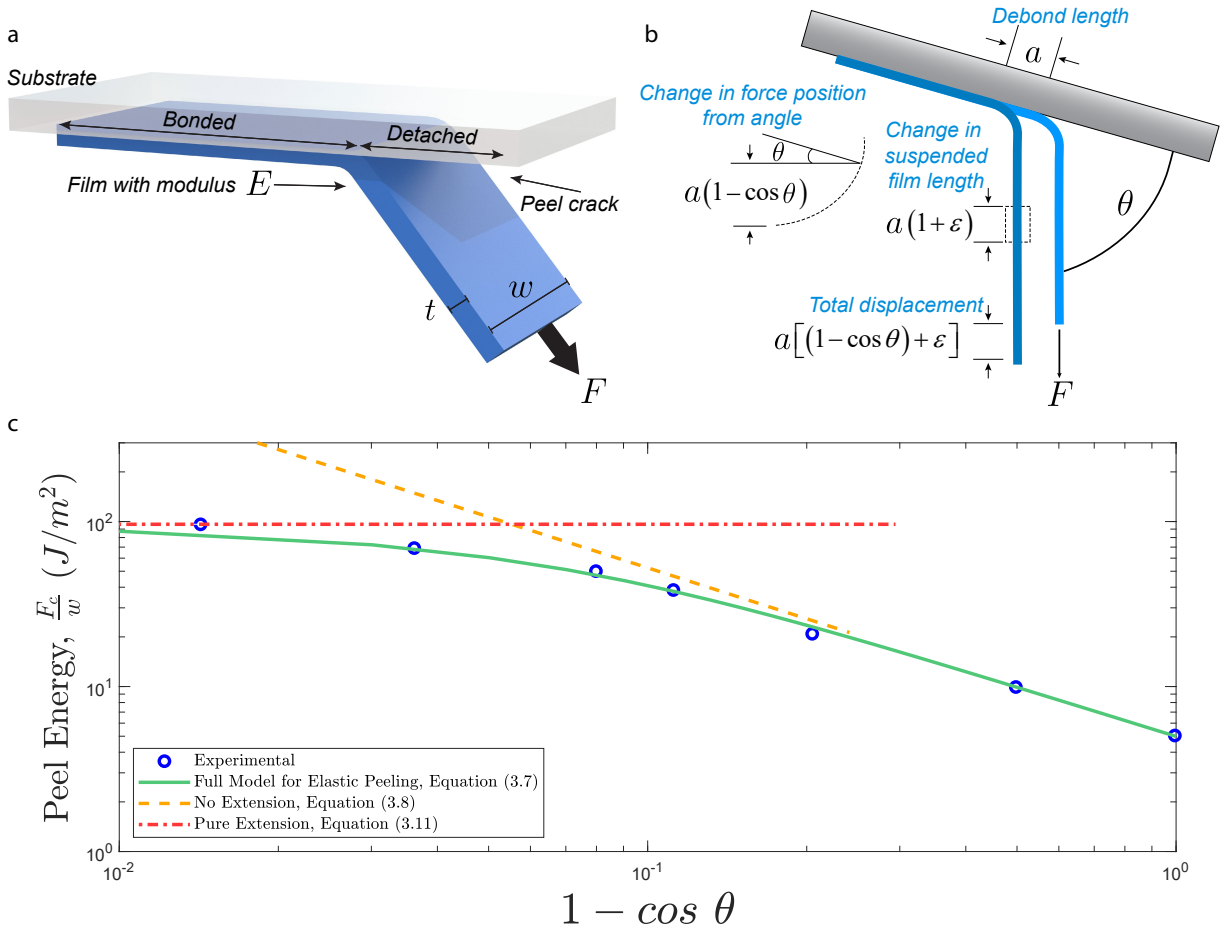

Figure 9: Film peeling. a) Peeling a film from a substrate with the relevant parameters labeled. b) Showing the progression of the debonding film. Source for a,b: ©M.D. Bartlett et al., CC BY-SA 4.0. Available at http://hdl.handle.net/10919/113716. c) Experimental results on peeling rubber showing how elastic extension at low peel angles (i.e. small $(1 - cos\theta)$)

causes deviation from Rivlin's equation.[10]

available energy release rate G can then be written for the linear-elastic case as:[61]

$$G = \frac{F}{w}(1 - cos\ \theta) + \frac{F^2}{2Ew^2t} \tag{3.6}$$

so that the force required to separate the interface, F_c, when $G = G_c$ is given as:

$$\frac{F_c}{w} = -Et(1 - cos\ \theta\ ) + \sqrt{E^2t^2(1 - cos\ \theta)^2 + 2EtG_c} \tag{3.7}$$

Equation 3.7 is understood to be applicable to a full range of peeling angles provided the the peel arm extends linearly elastic. For example, a comparison of experimental results for peeling rubber is shown in Figure 9c where peel force per unit width is plotted against $(1 - cos\ \theta)$. For very small peel angles, the elastic energy term dominates, while the work

potential energy term dominates at high angles. This can be seen in the plot where the experimental data is well captured with the elastic term at low angles and with just the work potential energy term at high angles. Consequently, two different limiting conditions arise in this elastic, self-similar peeling. First, we have the case where the change in elastic energy is negligible in comparison with the change in work potential energy. Specifically, this case occurs when $\sqrt{2G_c/Et} \ll 1 - cos\ \theta$ so that the critical force for peeling in cases of inextensible adherends is given by:

$$F_c = w\left(\frac{G_c}{1 - cos\ \theta}\right) \tag{3.8}$$

To reduce elastic deformation during peel tests and improve the assumption that the work potential energy is driving the separation and hence the validity of Equation 3.8, an inextensible backing can be attached to the peeling arm or a reinforcing layer can be embedded within, as recommended by standards such as ASTM C794 for 180° peel tests of sealants.

Special cases of Equation 3.8 often arise in practice. For example, for the the 90° peel test with inextensible adherends, direct substitution into Equation 3.8 gives the critical force for peeling as:

$$F_{c,\theta=90^\circ} = wG_c \tag{3.9}$$

In a similar manner, the critical force for peeling in the 180° peel experiment is:

$$F_{c,\theta=180^\circ} = w\frac{G_c}{2} = \frac{F_{c,\theta=90^\circ}}{2} \tag{3.10}$$

In contrast to the 90° and 180° peel tests, we can also consider the 0° peel test which is often referred to as a shear experiment. Here the tape is pulled parallel to the substrate (see the first entry in Table 1). For low peel angles, the change in work potential energy is nearly zero, so the stored elastic energy dominates in Equation 3.7, and the critical force for peeling can be approximated for linear-elastic peel arms by:

$$F_{c,\theta=0^\circ} = \sqrt{2EG_c t w^2} \tag{3.11}$$

When utilizing these different geometries to evaluate material or adhesive properties, the parameter of interest becomes the fracture energy, G_c. The equations can then be solved for G_c, the dependent variable of interest, for the different testing conditions. For inextensible peel arms, the 90° peel test results in:

$$G_{c,\theta=90^\circ} = \frac{F_c}{w} \tag{3.12}$$

and the 180°peel becomes:

$$G_{c,\theta=180^\circ} = \frac{2F_c}{w} \tag{3.13}$$

Another common configuration used to evaluate peeling is the T-peel test.[††] When both

[††]BS-EN-1895 refers to this as a 180° or T-peel test, and indeed the equation is the same as for 180°

peel arms are flexible in bending and inextensible in tension, this test results in:

$$G_{c,T-peel} = \frac{2F_c}{w} \tag{3.14}$$

These key equations for Category I behavior are summarized in Table 2. It should be noted that varying the peel angle, θ, for a test raises the question of the 'fracture mode-mixity' and its effect on the value of G_c as determined from that test. This is a complex and controversial area of research and therefore discussion of this topic is reserved for later in the present review, see Section 5.2.

Table 2: Common peel geometries and equations for Category I. The width w is into the page. Source: Schematics ©M.D. Bartlett et al., CC BY-SA 4.0. Available at http://hdl.handle.net/10919/113716.

Summary of peel geometries and equations			
Test name	Critical Force for Peeling (N)	Fracture Energy (J/m^2)	Assumptions
90° peel 	$F_c = wG_c$	$G_c = \frac{F_c}{w}$	Inextensible adherends
180° peel 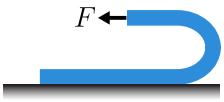	$F_c = w\frac{G_c}{2}$	$G_c = \frac{2F_c}{w}$	Inextensible adherends
T-peel 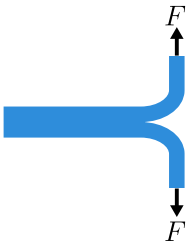	$F_c = w\frac{G_c}{2}$	$G_c = \frac{2F_c}{w}$	Inextensible adherends
0° peel 	$F_c = \sqrt{2EG_c t w^2}$	$G_c = \left(\frac{F_c}{w}\right)^2 / 2Et$	Long adhesive joint and linear-elastic extension

When utilizing these equations to calculate G_c for steady-state peeling, the value for F_c

peeling for the case where no plasticity is present.

should be taken from the plateau region when the adhesive has reached a nearly constant peel force (where F_c does not change substantially with displacement). Strictly speaking, these analyses are appropriate when the adherends are in the elastic regime and inelastic deformation in the adherends is not substantial. Furthermore, thickness and width of the adhesive can also play a role.[80,81] As will be discussed, the behavior of the adherends can dramatically impact the perceived G_c values, which can be artificially increased by processes like plasticity in the adherends. It is also worth noting that the ASTM D624 Type T specimen for rubber tearing correctly includes the factor of 2 and stretching, citing Rivlin and Thomas,[82] but the 180° type peel tests for adhesion ignore both (e.g. see D903, D1876, D6862). As noted previously, this leads to the difference in values of "peel strength" for 90° versus any of these 180°-type tests.

3.2 A review of Category II: Inelastic self-similar debonding

3.2.1 Introduction

In our analyses of the Category I behavior of the high peel angle tests (i.e. 90°, 180°, and T-peel configurations), we found that the thickness of the strip, t, does not appear in the result given in Equation 3.8, nor do any material properties. This key result is because we have assumed that the peel arm is inextensible in tension while also dissipating no energy in bending. Thus, the peel arm simply transfers the external work to the surface in a non-prescribed way. In the case of Category II behavior, this simple energy transfer no longer occurs, as significant energy may go into plastic bending and heat dissipation, as demonstrated for polyimide coatings using deformation calorimetry by Farris et al.[83,84] To illustrate how this complicates the understanding of even a simple peel test, we can consider the case of the 90°peel test in which the fracture energy is sufficient for the peel arm to be plastically deformed in bending. The steps involved in this deformation for an elastic-perfectly plastic peel arm are shown in Figure 10a,b, where the applied moment M and curvature κ are normalized by their respective elastic limits, M_e and κ_e. As the peel arm lifts from the substrate, it initially deforms elastically. Such behavior occurs from the peel front to point A. On the moment-curvature diagram in Figure 10b, this portion of the behavior is from the origin to point A. The peel arm is then further deformed plastically from A to B as the moment and curvature increase. From B to C, the arm unloads elastically to zero moment, but because of the prior plastic deformation, this region no longer has zero curvature. From C to D, the arm continues to deform elastically as the curvature decreases. At D, the moment is sufficient to begin reverse plastic bending which continues to E. From E to F, the arm unloads elastically to zero moment with a residual curvature observed after the test is completed and as suggested by the dashed curve. Additional details can be found in Refs. [22, 23, 85–87]. Similar behavior occurs throughout a range of peel angles, including 180°peel tests, as illustrated in Figure 10c. For both 90°and 180°peel tests this plasticity behavior is schematically shown in Figure 10d,e, where plastic bending initiates near the peel front and reversed plastic bending often occurs as the peel arms continue to straighten.

It is clear that for this complicated behavior from a simple test, the assumptions outlined in Section 3.1 for Category I peeling and in Equation 3.7 are not present. To cope with the consequences, it is necessary to relax the assumptions made in the Category I analysis. To

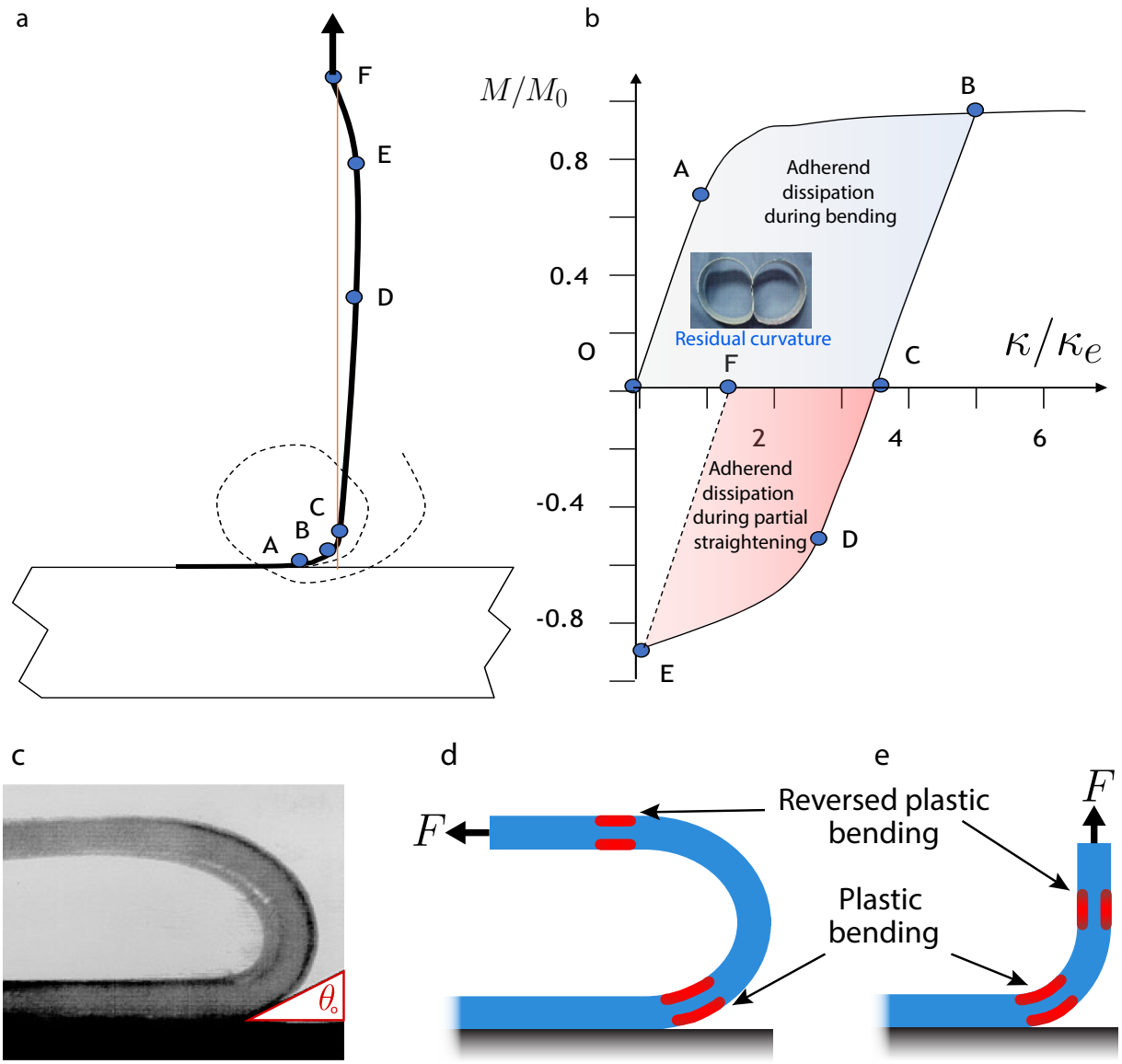

Figure 10: Peel test with plasticity in the peel arm. a) Regions of deformation of the peel arm. Dashed line suggests possible final shape of peel arm, as if removed from substrate. Adapted with permission from Ref. 23. Copyright 1988, ASME. b) Corresponding normalized moment-curvature behavior, Adapted from Ref. 23. c) Image of a 180°peel experiment showing the local angle (θ_o) at the contact point in a peel test. d) A 180°peel arm and e) a 90°peel arm with plastic bending that undergoes reversed plastic bending upon straightening.

do so, an energy-based analysis is usually written in terms of the critical energy release rate,

G_c, when the crack propagates stably:

$$G_c = \frac{\partial W}{\partial A} - \frac{\partial U_E}{\partial A} - \frac{\partial U_{dt}}{\partial A} - \frac{\partial U_{db}}{\partial A} - \frac{\partial U_k}{\partial A} \tag{3.15}$$

$$= \frac{1}{w}\left(\frac{\partial W}{\partial a} - \frac{\partial U_E}{\partial a} - \frac{\partial U_{dt}}{\partial a} - \frac{\partial U_{db}}{\partial a} - \frac{\partial U_k}{\partial a}\right) \tag{3.16}$$

where the following increments in energies are associated with the increment in crack growth:

$\frac{\partial W}{\partial a}$ = Change in the external work done

$\frac{\partial U_E}{\partial a}$ = Change in the stored strain-energy in the peel arm

$\frac{\partial U_{dt}}{\partial a}$ = Change in the energy dissipated during tensile deformation of the peel arm

$\frac{\partial U_{db}}{\partial a}$ = Change in the energy dissipated during peel arm bending near the peel front

$\frac{\partial U_k}{\partial a}$ = Change in the kinetic energy

per unit extension of the crack length, a.

First, in our consideration of Category II behavior, the kinetic energy term, U_k, will be ignored, but we note that it is determined entirely by the test speed, V. Generally the test speeds used in peel tests are relatively slow so there is little change in the kinetic energy, U_k. However, such effects may be easily included.[88] Second, obviously, if the terms U_{dt}, U_{db}, and U_k are all assumed to be zero then Equation 3.15 reverts to Equation 3.5. Third, therefore, the next step is to consider the effects on the analysis of the peel test when these terms are not zero in value.

3.2.2 Inelastic tensile deformation in the arm

Provided that bending remains elastic or that energy dissipated in bending (and partial straightening) is negligible, as might be the case if the peel arm is very thin, Equation 3.3 remains valid even if tensile deformation of the peel arm is inelastic.[61] Interestingly, this relationship holds regardless of whether the tensile behavior is nonlinear elastic or dissipative (e.g. includes plasticity). The reason for this is that during a test, tensile loading is not reduced so stretching is not reversed. This is in contrast to inelastic bending behavior, as bending of most peel tests involves partial reversal, thus introducing dissipation and requiring a larger work input. We rewrite Equation 3.3 as:

$$\frac{\partial W}{\partial a} = F_c\,(1 - cos\ \theta + \varepsilon) \tag{3.17}$$

and there will also be an accompanying change in the sum of dU_E and dU_{dt}:

$$\frac{\partial U_E}{\partial a} + \frac{\partial U_{dt}}{\partial a} = wt \int_0^{\varepsilon} \sigma d\varepsilon \tag{3.18}$$

Thus, we have for the value of G_c for the case of non-linear extension of the peel arm, but where solely elastic bending (denoted by the superscript "eb") is still assumed to occur or that bending dissipation is negligible:

$$G_c^{eb} = \frac{F_c}{w}\left(1 - cos\ \theta + \varepsilon\right) - t\int_0^{\varepsilon} \sigma d\varepsilon \tag{3.19}$$

3.2.3 Plasticity corrections

If plastic or viscoelastic bending of the peel arm occurs near the crack front, then the determination of G_c also needs to consider such energy losses, as shown by Gent and Hamed.[56,89,90] Thus, from Equation 3.15, the value of G_c is given by:[24]

$$G_c = \frac{F_c}{w}\left(1 - cos\ \theta + \varepsilon\right) - t\int_0^{\varepsilon} \sigma d\varepsilon - G_{db} \tag{3.20}$$

where $G_{db} = \partial U_{db}/\left(w\partial a\right)$. From Equation 3.19, an alternative representation of Equation 3.20 is:

$$G_c = G_c^{eb} - G_{db} \tag{3.21}$$

Obviously, the value of G_c^{eb} can be evaluated simply from Equation 3.19. However, the evaluation of the term G_{db}, which takes into account the energy dissipated per unit area of crack growth during bending of the peel arm near the peel front, is a complex problem. Nevertheless, this term is often of major importance and leads to the very strong dependence of the measured critical for force for peeling, F_c, per unit width, w, on 1) the peel angle, θ, 2) the thickness, t, of the peel arm, and 3) the stress versus strain behavior of the material(s) forming the peel arm.

Spies recognized that elastic and plastic bending combined to induce high peel arm curvatures near the debond tip, as well as that the debonded peel arm would become straight farther away.[5] Modern analysis methods often follow the results of Kim and coworkers[22,23,86] to quantify the energy dissipation associated with both bending and partial straightening of the peel arm as it moves away from the peel front. To the authors' knowledge, most models since this time thus account for plastic dissipation over the full excursion in curvature as a given segment approaches and retreats from the crack tip. One approach to determining an expression for G_{db} has been to model the peel arm either as 1) a non work-hardening elastic-perfectly plastic material, or 2) a bilinear work-hardening, elastic-plastic material or 3) a power-law work-hardening, elastic-plastic material and to input the appropriate stress versus strain relationship into the analytical equations derived for G_{db}. These equations have been derived using large displacement beam theory considering elastic-plastic loading, elastic-plastic unloading and root-rotation at the peel front.[22–24,85,86,91,92] Equations for both the cases of 1) the peeling of one material directly from another and 2) when the two materials were adhesively-bonded using an adhesive layer were analysed, with somewhat different expressions being derived for these two cases.[24] Two noteworthy aspects are, first, that the determination of the value of G_{db} for a given peel test requires an iterative solution. However, a spreadsheet implementation that calculates the values of G_{db}, and so gives the value of G_c, from inputting the measured peel test results, the geometry of the peel test, including the peel angle, θ, and arm thickness, t, and the elastic-plastic stress versus strain curve of the peel arm has been developed which may be downloaded to facilitate the analysis of experimental peel data.[93] Second, in these analytical equations the angle at the separation

point in the peel tests is taken to be θ_o, as shown in Figure 10c, and its value is determined in the course of the calculations of G_{db}. The predicted values of θ_o may be compared to the experimentally measured values of θ_o in order to provide a validation of the accuracy of these analytical/numerical calculations.

3.2.4 Effect of peel angle

Kinloch et al. have studied the failure of peel tests of polyethylene/aluminum-foil laminates where the aluminum foil was bonded down to a rigid substrate and the polyethylene film was peeled away at various angles.[24] The results are shown in Table 3. For comparison purposes, the analysis results for the Category I case of inextensible elastic peel arms:

$$G_c^{\infty E} = \frac{F_c}{w}(1 - \cos\theta) \tag{3.22}$$

are shown as the second column of the table. For the tests conducted by Kinloch et al., the values of $G_c^{\infty E}$ are very similar to those of G_c^{eb} from Equation 3.19, since the strain, ε, in the peel arm during the test was relatively low. Note that the values of $G_c^{\infty E}$ are highly dependent upon the value of the peel angle, θ, employed. This arises from the plastic bending of the polyethylene peel arm that occurs near the crack front and the extent of such plastic energy dissipation is a strong function of the peel angle. This can be seen in a similar system when peeling a PSA tape from stainless steel (SS) and high density polyethylene (HDPE) (Figure 11a). Due to plastic deformation, the measured peel force is higher than expected with Equation 3.8. This can be seen in the shape of the tape after removal, where at higher peel angles the tape becomes more tightly coiled, indicative of the plastic deformation in the adherend (Figure 11b).[‡‡]

We recall that the terms $G_c^{\infty E}$ and G_c^{eb} do not take any such plastic bending of the peel arm, via the term G_{db}, into account. However in Table 3, the values of G_c were ascertained by accounting for and subtracting the plastic energy dissipation that occurs in the peel test from using Equation 3.21 and by modeling the peel arm as a material which work hardens according to a bilinear elastic-plastic stress versus strain relationship. Clearly, when the plastic deformation is taken into account, the values of G_c obtained are not significantly dependent upon the peel angle used. The values of the local peel angle, θ_o, determined from both the analytical theory and by direct experimental measurements are also quoted in Table 3. As may be seen, there is very good agreement between the values of θ_o from the different methods and this acts as a direct check on the soundness of the analytical approach outlined above. Thus, this analytical approach does indeed yield a characteristic value of the fracture energy, G_c, from the peel tests which is independent of the peel angle.

3.2.5 Effect of thickness of the peel arm

The thickness, t, of the peel arm may influence the measured peel force, as shown by the variation of the values of $G_c^{\infty E}$ as a function of t in Table 4.[24] Again, this behavior arises from the plastic bending of the polyethylene peel arm that occurs near the crack front and

[‡‡]These experiments can be carried out at your desk by changing the peel angle during the removal of common PSAs and observing how the tape coils with different peel angles.

Table 3: Results for polyethylene (PE)/aluminum foil laminates for various peel angles.[24] (The thickness of the PE peel arm was 35 μm.)

Peel angle (°)	F_c (N)	$G_c^{\infty E}$ (J/m^2)	θ_o (theory) (°)	θ_o (expt.) (°)	G_c (J/m^2)
45	15.6	183	20.4	24 to 30	236
90	8.3	333	34.5	40 to 47	228
120	6.2	373	41.7	48 to 58	218
135	6.0	412	46.1	50 to 60	223
150	6.3	467	51.7	55 to 62	236

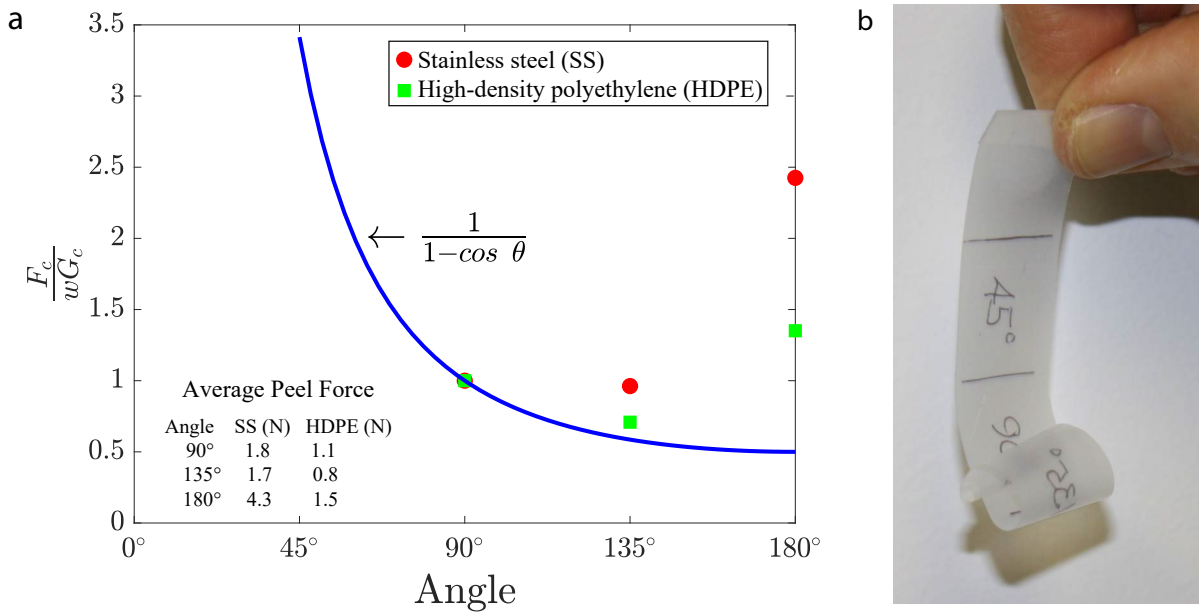

Figure 11: Adherend curvature as result of plasticity. a) Plastic deformation during peeling often increases with peel angle. Thus, there is interest to use smaller peel angles to reduce plastic dissipation that amplifies the apparent peel energy. Here are results for a PSA tape being pulled from either stainless steel (SS) or high density polyethylene (HDPE), showing the amount of dissipation depends on the substrate, which affects the peel energy. Here, both sets of data were normalized by their respective peel values at 90° peeling, with the stronger adhesion to SS showing the greatest dissipation with respect to the blue curve for Rivlin's solution. b) This increasing dissipation is seen in successively going from 45° to 90° to 135° to 180° for a demonstration of a PSA tape, where increasing plastic deformation results in increased coiling after peeling.

the extent of such plastic energy dissipation is a strong function of the thickness of the peel arm. However, when the analysis appropriately accounts for the term G_{db} as a function of t, the resulting value of G_c is independent of the value of t. Furthermore, there is good agreement between the values of the measured and theoretically calculated local peel angle,

Table 4: Results for polyethylene/aluminum foil laminates with various thicknesses, t, of the polyethylene peel arm.[24] (Peel angle, θ, was 180°.)

Thickness (μm)	F_c (N)	$G_c^{\infty E}$ (J/m^2)	θ_o (theory) (°)	θ_o (expt.) (°)	G_c (J/m^2)
30	2.4	195	59.5	54 to 66	69.8
45	2.6	205	50	41 to 49	62.3
60	3	240	46	38 to 46	69.3
75	3.3	260	43.4	38 to 45	71.5
105	3.3	260	36.1	24 to 32	67.3
135	2.8	225	29.1	22 to 28	59.5
165	3	240	27.1	22 to 28	65.4
215	2.8	220	21.9	17 to 21	68.2

θ_o, at the crack front. Finally, it is interesting to note in Table 4, whilst that the value of G_c is independent of the value of the thickness of the peel arm, the value of $G_c^{\infty E}$ at first increases with increasing thickness and then decreases. This observation has been suggested[59] to arise because, for a given degree of adhesion, a very thin peel arm will undergo complete plastic yielding on detachment.[56] However, the total amount of such energy dissipated will be small since the thickness of the peel arm is small. As the thickness of the peel arm increases, more energy will be dissipated and the value of $G_c^{\infty E}$ will rise. However, at relatively large thicknesses, the peel arm will not experience large bending stresses and the value of $G_c^{\infty E}$ will now decrease.

3.2.6 Limitations in the analysis as a result of plasticity in adherends

A study by Kinloch et al.[94] has subsequently revealed that, while this analytical approach works well for the above and similar thin-film laminates, there are major problems if this approach is applied to peel tests consisting of structural adhesives, such as epoxy adhesives bonding aluminum and steel alloys when a relatively thick peel arm of the metal is used. Basically, the challenge here is that the value of $G_c^{\infty E}$ ($\approx G_c^{eb}$), which is equivalent to F_c/w for a typical such peel test with θ= 90°, invariably has a very high value, as does the plastic dissipated energy term, G_{db}. Thus, the calculation of G_c from Equations 3.21 involves the subtraction of two relatively large values. This may often lead to a very high scatter and uncertainty being associated with the resulting value of G_c and also obviously depends upon the accuracy of the analysis used to determine the value of G_{db}.

Some data to illustrate these problems are shown in Figure 12, where in all the peel joints the locus of failure was cohesive failure through the adhesive layer. (The two commercial adhesives, i.e. ESP110 (Permabond, UK) and XD4600 (Dow, USA), are both rubber-toughened epoxy adhesives. However, the latter is significantly tougher, as may be seen from the relative values of G_c.) The first aspect that was considered was the form of the model used for the elastic-plastic behavior of the aluminum-alloy peel arm that was used in the calculation of

the term G_{db}. Three different approaches were examined: a bilinear representation, a classic power-law representation, and the digitization of the experimentally-measured elastic-plastic stress-strain curve for the peel arm material. As may be seen from Figure 12, the type of representation used for the elastic-plastic behavior of the aluminum-alloy peel arm had no significant effect on the scatter apparent in the values of the fracture energy as determined from the peel tests. The second aspect was to consider the assumptions made in the equations used in determining the value of the plastic dissipated energy term, G_{db}, see Section 3.2.3. Consideration of these equations led to the suggestion that the maximum strain, e_{max}, at the root of the bending, flexible peel arm must not exceed $e_{max} \geq 4\%$. If values of $e_{max} \geq 4\%$ were found to arise in the peel test the measured data were rejected and 'filtered' out from the set of peel test measurements used to determine a valid value of the fracture energy, G_c, from the peel tests. Thirdly, to try to resolve the problem of the subtraction of two relatively large values, i.e. $G_c^{\infty E}$ and G_{db}, which leads to a high scatter for the term, G_c, as discussed above, it was suggested that a rejection criterion for the data should be applied if a 'correction factor' ($CF\ \% = 100.\ G_{db}/G_c^{\infty E}) \geq 85\%$ was found to be needed. If values of $CF \geq 85\%$ were found to arise in the peel test, the measured data were rejected and "filtered" out from the set of peel test measurements used to determine a valid value of the fracture energy, G_c.

The effects of the latter two rejection criteria are also illustrated in Figure 12. For both rubber-toughened epoxy adhesives, the left-hand side (i.e. "Before filtering") shows all the values of G_c from the replicate tests and the scatter in the data for all these cases is relatively high. The LEFM $G_{c(bulk)}$ value is also given for each adhesive. When the rejection criteria for the values of G_c of $e_{max} \geq 4\%$ or a CF $\geq 85\%$ are applied, then the results reduce to those shown on the right-hand side of Figure 12, termed "After filtering." For the moderately tough "ESP1110" adhesive, then the scatter associated with the values of G_c from the replicate tests is indeed reduced, but is still relatively high. For the very tough 'XD4600' adhesive, virtually all the values of G_c from the replicate peel tests are rejected, since the high toughness of this adhesive leads, of course, to high values of strain and the CF. Hence, many calculated values of G_c are rejected and the two remaining values of G_c are in poor agreement with the value of $G_{c(bulk)}$ from the LEFM tests. Additionally these observations are relatively independent of the modeling method used for the elastic-plastic stress versus strain curve of the peel arm adherend material, i.e. using either a bilinear or power-law work-hardening model (see above), which indicates the robust nature of this modeling approach. This low sensitivity to the employed model likely reflects the fact that all models are fits (of varied fidelity) of the same experimental stress versus strain behavior, which averages the effect. There is also the self-correcting nature of higher stiffness leading to higher moments, and hence larger curvatures, thus further reducing output variation. Because these models are typically independent of time (i.e. it is only the extent of the forward and reverse plasticity excursion that matters, not the duration along this path), we would recommend that ideally the fits be optimized over the expected extent of plastic deformation unless the option taken in IC Peel is used, in which a high fidelity direct fit of an empirical equation to the measured stress versus strain curve accurately tracks the extent of plasticity.

All the various methods used to circumvent the assumptions used in the calculation of G_{db} and the mathematical problem of subtracting two very large numbers to get an accurate value of G_c were found to be inadequate. Thus, the final conclusion from these studies was that

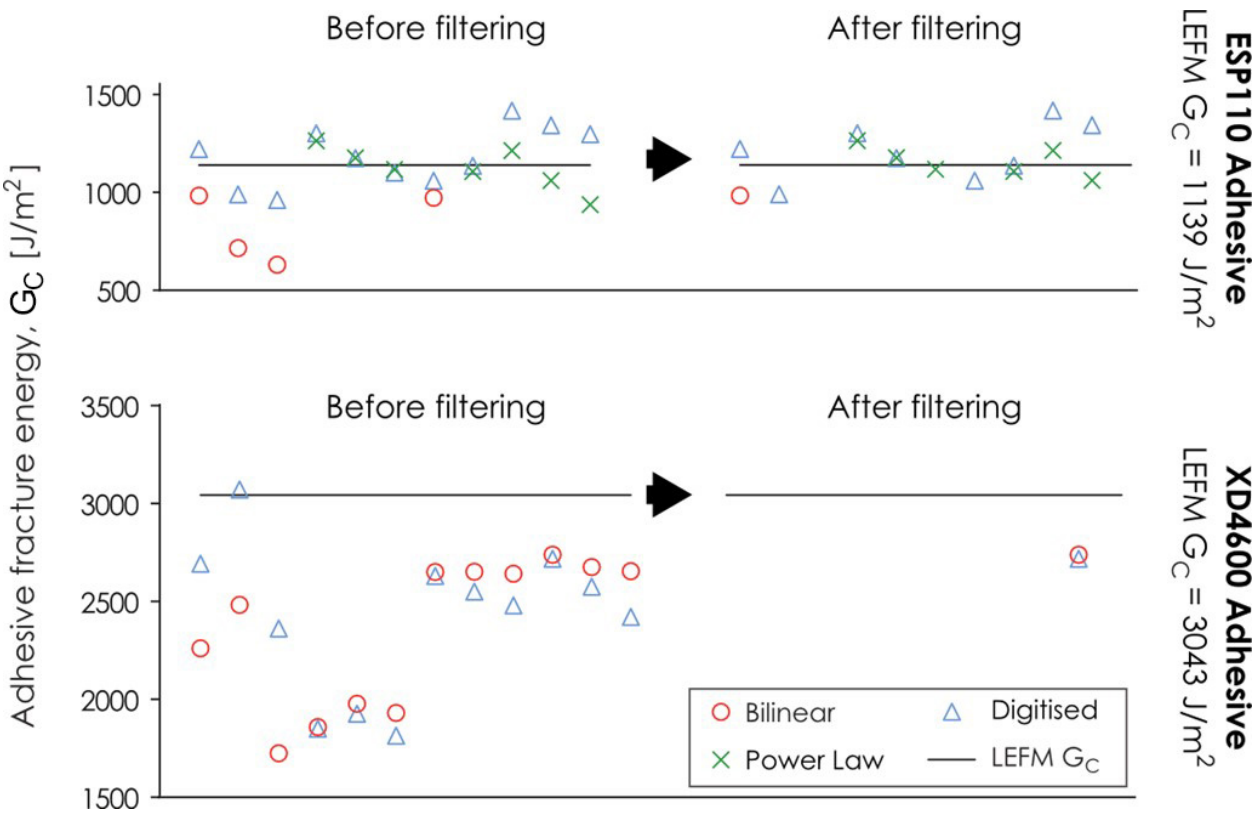

Figure 12: Toughened epoxy/aluminum-alloy arm 90° peel tests. Before filtering and after filtering the measured peel tests data by applying a rejection criterion. Namely, 'Reject data if $CF > 85\%$ OR $e_{max} > 4\%$', for the ESP110 adhesive (top) and the XD4600 adhesive (bottom). The values of G_c determined from standard linear-elastic fracture mechanics (LEFM) ISO 25217: 2009 tests, using DCB and the TDCB specimens, are also indicated. Failure was cohesive though the adhesive layer in all cases.

to ascertain an accurate value of the fracture energy, G_c, for such structural adhesive joints then it is usually far better to use the ISO Test Method (ISO 25217: 2009),[95] which employs the LEFM double-cantilever beam (DCB) or tapered double-cantilever beam (TDCB) test specimen, rather than any form of peel tests.

3.2.7 Peel diagrams and insights

Early studies of peeling involving elasto-plastic adherends include Spies'[5] theoretical framework for stresses within the bonded and debonded regions for thin metallic adherend peeling. Numerous researchers have built on this pioneering work for self-similar debonding, including Kim and colleagues,[22,23,86] Kinloch et al.,[24,88,95] and Moidu et al.,[96,97] and refinements to these approaches continue to be made.[98] Kim and Kim's formulation[23] allowed them to propose the Universal Peel Diagram (UPD), where the ordinate axis is $\bar{p} = (F_c/w)/G_c$, the ratio of the 90° peel energy, $\frac{F_c}{w}$, to the fracture energy of the adhesive, G_c. The abscissa is a nondimensionalized adherend thickness given by $\bar{t} = (t\sigma_y{}^2)/(6EG_c)$ where t, E, and σ_y are the adherend thickness, Young's modulus, and yield stress, respectively. A diagram of this

type had been suggested by Gent and Hamed.[56] The essence of such a diagram is understood by considering a fixed value of fracture energy of the peel joint and examining the effect of peel arm thickness. For example, at a given value of the fracture energy, a sufficiently thin peel arm will undergo complete plastic yielding after debonding. Because the total thickness is small, the dissipated energy will also be small. As the thickness increases, the amount of dissipated energy increases, increasing the apparent peel energy. However, when the thickness of the peel arm becomes sufficiently large, it becomes increasingly difficult to yield the arm in bending, decreasing the apparent peel energy. At a critical thickness, yielding no longer occurs and the peel energy is equal to the critical fracture energy, G_c. Thicknesses beyond this level would be sufficient to avoid yielding, as is typical in DCB tests.

Because of the relationships among these quantities and the peel force and fracture energy, Kim and Kim included a second set of guidelines/axes on the UPD as well, where an alternate nondimensionalized form of peel force, $\eta = 6EF_c/t\sigma_y^2$, and the fracture energy are plotted on orthogonal axes rotated with respect to the original coordinates, as shown in Figure 13a.[23] The axes create a space in which to plot experimental results or predicted behavior for self-similar peeling and then interpret in terms of the relevant parameters. They demonstrated their analysis by examining the influence of the thickness of copper/chromium films deposited onto silicon substrates with good agreement. Though subsequent studies do not often present their analysis in this form, we find that between the experimental results and the predictions, for example using IC Peel, produce a similar behavior (IC Peel[93] is a free-to-download software in the form of an Excel Spreadsheet which undertakes the calculations outlined in Sections 3.2.1 to 3.2.3, where the appropriate main equations are also given.).[24,88,95] Specific results using IC Peel[93] are shown in Figure 13b. Here, the predictions for aluminum and copper adherends of different thicknesses over a range of fracture energy values are presented in the UPD space. We observe that the resulting predictions do not result in a single curve, but rather a family of curves that depend on the specific nature of plastic hardening behavior of the adherend, the foundation stiffness, and the resulting root rotation at the peel front. We also show the limiting case of a thin peel arm with high Young's modulus and low yield strength (i.e. the analog of Kim and Kim's no hardening-rigid base case). The results here highlight that the apparent fracture energy given by F_c/w can vary significantly from G_c depending upon the material properties of the adherend (i.e. its Young's modulus and yield strength) as well as its thickness. Thus, the ratio of the "practical adhesion" (i.e. the measured peel energy, F_c/w) to the fracture energy, G_c can vary greatly from unity depending upon the amount of energy dissipated elsewhere within the system.

3.3 A review of Category III: Inelastic Not self-similar debonding

Category III behavior is perhaps the most challenging category to analyze as the complexities of both inelastic peel arm behavior and non-self-similar configuration are present. The intent of peel tests is to achieve the stable force for debonding associated with self-similar peeling and most analyses have rightfully focused on self-similar debonding, greatly simplifying the analysis by effectively moving a section with a known pre-existing stress state well ahead of the complex process zone into another (comparatively) easily modeled region in the wake of the process zone.[40] Analyzing the stored and dissipated energy states within these relatively simpler regions, along with input work to the system, allows one to evaluate the fracture

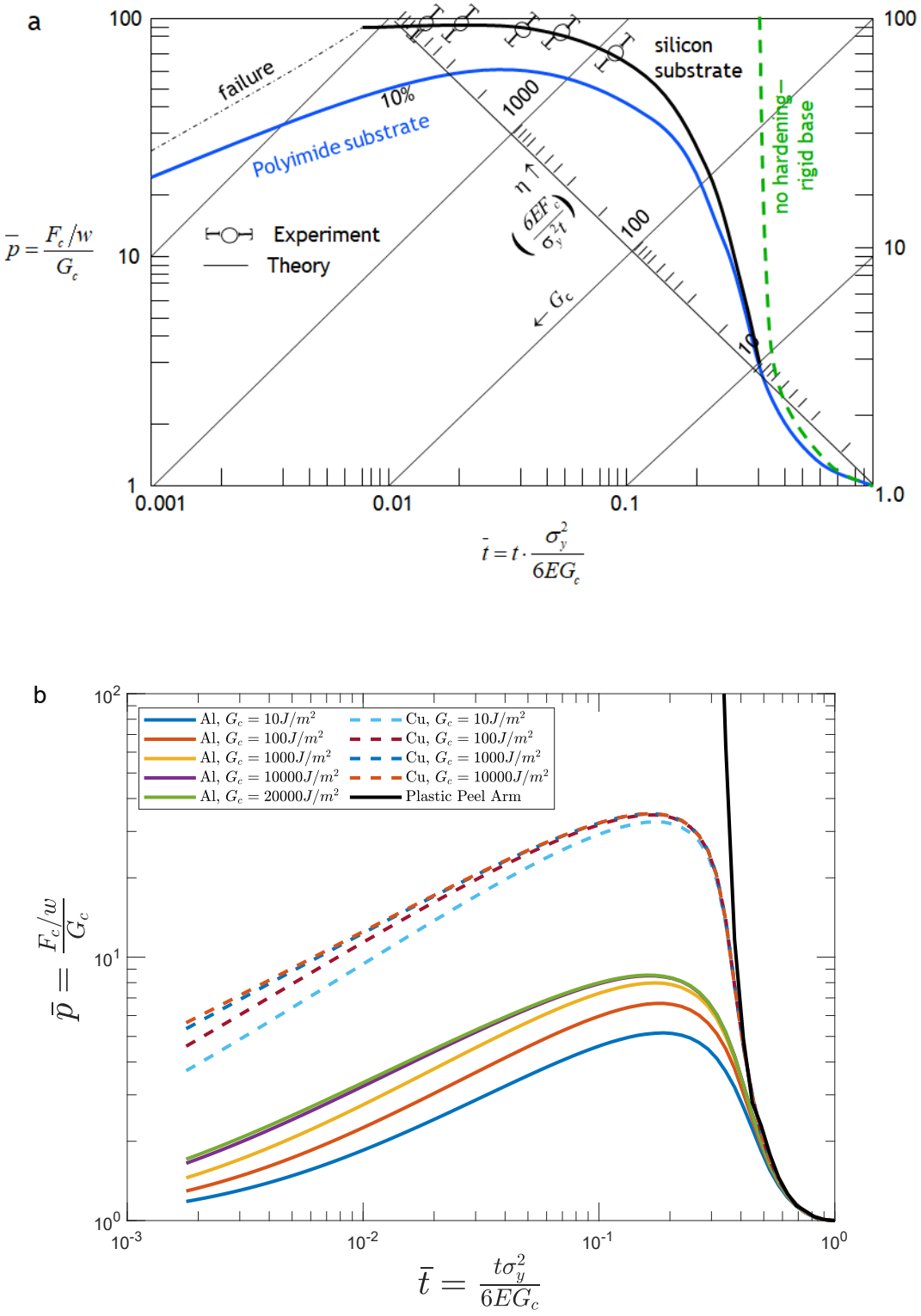

Figure 13: Universal Peel Diagrams. a) Representation of Kim and Kim's Universal Peel Diagram for soft copper film. Adapted with permission from Ref. 23. Copyright 1988, ASME. b) Universal Peel Diagram for aluminum and copper adherends of different thicknesses over range of fracture energy values calculated using IC Peel.[93]

process analytically. The approach to self-similar debonding is asymptotic, so there is no clear demarcation separating Category III from Category II behavior, though the latter typically results if peeling proceeds far enough in a sufficiently long bond. While analytical solutions for Category III are potentially possible, they undoubtedly would involve extensive computational efforts, so finite element analyses are the only known (to the authors) reports of addressing this category. In fact, if one wants to analyze Category II behavior, then finite element analyses typically start on an undeformed specimen, so naturally include the initial Category III behavior as well as the transition from Category III to Category II. When conducting practical peel tests, it is likely beneficial to plan or to conduct tests that move beyond this category into self-similar debonding regions, where Category II analysis methods are applicable. Nevertheless, recent efforts to reduce the bond length to save cost and test time can, however, result in specimens too short to achieve significant propagation within the self-similar plateau region of Category II. Additionally for the case of biological materials, it may be impossible to obtain larger samples. The necessary use of specimens which are too short to achieve significant propagation within the self-similar plateau region of Category II necessitates consideration of this category of behavior. Otherwise, erroneous interpretations of the resulting test data are almost certain to occur.

Examples of reported literature concerning Category III includes the finite element analysis of Yang et al.,[45,46] who considered debonding of T-peel specimens composed of 5754 Al adherends bonded with a commercial adhesive. In their finite element study, their embedded process zone (EPZ) parameters were calibrated with data from wedge tests to predict the results from T-peel tests with good quantitative agreement between the experimental and numerical results.[45] Yang and Thouless also considered asymmetric T-peel test configurations in exploring mode-mixity effects with their mode-dependent EPZ approach.[99] Li et al. conducted experimental and numerical modeling of T-peel specimens consisting of 1010 cold-rolled, electrogalvanized, and hot-dip galvanized steels as well as 6061 aluminum adherends of several thicknesses, bonded with two different commercial acrylic adhesives.[44] Using a cohesive zone model (CZM) in a commercial FEA code (ABAQUS), they obtained accurate predictions of the load-displacement behavior, the onset of self-similar debonding, and residual curvature following peeling. They also demonstrated that the load plateau is achieved when the distance from the line of action of the grips to the crack tip stabilizes, as shown in Figure 14. Furthermore, their work suggested that although ASTM D1876[12] recommended bond lengths of 230 mm would result in self-similar debonding for all the systems considered (except the cold-rolled steel), shorter specimens, such as the 100 mm bonds favored by some industries to expedite testing,[44] failed to achieve self-similar debonding for any significant length, thus precluding determination of meaningful peel properties using Category II approaches. For an example of such an analysis, Alfano et al.[100] considered the T-peel behavior of 6082-T6 aluminum-alloy with a commercial epoxy adhesive in which samples consisted of a bond length of only 45 mm. They tuned values of the cohesive strength and fracture energy until a good match between the experimental and simulated load-displacement curves was achieved. For the case in which self-similar behavior was not achieved, the tuned values of the fracture energy that spanned the range of the experimental data differed by more than a factor of two. There are also reports of so-called "coach peel" specimens (e.g. in the work of Yang et al.[101]) where the bond length is only 25 mm long – far too short to reach self-similar debonding for most automotive adhesive systems for which this specimen is used.

Thus, practitioners are cautioned about the use of shorter bond lengths and encouraged to consider longer bond lengths that ensure that self-similar debonding plateaus are clearly established to allow meaningful interpretation of results. Finally, of course, if a rising R-curve exists for the adhesive or interface used in the peel test, i.e. the value of the fracture energy, G_c, increases as the peel crack advances, then self-similar peeling will not be observed as defined for Category I and Category II behavior until after G_c has plateaued. (Such an R-curve may arise, for example, due to fibrillation increasing in extent across the peel front as the peel crack advances, see Section 7.2). The effect of the presence of an R-curve has been modeled in detail by Tvergaard and Hutchinson as a function of the extent of work hardening, the yield stress, the mode-mixity, etc.[102–105]

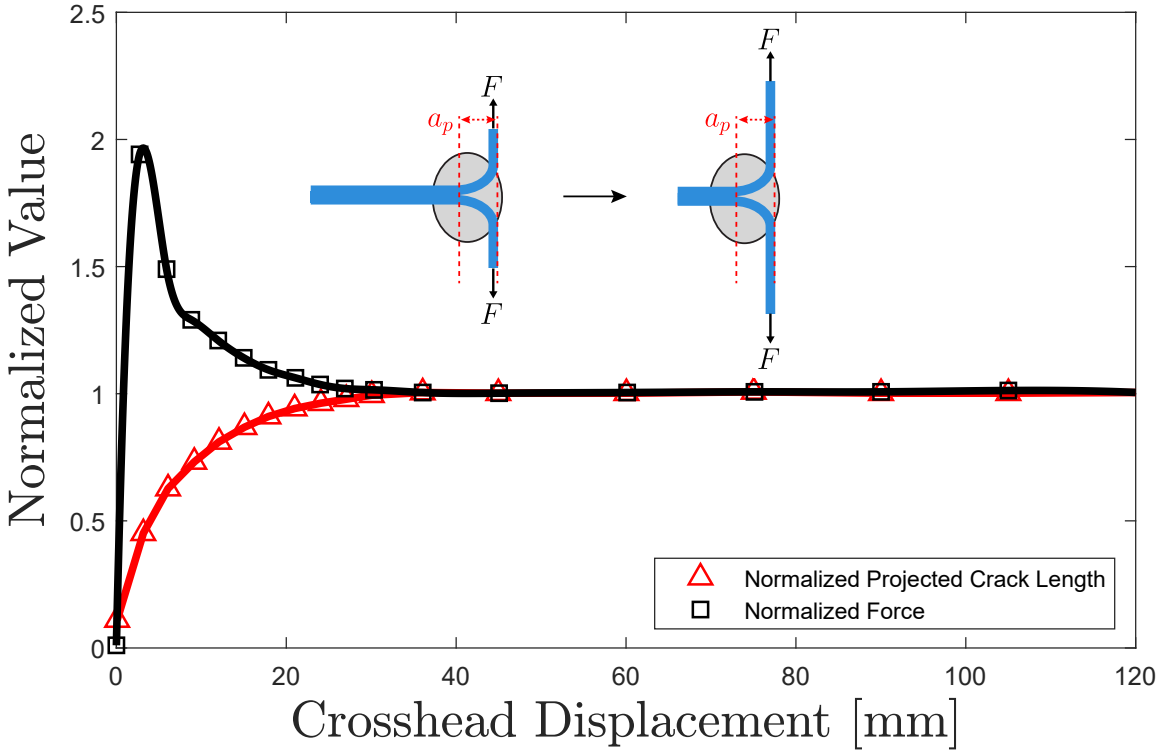

Figure 14: Steady-state debonding. Illustration of FEA results for 6061 aluminum-alloy adherends bonded with an acrylic adhesive showing that the predicted load plateaus when the projected crack length (a_p) stabilizes.[44]

Nevertheless, rather than relying on the simpler approaches of Categories I and II, it appears one can still extract meaningful fracture properties from Category III tests by using more involved numerical approaches. For example, peel tests sometimes involve the tabs being bent at 90° angles to facilitate gripping of 90° and T-peel specimens. This initial bend can significantly influence the non-self-similar behavior, as other portions of the specimen are typically flat. (In most finite element models, the plastic deformation history and strain hardening effect associated with this bending process is often not included. A notable exception is the work of Bruce and Holmqvist[106] who used 90° and 180° peel tests to study the behavior of adhesives used in packaging.) Perturbations then, such as the plastic bend, are

seen to delay the approach to self-similar debonding. The above tacitly assumes that the peel arm and intrinsic adhesion is uniform along the length, but any nonuniformity along the length can essentially reinitiate non-self-similar debonding until these nonuniform transition regions are well outside of the bending zone. Examples of this include: nonuniform or intermittent adhesion,[107] differential peel arm thicknesses,[108] and even switchable adhesion approaches to alter peel arm stiffness during a test.[25] Depending on whether the behavior is linear elastic or not and the magnitude of the fracture energy, such configurations could fall into either Category III or Category IV. One frequently encounters behavior which is stick-slip debonding, where debonding can proceed in a non-self-similar manner because the fracture resistance alternates between slow and rapid states, as discussed in detail in Section 5.5. In some cases, debonding will alternate back and forth across a brittle adhesive layer, inducing localized plastic hinges as the debond reinitiates at the opposite interface, as will be shown in Section 5.3.

3.4 A review of Category IV: Elastic Not self-similar debonding

At first glance, one might think that few peel test configurations fall into Category IV, where the peel arms remain elastic and yet self-similar debonding does not occur. In fact, this region would include many of the popular fracture tests including double cantilever beam (DCB) specimens. This category thus encompasses a vast array of test configurations that are often preferred for meaningful fracture evaluation, precisely because they avoid complications of inelastic behavior within the adherends. Relatively small deformations and slopes are often preferred, as they permit the use of Euler-Bernoulli beam approximations for the deforming arms, although corrections have been added to the ISO standard for DCB beams and in Imperial College spreadsheets for the DCB analysis.[109] In a sense, such tests do involve peeling (Mode I or mixed, depending on symmetry of specimen and loading), though such tests are seldom considered to be peel tests *per se*.

Although uncommon, examples of Category IV behavior can be seen for classic peel configurations, such as illustrated by cold-rolled steel adherends bonded with an epoxy in a T-peel configuration.[44] The combination of high yield strength adherends, coupled with what was likely weaker adhesion in their experiments, prevented yielding, meaning that the adherends remained elastic and the distance between the grip axis and debond tip continued to increase as the crack tip progressed along the specimen. If the tabs are fully gripped and the ends can be considered encastred, the resulting energy release rate is given by:[110]

$$G = \frac{F^2 a^2}{4wEI} \tag{3.23}$$

where I is the second moment of area of the adherends (here assumed symmetric.) This G value is just one quarter that of the simple beam theory result for a DCB specimen subjected a given load level.

3.5 Evolution of peel category during peeling

As discussed in Li et al.,[44] specimens undergoing peeling often move from one category to another as debonding proceeds. Initially, at sufficiently short debond lengths, nearly all but

the most flexible or poorly adhered peel specimens are likely non-self-similar. If the bonded region is sufficiently long and peeling proceeds far enough, most will eventually approach a self-similar configuration, where most of the analytical analyses are of use.

3.5.1 Initiation

Although the focus of peel testing is often directed at self-similar configurations, all peel tests must begin with initiation. For thin, flexible, and elastic materials, the end(s) of bonded flat strip(s) may be easily bent to allow testing in a load frame. For other systems, however, the end must be bent with plastic deformation occurring to permit alignment for testing. Often induced after bonding, the bend is typically very near the end of the adhesive bond, invariably leading to non-self-similar propagation for at least a portion of the test. Although standards and most practitioners avoid including the first portions of the load-displacement response in their calculations, others have been known to record and use the peak force for their purposes. Some analysis efforts have been devoted to understanding the peak force in T-peel configurations, for example, as a function of bend angle, spew details, and bend radius for automotive applications,[58] where T-peel configurations may be used for panel-bonding applications. Geometric details such as these will affect the applied moment, stress gradients, and resulting initiation load. The lack of a sharp crack tip can be due, for example, to a relatively thick release film of poly(tetrafluoroethylene) being used to start the peel crack. The aim of the peel test is to measure the peel force associated with a relatively sharp, naturally-occurring crack in the joint.

One of the challenges with any fracture test is introducing an appropriate initial flaw. When intentionally bonding specimens for peel testing, one can often leave portions of the peel arm(s) unbonded by limiting the extent of the adhesive application or using a release agent or bond breaker. This can be immensely more difficult if one is simply pulling a laminate off of the production line for manufacturing processes that have been optimized to achieve consistently good adhesion with minimal flaws. Some have found success by dipping an end of specimens in water or other liquids to weaken an interface, or by bonding auxiliary tabs on peel arm(s) to initiate debonding, resulting in "handles" to grip specimens for peel testing. This has worked well in some laminated systems, though inducing fracture at the desired interface in multi-layer systems remains a challenge, though mode-mixity concepts have been attempted with some success, see Sections 5.2 and 5.3

Alignment and adhesive spew which are not always consistent from one bond to the next, have been shown to have a substantial effect on this peak force.[58,111] The evolution of moment arm, measured from the line of action of the applied forces to the debond tip, for example in a T-peel specimen, often starts out quite short and steadily grows until self-similar debonding may be achieved, as shown in Figure 14. Clearly, the initially shorter moment arms may necessitate a larger force for initiation, and this may continue well after a natural crack develops.[44] This portion of the peel force versus displacement traces should not be used with Category I or II analyses methods. This includes debonding near the plastically bent end-tabs, where plastic bending, reverse bending, and other complications would be inconsistent with model assumptions.

3.5.2 Transition to self-similar peeling

Following initiation, there may be an extensive transition region in which the force required to propagate the debond typically drops. The transition is associated with multiple phenomena, including establishing a stable, self-similar process zone involving both adhesive damage region and local adherend plasticity. In addition, the initial bend and specific curvatures induced earlier in the peeling process move further away from the growing crack tip and process zone. Becoming more remote, their lingering influence decreases as the specimen transitions to Category II. Increasing the adherend modulus and decreasing the yield strength tend to shorten this transition region. The transition region does not lend itself easily to analytical methods, though finite element analyses have been used to address this complex behavior, as noted earlier, including for bonds too short to achieve self-similar peeling and the range of behaviors as length and properties change.[44–46,99,112–114] As confirmed in Figure 14, development of a plateau in the load versus displacement behavior coincides with a fixed distance from the line of action of the grips to the crack tip for T-peel configurations.[44]

3.5.3 Short beam and terminal behavior

The bulk of peel analysis literature has, perhaps rightfully, focused on self-similar debonding, and the transitions from initiation to this region have been described above. One additional complication can arise, however, if the debond approaches the bond terminus, as the remaining bond enters the short beam realm, defined as $3\pi/2$ times the characteristic beam on elastic foundation length.[115] As the growing debond approaches the end of the bond, additional compliance alters the available energy release rate and can return the terminal debonding to non-self-similar behavior. Such phenomena were recently analyzed by Plaut et al. for both a Winkler beam on elastic foundation[116] and for the 6^{th} order plate on elastomeric foundation formulations,[11,117–119] revealing instabilities that lead to rapid debonding and separation.

4 Additional peel geometries and test methods

4.1 Shallow angle geometries

Shallow peel angle configurations offer some advantages for simplifying testing, reducing peel arm plasticity, and resulting in practical work of adhesion values that better approximate the fracture energy.[97] Although mentioned earlier, it is worth commenting on the 0° peel test. For common peel specimens consisting of a flexible peel arm bonded to a rigid substrate, testing specimens at angles between 0° and 180° often requires free hanging weights, a translating peel carriage, or a bisected angle configuration where the specimen translates at an angle to the applied force. For both 0° and 180° peeling, conventional load frames can be used without special fixtures, making them especially common tests. The 0° peel does not involve the large-scale adherend bending and deflections common to most other peel specimens. This geometry is widely employed in assessing time-dependent failures of pressure sensitive adhesive tapes by suspending a mass from a bond of given area and measuring the time to failure, often at controlled temperature and humidity levels; these tests for PSAs are often

referred to as shear holding power or static shear tests rather than peel tests, *per se*, as the propagation lengths are often quite short. Concerns for this geometry have been raised for adhesives that can reattach, adding some further complications.

Applications of 0° peel to structural bonds using the cracked lap shear (CLS) test[120] are popular because they enable simple load-frame testing, an attribute that has led to their use, especially for fatigue assessment of aerospace adhesives.[121] Mode-mixity of Brussat's strap and lap configuration can be varied slightly from approximately $G_{II} : G_I :: 4 : 3$ for symmetric adherend by altering their relative stiffness. Numerical and analytical analyses have suggested modest variations from the constant energy release rate and mode-mix ideals for realistic geometries.[121–123] This combination of shear and opening mode fracture offered the additional benefit of relevance to aerospace joints, where considerable effort is given to minimize peel-dominated loading through design.[124,125] Extensions of this geometry have also been made to coating adhesion measurements, in the form of the notched coating adhesion test (NCA),[126–128] though here the more massive substrate may experience extensive plastic elongation before stored energy in the severed coating is sufficient to induce debonding. Energy for debonding can also be supplied by residual stress in the adherend (e.g. Ref. 40) or through that of a superlayer, as discussed in detail by Yu and Hutchinson for epoxy layers with a nickel superlayer.[129] For a given residual stress state, spontaneous debonding can occur when the coating exceeds a critical thickness, though debonding from a circular hole has been proposed to assess fracture energy for such cases.[130]

An interesting shallow-angle peel test was proposed by Gent and Kaang as the pull-off test,[131] though similar embodiments have been referred to the V-peel and strip blister (Figure 15a).[132,133] Gent and Kaang formulated this as a simple out-of-plane stretching analysis assuming an initially just-taut but stress-free state, leading to the classic solution that the central deflection at given debond length results from elastic stretching of the debonded adherends and is proportional to the cube root of the applied central force.[131] Assuming the fracture energy is independent of debond length, the angle of peeling remains constant and the applied energy release rate is given by:

$$G = \frac{3}{8}\frac{F\theta}{w} \tag{4.1}$$

Liechti et al. have performed interferometric and numerical analyses of this geometry (aka strip blister) epoxy/glass bonds[134] and elastomer/steel bonds,[135] the latter of which were extensively used for cathodic delamination studies.[136] Extensions of the pull-off test have also addressed the (aka V-peel) bending-stretching transition,[132] and 3-D aspects of debond initiation.[137]

As with the pull-off test, blister tests also offer low angle peel opportunities, and have been used extensively in electronics, thin-film coatings, and MEMS.[138–141] Beginning with the work of Dannenberg[142,143] who measured paint adhesion by pressurization of a suspended coating, allowing paint to debond and expand into a linear, shallow groove, a variety of blister test configurations have been proposed and used. One advantage of blister tests is that they offer gentle ways to introduce loads into the peeled adherend, thus facilitating debonding of more fragile materials.[144] Perhaps the most common blister configuration is the circular blister (Figure 15b) proposed by Williams[145] where bending stiffness dominates, or the blow-off test,[146] where membrane stretching stiffness dominates. Williams has sum-

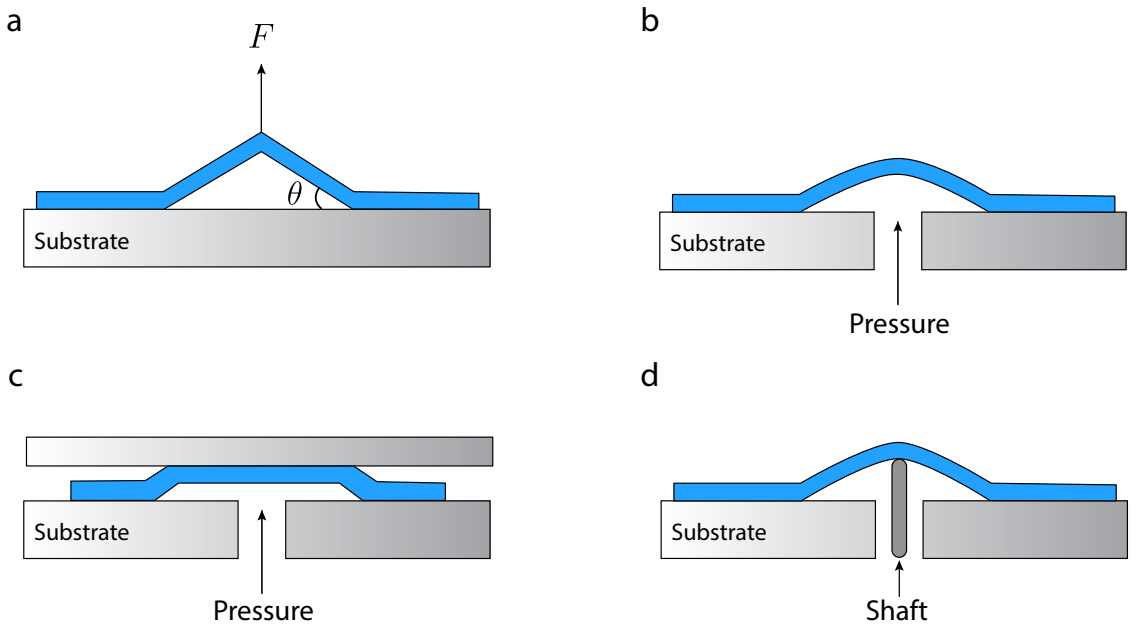

Figure 15: Additional peel geometries. a) Pull-off geometry. b) Axisymmetric blister geometry. c) Constrained blister geometry. d) Axisymmetric shaft-loaded blister geometry. Source: ©M.D. Bartlett et al., CC BY-SA 4.0. Available at http://hdl.handle.net/10919/113716.

marized relations for energy release rates for a variety of peel and blister tests.[147] Extensions of these to bridge bending and stretching domains and including residual stresses have been made.[148,149] Other blister configurations have been suggested, including the island,[150,151] constrained[152,153] (Figure 15c), and peninsula[154–156] blister configurations, the latter two of which nominally allow for constant applied energy release rate peeling at a fixed pressure. Although pressurizing blister specimens has advantages, pressurization equipment is less common than axial load frames, so the shaft-loaded blister has also received interest (Figure 15d),[157] and can be conducted in universal test frames or even dynamic mechanical analyzers (DMA) for PSAs.[158]

4.2 Floating roller, climbing drum, mandrel peel

The presence of a roller or drum in the floating roller[159] and climbing drum[160] tests can supposedly limit the curvature as the adherend is debonded, thereby reducing or even eliminating plastic bending (Figure 16a,b). Such methods had proven successful for eliminating plastic bending and providing consistent work of debonding measurements for Gent and Hamed,[56] but they supplied sufficient force at an appropriate angle to ensure that the peeled adherend appeared to remain in contact with the roller. As the value of G_c increases, greater forces on the roller are required to prevent the adherend from lifting off the roller in the vicinity of the propagating debond. (Large peel stresses at the debond tip act normal to the roller surface, providing a very strong lifting action off the roller.) Because the floating roller and

climbing drum tests, as practiced, may not apply sufficient force for the roller to maintain contact, there can be localized regions with higher curvatures and greater possibility of plastic bending. Indeed, higher values of fracture energy will inevitably require greater bending moments, and these can exceed the plastic limit of the adherend. To address this limitation, Kawashita et al.,[161] following the concepts of Gent and Hamed,[56] introduced the mandrel peel test in which an opposing force is imposed on the carriage in an attempt to cause the adherend to conform to the mandrel and limit plastic bending and energy dissipation (Figure 16c). This method shows promise, though it will be limited such that combinations of bending and tensile stresses remain below the yield strength of the peel arm. They went on to further evaluate and use this method.[162,163]

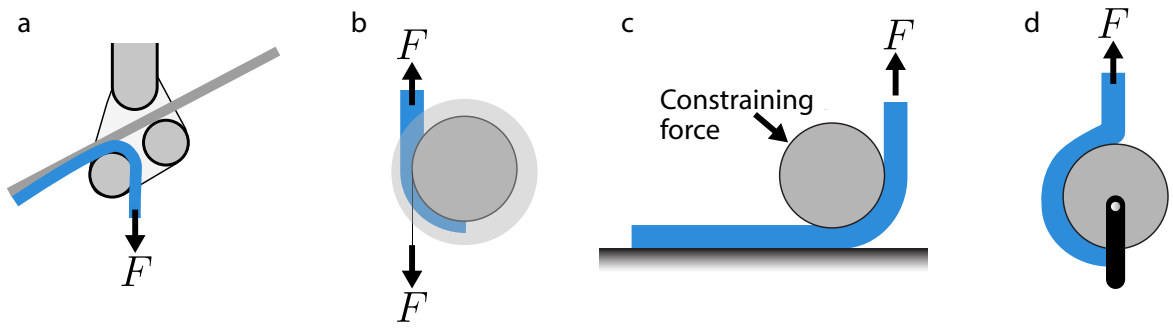

Figure 16: Roller and wheel peel geometries. a) Floating roller. b) Climbing drum. c) Mandrel peel. d) German wheel peel. Source: Schematics ©M.D. Bartlett et al., CC BY-SA 4.0. Available at http://hdl.handle.net/10919/113716.

Another circular peel configuration involves peeling a bonded layer from a rotating wheel, essentially in a 90° manner. This is distinct from the above mandrel methods since a roller is not used to nominally limit the curvature of the peel arm. The German wheel, such as used by Spies in his seminal paper,[5] allows constant 90° degree peel tests to be performed in a universal load frame without the need for a carriage system to translate the specimen (Figure 16d). The German wheel was once a popular test method for characterizing interlayer adhesion in flexible electronic laminates, though relevant standards have now been withdrawn (e.g. ASTM D5109, German Standard DIN 53357). As with the lift-off issue for roller peel tests described above, lifting of the bonded laminate away from the wheel can alter the peel angle, leading to modifications of this method by bonding the laminate to the wheel with a PSA tape, or, for tougher systems, bonding the laminate to be tested to a sacrificial metal strip using a tough epoxy adhesive, where the sacrificial strip is then screwed to the wheel to facilitate testing of multiple specimens.[65,164]

4.3 Wedge peel

Peel tests have been widely employed for aerospace and automotive adhesive characterization for several reasons, including that they are often deemed appropriate for testing light gauge stock that is common in these weight-critical products. Although many peel methods have been used, including those discussed earlier herein, two wedge peel test methods are discussed

here, and both typically induce large-scale adherend plasticity in well-formed bonds with tough adhesives.

4.3.1 Wedge-induced curvature measurements

Thouless, Ward, and colleagues developed a test where a drop hammer drives a bonded specimen over a wedge, a process that induces considerable plastic bending of the adherends for relevant adhesive systems.[20] The fracture energy of the bond was then extracted by analyzing the permanent plastic curvature of the adherends in the wake of the wedge. In most peel tests involving plastic adherend bending, portions of induced plastic bending are reversed as a point on the adherend moves from debond tip to the often straightened region of the debonded adherend, as shown in Figure 10, an additional dissipation process that can be quite pronounced, though is mitigated by low modulus and high yield strength adherends. Their method is unique in that adherends remain unloaded in the wake of the wedge, thus preserving the initial plastic bending. By using an appropriate elastic-plastic constitutive model, they could extract the fracture energy of the bond from this remaining and unperturbed curvature. Such approaches may not be appropriate for other peel geometries due to the likelihood for reverse plastic bending occurring in adherends that remain under load following peeling, as happens in many standard tests. The analysis of such specimens is discussed further in Section 4.3.2 below.

4.3.2 Impact wedge peel

The use of structural adhesives in industry is increasing steadily in the automotive industry as car manufacturers have become aware of the advantages that adhesives can offer, compared with conventional joining techniques, in the assembly of engineering components and structures, especially when very dissimilar materials need to be joined. However, the toughness of an adhesive joint may decrease considerably under impact-loading conditions. This arises because adhesives are polymeric materials that exhibit plastic and viscoelastic deformations, and thus their fracture behavior may be very dependent upon the rate of loading and the test temperature. Hence, for applications such as in the automotive industry, for example, where adhesives are being used increasingly in safety-critical areas, it is necessary to evaluate any possible decrease in performance that may occur when the adhesively-bonded joints are subjected to impact loading. The needs of the automotive industry led to the development of an International Standard Organisation (ISO) method that is termed the impact wedge-peel (IWP) test, which measures the resistance to cleavage fracture of structural adhesives at higher rates than most other adhesive bond tests are performed.[165] The IWP test specimen is shown in Figure 17.

The wedge, made from hardened steel, is drawn through the bonded joint, in the form of a "bonded tuning fork," at a relatively high test-rate of 2 to 3 m/s using a high-rate or an impact test machine (Figure 17). The average cleavage force is measured via an appropriately placed piezoelectric transducer, for example, providing quantitative results . Two important and interlinked prerequisites are required for demonstrating significant impact resistance.[166] First, that stable crack growth occurs in the adhesive layer, with the crack propagating at about the same velocity as is being applied to the wedge. (Rather than unstable crack

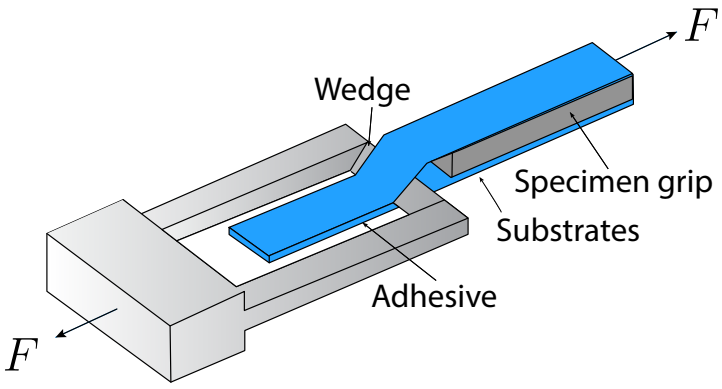

Figure 17: Impact wedge-peel. An additional peel geometry where a wedge is used to drive peeling. Source: ©M.D. Bartlett et al., CC BY-SA 4.0. Available at http://hdl.handle.net/10919/113716.

growth with the crack propagating at a velocity far greater than that of the wedge). Second, and very importantly, that significant plastic deformation of the substrate arms occurs, since this will greatly increase the cleavage force, and energy, needed to separate the arms. Thus, desirable performance involves very substantial plastic deformation of the substrate arms, which mimics the required controlled plastic collapse of the metal in a bonded (safety) crush zone in the front-end and rear-end of a car. (Obviously, in a successful IWP test result, the overall energy absorbed by the thin adhesive layer will be relatively insignificant compared to the energy absorbed by the plastic collapse of the surrounding metal. The vital role of the adhesive is to not fracture until such plastic collapse of the surrounding metal has fully occurred.)

Now, the value of the fracture energy, G_c, cannot be readily obtained from the IWP test. This is due to the problem of accurately estimating the energy dissipated, G_{db}, per unit area of crack growth during bending of the peel arms near the peel front, as discussed in Section 3.2.6. Further, there is the problem in determining the contribution from the energy absorbed due to friction between the wedge contact point and the substrate or fractured surface of the adhesive. Notwithstanding this, Blackman et al. have shown, when the locus of joint failure is cohesive through the adhesive layer, that there is a direct correlation between the measured wedge cleavage force and the fracture energy, G_c, of the adhesive, where the value of G_c was determined using a LEFM approach via the DCB or TDCB specimen.[166] They identified that a linear correlation existed between the IWP cleavage-force and the fracture energy, G_c. The gradient of this correlation was dependent on the properties of the substrate material used. However, the relationship between the IWP cleavage force and the fracture energy, G_c, did not pass through the origin of the graph. Instead, a limiting value of G_c was observed, which represented a lower limit. Below this limiting value of G_c, the toughness of the adhesive was inadequate to enable sufficiently high stresses to be developed in the substrates to give rise to extensive plastic deformation of the arms of the substrate. Hence, unstable crack growth was seen in the IWP test specimen and a zero value of the wedge cleavage force was recorded. In contrast, for adhesives with G_c values above this limiting value, extensive plastic deformation of the arms of the substrates did occur, and stable crack

propagation was observed in the IWP test. For such tests, relatively high values of the cleavage force were recorded. This limiting value of G_c was dependent of the properties on the substrate material used.

As stated in Section 4.3.1, Thouless et al. published a very interesting paper on a wedge peel test for measuring the fracture energy, G_c, from two bonded flat substrates which are split apart by driving a wedge through the bonded peel joint.[20] They derived an analytical equation relating the value of G_c to the measured radius of curvature after the test had been completed, assuming a power-law relationship for the plastic deformation behavior of the substrates. However, as the authors commented, their calculated values of G_c were about a factor of two lower than previously published values, and the results from the aluminum and steel substrates differed considerably, although cohesive failure in the adhesive layer was observed in both cases. Such discrepancies may be explained from earlier work on peel tests by Kinloch et al., who showed the importance of including the effects of root rotation at the peel front.[24] Indeed, when such a correction was applied to the original Thouless et al. analysis the recorded discrepancies essentially disappeared.[20,167]

On the other hand, Martiny et al. have undertaken quasi-static tests on a similar peel test to the above but where they forced a wedge, at a relatively slow quasi-static velocity, through two bonded, flat substrates forming a peel test.[168–170] Following earlier work,[171] and in a similar manner to later work by Geers et al.,[172,173] they developed a relatively sophisticated model that used a FEA approach with a single CZM which possessed zero height and had material parameters which defined the shape and size of the CZM.[168,169] The local fracture process was simulated by this cohesive zone and the local energy plastic dissipation in the adhesive, ahead of the crack front, was accounted for by embedding the CZM between layers of elastic-plastic solid elements which represented the adhesive layer. A main feature of the model was that the values of the material parameters for the CZM zone, for a given adhesive, were held constant throughout the various modeling studies. This approach was successful when a relatively brittle adhesive was used but gave poor agreement with the experimental results when a relatively tough adhesive was employed. Thus, they turned to the idea of using a two-parameter failure criterion based upon the attainment of a critical value of the (macroscopic) maximum principal stress, σ_c, at a critical distance, r_c, ahead of the crack tip.[170] This failure criterion, proposed by Ritchie et al.[174] in the context of cleavage fracture in steel, has often since been used for very different applications and materials (e.g. [175–178]). The key feature of this failure criterion is the introduction of a characteristic length which, in principle, is connected to the microstructure and damage phenomena. The advantage of this model was that it did not *a priori* partition the fracture energy between an "inner" energy dissipated in a cohesive zone and a "far-field" energy-term dissipated in the surrounding plastic zone(s). Indeed, such an arbitrary statement of the fracture process zones, their dimensions, and associated energies, can be difficult to define and justify in polymers. The material parameters were identified for three different structural, epoxy-based adhesive systems which showed very different values of their fracture energies, G_c, spanning the range of about 200 to 6500 J/m^2. It was found that the critical stress was related to the principal stress that was needed to debond, or cleave, second-phase filler particles present in the adhesive formulations, and so initiate a void or micro-crack that would cause crack propagation. The order of magnitude of the critical distances was linked, with the help of micrographs of the fracture surfaces, to the average size and/or spacing

of the second-phase particles in the adhesive. The numerical predictions were in excellent agreement with the experimental data, using constant values of the material parameters, σ_c and r_c, for a given adhesive. This observation was valid over a very wide range of thicknesses of the adhesive layer between 0.1 and 1.0 mm and for two very different test configurations, namely the LEFM TDCB test and the EPFM wedge-peel test.

5 Additional peel test parameters - Issues and phenomena

5.1 Peel strength versus peeling energy metrics

Most peel test standards, such as ASTM D1876, focus on self-similar debonding scenarios (Categories I and II), where plateaus are reached in the debonding process. As practitioners vary the adherend and adhesive materials and dimensions, such debonding is not guaranteed. For example, some industries have pushed for shorter bond lengths to reduce material consumption and facilitate testing without realizing that such changes may preclude them from achieving the self-similar debonding intended. We have discussed the "peel strength" and fracture energy metrics and their relationships based on the peel configuration. Most specimens tested will have an initial peak load as debonding initiates, though this is a less commonly used metric, for reasons previously cited. For Category III and IV debonding, the force fails to reach a plateau (to varying extents), introducing a significant risk that any average load level used will be higher than the plateaus for which equations, presented for Category I and II debonding above, are intended, thus invalidating such analyses. Figure 18 illustrates how using different metrics can impact interpretation from data included in Refs. 44 and 110 for LORD 406 acrylic adhesive T-peel samples involving hot dipped galvanized (HDG) and cold-rolled (CRS) steels as well as an aluminum alloy (Al) as adherends. The load trace plateau is clearly established for the ductile HDG system. The aluminum-alloy specimen is transitioning from Category III to Category II, with a plateau barely being reached. Although the CRS peel test might appear to have reached a plateau, the specimen exhibited no plasticity and a very low displacement at break; in fact self-similar debonding was never achieved so this fell into Category IV. Also shown are comparisons, normalized to the respective HDG values, for displacement at break, peak force, "T-peel strength" as might be reported on the basis of standards, and the mechanical energy input per unit area of debonding, the apparent fracture energy. The CRS specimen resulted in non-negligible fractions of HDG metrics (35% of peak force and 21% of plateau force or "peel strength,") yet only 3% as much energy per unit area to debond! Clearly, one's choice of metric is important, and "peel strength", as recommended by the standards, only reflects one aspect of the capability to prevent debond propagation, as it fails to capture crosshead displacement. We note that because the "T-peel strength" only depends on average force and ignores displacement, it misses the important contribution of distance traveled to energy input and dissipation.

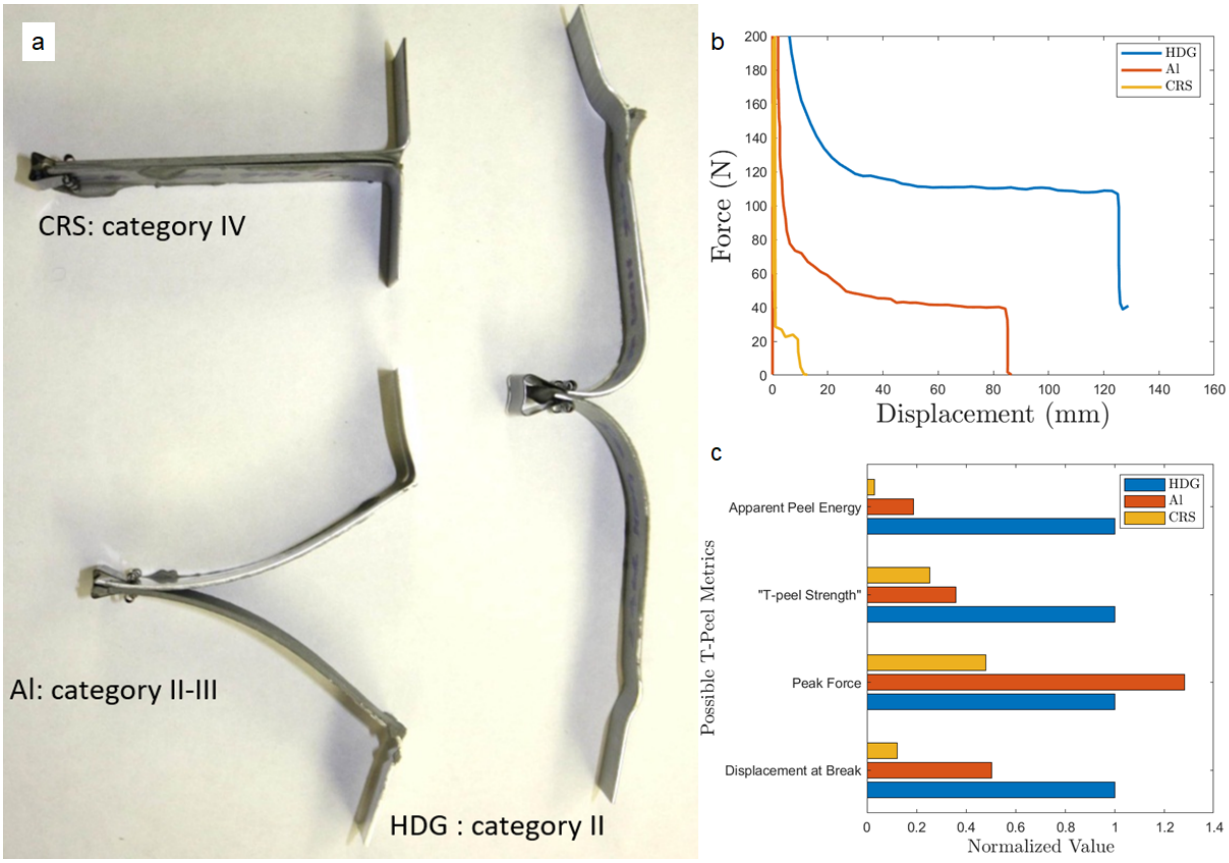

Figure 18: T-peel examples and metrics. Results for LORD 406 acrylic adhesive T-peel samples involving hot dipped galvanized (HDG) and cold-rolled steels (CRS) as well as an aluminum alloy (Al) as adherends. a) Images of three representative T-peel specimens, clipped together after failure. Note the various categories for the resulting geometries involving the same adhesive: Category IV for CRS adherends debonding at interface and resulting in low adhesion values, Category II to III transition for Al adherends debonding cohesively and resulting in intermediate adhesion values, and Category II for HDG adherends debonding cohesively and resulting in high adhesion values. b) Representative load traces; and c) Comparison of several T-peel metrics, normalized by the value for representative hot dipped galvanized (HDG) adherend results. Adapted with permission from Ref. 110, Copyright 2012, John Wiley & Sons.

5.2 Mode-mixity implications

5.2.1 The concept of mode-mixity

Taking on special significance for cracking in layered materials, where fracture processes may be constrained to grow at an interface or within an adhesive layer, the topic of fracture mode-mixity has been widely studied by proponents as well as those questioning its validity and general applicability, especially in tough and/or layered systems. In fracture-mechanics terminology, a crack tip may be loaded by, and potentially propagate in, one of three modes, or some combination of these. There are two in-plane scenarios: Mode I (an opening tensile)

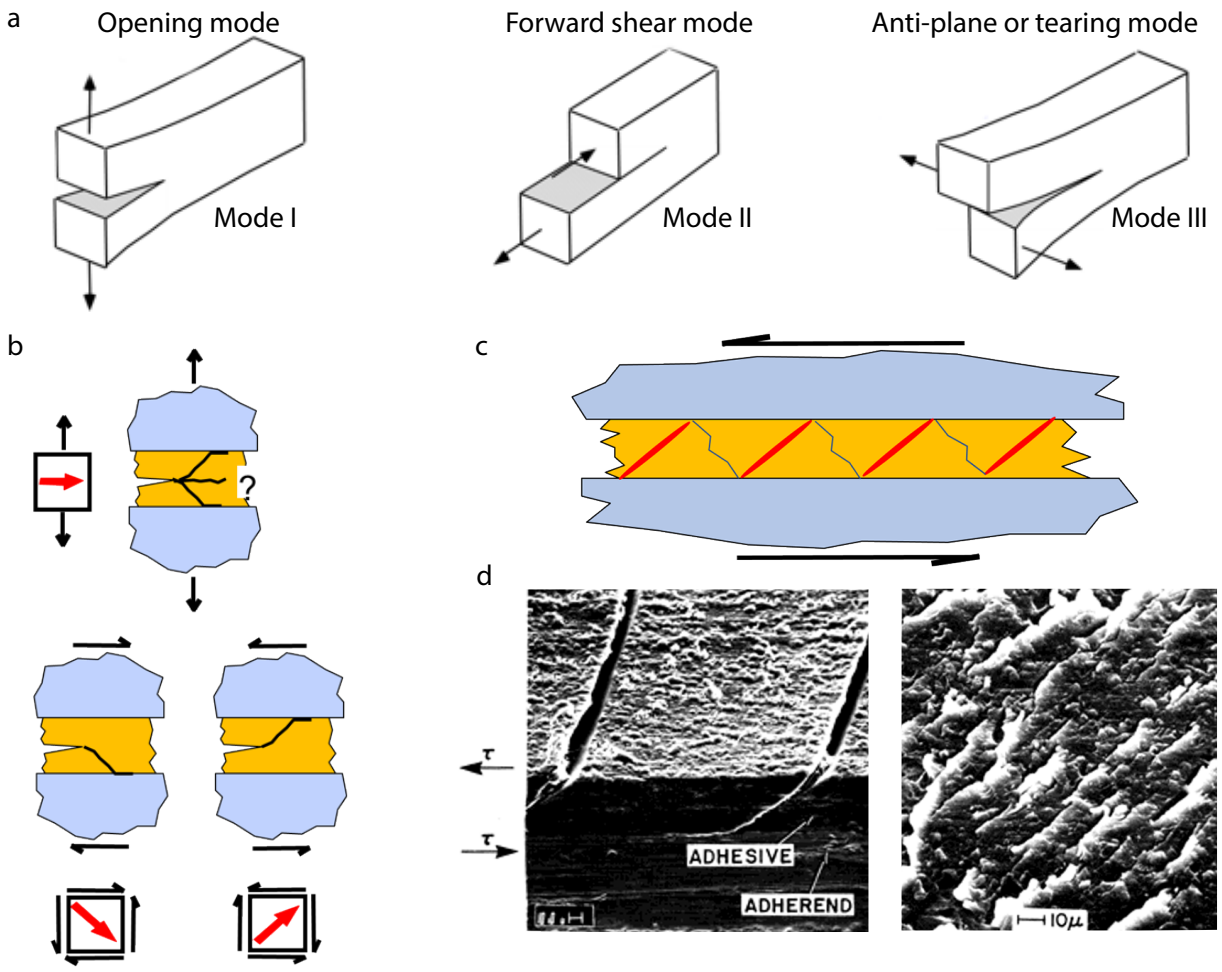

Figure 19: Fracture modes and their influence on failures. a) Illustration of the two in-plane fracture Modes (I and II) and of Mode III. b) Illustration of the effect of in-plane shear mode application to a bonded joint. Though there is no tendency for Mode I, the sign of the shear for Mode II can direct the growing crack to grow perpendicular to the largest tensile stress, towards the lower or upper adherend. Adapted with permission from Ref. 179, Copyright 2005, Wiley. c) Illustration of hackle patterns (for rightmost figure in b)) showing growth of the initial Mode I cracks (red) growing perpendicular to largest tensile stress and subsequent tearing to connect the mode I cracks, thereby severing material along the length of the bond. d) Micrographs of hackle patterns observed in bonded joints loaded in Mode II manner. Adapted with permission from Ref. 180, Copyright 1988, Springer.

and Mode II (an in-plane shear), and an out-of-plane tearing Mode III as shown in Figure 19a. The distinction between friction (as studied in tribology) and peel experiments in Mode II crack propagation (shear) becomes somewhat blurred for weak adhesives based on reversible van der Waals bonds. However, for practical adhesive systems, the energy in Mode II crack propagation is largely driven by dissipation and becomes distinct from friction alone. The two in-plane modes are widely considered for plane problems, and are the focus herein for their potential relevance to known peel geometries.

For cracks in monolithic systems when LEFM is applicable, in-plane loading results in specific stress fields surrounding crack tips[181] and mode-mixity can be unambiguously determined.[68] This mode-mixity can be expressed in several ways, including the commonly used "phase angle," defined as:

$$\psi = tan^{-1}[K_{II}/K_I] = tan^{-1}[\sqrt{G_{II}/G_I}] \tag{5.1}$$

where the components of the applied energy release rate are G_I and G_{II}, the sum of which is the total applied energy release rate, G, which can also be designated as the mixed-mode applied energy release rate, $G_{I/II}$. K_I and K_{II} are the corresponding components of the related applied stress intensity factor. One can use analytical or numerical methods to determine the K components from the stress field within the K-dominated region,[68,182] or equivalently, the G components based on opening and tangential tractions and displacements near the crack tip.[183,184]

5.2.2 Relevance of mode-mixity to peeling in bonded systems

The applicability of fracture modes and mode-mixity concepts for bonded or laminated systems revolves around several important questions, and these issues are discussed in more detail below.

1. *Is there such a thing as Mode II fracture, as fracture seldom occurs on a planar surface as shown in Figure 19a in an adhesive bond when Mode II loading is applied?* In reality, shear loading often results in tortuous fracture paths (e.g. hackle patterns shown in Figure 19c,d[180]), potentially leading to impingement, frictional dissipation, smearing of protruding features, etc.

2. *If mode-mixity is important, can the applied energy release rate be accurately partitioned into the various modes?* Mode-mixities are often defined in terms of the stresses in the small, near-field, singularity-dominated region ahead of a crack in an elastic material, yet failures of many practical adhesive bonds involve very large-scale plasticity in the adhesive and, especially with peel specimens, the adherends themselves. If this plastic deformation zone is larger than the singularity-dominated region, can mode-mixity even be defined?[185,186]

3. *Does the fracture mode affect the measured fracture energy G_c?* Some have argued that it does not, but that a consistent amount of energy per unit area is required to create a fracture surface, regardless of the applied loading mode.[187] However, the experimental evidence often shows that G_c often increases when a higher Mode II loading component is applied. Plasticity, friction, and other phenomena can increase the measured fracture energy, G_c, required in the shearing loading modes, as has been observed for a wide range of bonded material systems.[102,188–193] Thus, typically, for example, $G_{Ic} < G_{IIc}$ but the effect of the applied Mode II loading on the value of G_c is also very dependent upon the actual adhesive being employed.[57] And, Mode II components of loading can effectively pry apart the crack tip, inducing Mode I loading due to sliding of hackle patterns or other roughness present on the failure surface, or when there is a material

mismatch across an interface, further suggesting the importance of G_{Ic} in controlling fracture.[194]

4. *Does the fracture mode affect the intrinsic fracture energy, G_0?* There is no experimental evidence on the effect of the mode-mixity applied upon loading a joint on the value of the intrinsic fracture energy, G_0; where the term G_0 is defined in Equations 2.11 and 2.12, see Section 2.5. However, it has been shown that for crack growth, even under a pure Mode II (shear) applied loading, the advancing crack may propagate locally in a Mode I (tensile) manner. Thus, it is to be expected that the value of G_0 would be mode independent. However, of course, where there is dissipation, the values of the terms G_D and ψ_v are likely to depend upon the extent of Mode II loading applied. Hence, this leads to a dependency of the measured fracture energy, G_c, upon the mode-mixity, as discussed above.

In light of complications such as these, O'Brien[195] authored a paper succinctly capturing some of these concerns in its title: "Composite Interlaminar Shear Fracture Toughness, G_{IIc}: Shear Measurement or Sheer Myth?" This paper concluded with the statement: "Therefore, as Shakespeare might have said, the controversy over Mode II fracture toughness measurement may turn out to be much ado about nothing."[196] In his subsequent work (e.g. Refs. [197–200]), Mode II (and Mode III) are included as being parameters that one can measure and are of use in engineering predictions, even if their physical micro-mechancial meaning is still open to debate. Herein, we critically examine these concerns, as well as explore the known implications of mode-mixity.

5.2.3 Mode-mix determination

Though seemingly straight-forward for homogeneous elastic systems, applications of the mode-mixity formalism to layered materials proves to be challenging for many systems.[40] Although beyond the scope of this paper, mode-mixity becomes considerably more complicated when cracks are present at an interface between dissimilar materials,[201] where alternate definitions of the fracture components are required and their relative magnitudes vary significantly with distance from the crack tip.[§§] Even without the complication of dissimilar materials, significant concerns have been raised regarding mode-mixity determination and applicability. For example, in specimens involving beam splitting, which is locally relevant to the debond region in peel testing, mode-mixity can be determined analytically using a local method by considering the crack tip stress field[202,203] or a global method based on partitioning the applied moments into portions that induce pure Mode I and pure Mode II loading, e.g.[192,204] For symmetric beams, global and local mode partitioning analyses agree, but if the geometry is not symmetric, local and global method results diverge substantially.[205,206] Conroy et al.[205] argue that the local method works well when the cohesive damage zone is small, and that the global solution is approached as the damage zone becomes larger.

[§§]These solutions also predict physically impossible interpenetration of the fracture surfaces, though these mathematical anomalies are thought to be highly localized at the crack tip and insignificant for practical bonds.

Turning specifically to mixed-mode analysis of peel joints, Thouless and Jensen[207] have undertaken a detailed (linear-elastic) theoretical analysis, using a stress-intensity factor approach involving the Dundurs' parameters,[208] of a bilayer peel test for when the levels of toughness were relatively low. They found that the mode-mixity, i.e. the ratio of Mode II to Mode I (i.e. in-plane shear to opening loading) as expressed by the phase angle, ψ,[207] was fairly insensitive to the peel angle, θ, assuming no elastic mismatch between the two layers for a crack growing along the interface, as can be seen from Figure 20. However, the degree of insensitivity was a function of the elastic strain in the peel arm, with more sensitivity being predicted when the strains were relatively high. When the strain in the peel arm tended to zero[¶¶], the ratio of Mode II to Mode I was constant and independent of peel angle with the ratio of $G_{II} : G_I$ being 0.606 (or $\psi = 37.9^\circ$), again assuming no elastic mismatch between the two layers for a crack growing along the interface (we note that a negative sign is used in the paper, indicating a tendency for the crack to be steered into the film). Indeed, from Figure 20, the value of the phase angle, ψ, is shown to vary at low values of the peel angle, θ, when the strains are relatively high. Furthermore, the analysis then predicted crack tip contact at the peel front and under such circumstances frictional effects may be expected to have an influence on the apparent toughness. Now, these studies assumed linear-elastic behaviour and are relevant when a very low toughness is present, such that a singular-dominated zone can be assumed to be acting at the peel front. However, the theoretical studies reported by Wei and Hutchinson[209] have reached the same conclusion, namely that relatively little variation in the mode-mixity with peel angle is to be expected, for the case of an elastic-plastic peel arm, especially when the extent of plasticity in the arm is relatively limited. One point to note is that though many of the mode-mix analyses are based on axial forces and moments ahead of and in the wake of the crack tip, peel tests, such as the 90°peel test, also involve large prominent lateral loads as considered by Kaelble's stress analysis[66] and several fracture analyses.[210,211]

Partitioning becomes less certain, however, if plasticity is sufficiently large that a singular-dominant region at the peel front no longer applies, as is often the case for most practical adhesive bonds, where large-scale plasticity occurs within the adhesive layer,[185,186] and often extends into the bonded substrate(s) for peel testing. Since, many analyses of the mode-mixity, including in adhesive joints, are based upon the assumption of a singularity at the crack tip, as described by a stress-intensity factor, K, approach.[40] If such a K-dominant stress-field is not present at the crack tip due to yielding, then partitioning based on a singular stress field may not be valid or even possible. Now, for purely elastic materials, or very brittle adhesives and interfaces, a K-dominant stress-field may indeed be present at the crack tip. However, the viscoelastic-plastic damage zones at the crack tip in many practical joints is sufficiently large to extend beyond the K-dominant stress-field.[102,212] Thus, in such cases, analysis of the mode-mixity via any form of a stress-intensity factor, K, approach[102,185,194,212,213] is invalid, since the singular fields have no physical meaning, invalidating any fracture analysis based on the near-tip singularity field. Nonetheless, these problems are tractable using numerical methods using a CZM approach and including peel arm plasticity, e.g.[209] Furthermore, in layered systems, cracks in interlayers are constrained,

[¶¶]As is often the case except at small peel angles where peel arm stretching becomes dominant, as discussed in Section 3.1.1

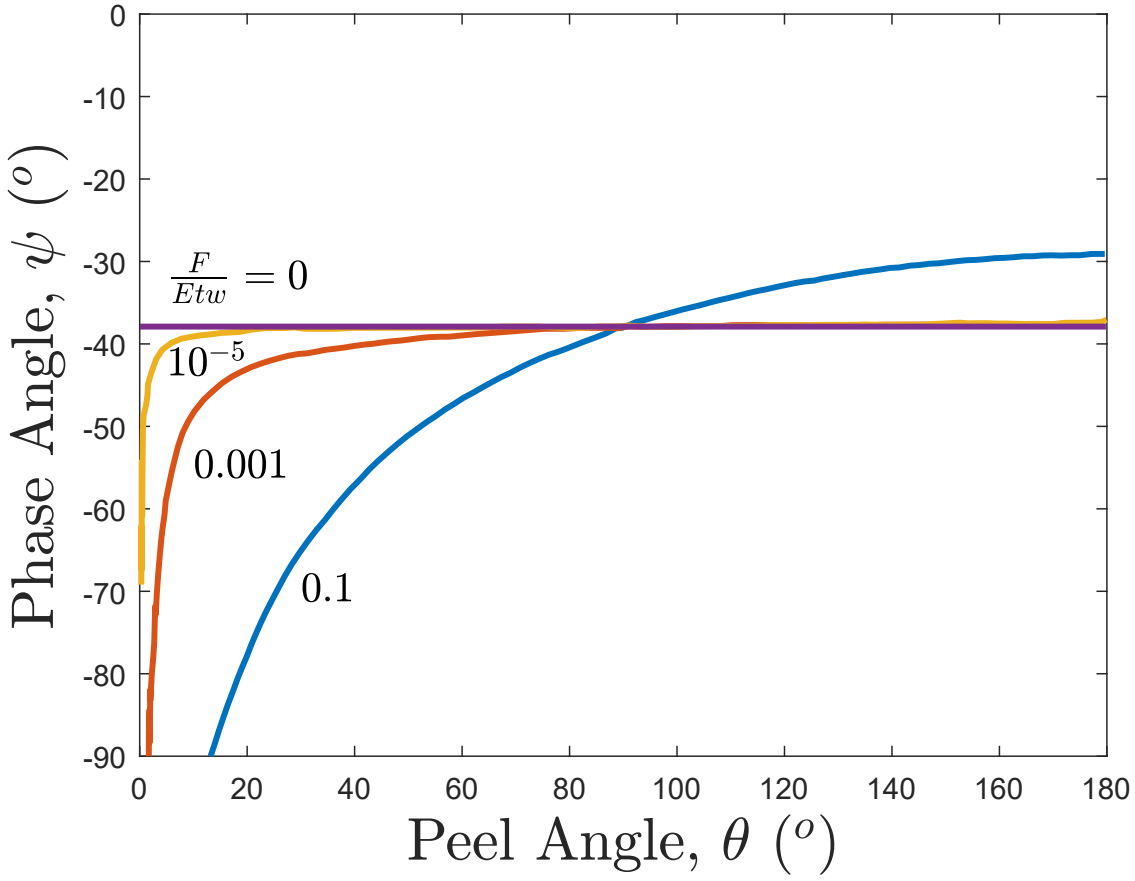

Figure 20: The phase angle, ψ, as a function of the peel angle, θ. These theoretical predictions assume 1) linear-elastic behaviour of the peel arm, 2) the level of toughness is relatively very low, and 3) no elastic mismatch between the film and the substrate.[207]

often by stiffer and tougher materials, significantly altering the stress state[212,214] and potentially affecting determination of mode-mixity. It should be noted, however, that even if yielding encompasses the singular or K-dominated stress field, the strains (from a continuum standpoint) remain singular, suggesting potential qualitative relevance, such as for crack path selection discussed below, even if stresses quantitatively differ from the classic K dependence.[215] Furthermore, many global analysis methods (e.g.[204]) as well as finite element analysis methods, rather than being based on the singular K-field, are in fact based on energy assessments (e.g.[183,184,216]), and continue to be potentially meaningful in spite of plastic deformation.

5.2.4 Mode-mixity steering cracks

Although one can load existing cracks in isotropic monolithic materials with any combination of the three fracture modes, cracks tend to grow in Mode I, as consistently predicted by the maximum opening stress criterion,[217] the path of maximum energy release rate criterion,[218] and by the growth in pure Mode I criterion .[219,220] The three criteria have been shown to

be experimentally indistinguishable and suggest that cracks in brittle, isotropic monolithic materials will turn or kink to grow via a Mode I. This can be thought of as saying that cracks will grow perpendicular to the largest tensile stress[221] (or strain), a useful rule of thumb in interpreting failure modes. The situation becomes more involved in anisotropic materials and also in layered systems, where cracks may be constrained to grow along specific planes (e.g. at an interface) or within a specific layer (e.g. within an adhesive layer). Thus, although cracks growing within an adhesive layer tend to follow the above criteria locally, they may be both *loaded in* and *constrained to globally appear to grow in* other modes or some combination, i.e. mixed-mode conditions.

When the crack growth in an adhesive layer under Mode II loading is examined in detail it has been found that the crack does not *locally* grow as a shear crack, even though a shear load has been applied to the joint.[215,222] Instead, the crack in the adhesive layer grows as microcracks, which are inclined at approximately 45° to the specimen axis (perpendicular to the largest principal stress) across the entire thickness of the adhesive layer until they intersect with an interface, as show in Figure 19c.[180] Further, this array of such microcracks typically grows for several millimetres, or more, down the length of the adhesive layer, essentially forming a relatively long damage zone.*** Thus, the main apparent crack grows as a series of Mode I tensile micro-cracks followed by the coalescence of the ligaments created by these failures, and not by the sliding of two planes relatively to one another that is assumed in illustrations of Mode II fracture mechanics. Clearly, such failure surfaces are considerably more complex, and we now turn to examining their possible effect on the measured fracture resistance.

5.2.5 Mode-mixity effect on G_c

There has been significant debate on whether the fracture energy required to create new crack surfaces should actually depend on the mode-mixity applied. We note that the corresponding measured fracture energies for Modes I and II, and for the combinations of the two, G_{Ic}, G_{IIc} and $G_{I/IIc}$, respectively, are often different, as has been widely reported for a variety of bonded and laminated systems. For thermodynamic (reversible) adhesion, the creation of new area requires a given amount of energy, often tens of $\mathrm{mJ/m^2}$, and is understood to be independent of the manner in which it is formed; hence the understanding that the intrinsic fracture energy, G_0, is mode independent. Where there is dissipation, however, it is plausible that plastic or other dissipative deformations might depend on the mode, and indeed many researchers, working in the area of layered systems where this is relevant, have shown that measured values give $G_{Ic} < G_{IIc}$, e.g.[191,192] Tvergaard and Hutchinson,[102] for example, have analyzed the effect of yielding for a crack at an interface, showing a significant increase in plastic zone size with an increasing Mode II loading component to the test. Further, following the above comments that cracks always basically grow as Mode I cracks at the peel front, some researchers[222,223] have reported that the value of G_{IIc} may be deduced simply from the values of G_{Ic}, the shear yield stress, the shear modulus, and the thickness, h, of the adhesive layer, though the broader applicability of this idea has yet to be established. However, this observation that upon Mode II loading that the cracks in a polymeric layer

***Though these process zones tend to be shorter with thinner substrates common in peel experiments due to the shorter characteristic lengths.[11]

essentially propagate as local Mode I (tensile) cracks is therefore typically inconsistent with the original definition of Mode II shear fracture,[222,223] where the crack growth occurs by a sliding motion of the crack faces, as suggested in Figure 19a, except for relatively weak adhesion. Finally, if the resulting fracture surfaces are non-planar, impingement may impose an opening mode as asperities ride over one another, even under what is considered pure Mode II loading.

Turning to experimental results for many real peel tests, i.e. where the toughness as measured by G_c is invariably more than a few J/m^2, then from the results shown above in Table 3, and in, for example, Ref. [24,168] one might surmise that there is no need to invoke the proposition that the mode-mixity varies as the applied peel angle, θ, or thickness, t, of the peel arm is varied, even when the extensional strain in the peel arm is significant. Or, is the independence on peel angle simply to be expected because of the mode-mix ratio itself is so insensitive to peel angle?[207] Martiny et al.[168] studied an epoxy adhesive bonding aluminium-alloy substrates and used a numerical elastic-plastic FEA model with a zero-height CZM to determine the value of the fracture energy, G_c, from both 1) fixed-arm peel tests, where the applied peel angle, θ, was varied between 45° and 135°, and 2) wedge-peel tests. The measured peel force per unit width, F_c/w, as a function of the applied peel angle, θ, for the fixed-arm peel test is shown in Figure 21a. As expected, the experimentally measured value of F_c/w is a strong function of the chosen value of the applied peel angle, θ. However, the calculated values of G_c were not significantly dependent upon the peel angle used for the fixed-arm peel test. Further, these values of G_c were compared to values measured from all the many different types of peel test and from using the ISO Standard Mode I LEFM DCB and TDCB tests.[224] (In all cases the locus of failure was cohesive in the adhesive layer.) The value of G_c was 1020±150 J/m^2 from the many types of peel test used and was not significantly dependent upon the geometry of the peel test specimens, see for example Figure 21b. This value of G_c was also again in good agreement with the results from the LEFM Mode I tests. These results clearly imply that there was no significant effect of mode mix from employing the very different test geometries.

5.3 Locus of Failure

The locus of failure, resulting during a peel or other fracture test, involves the material system's (often stochastic and spatially and directionally dependent) resistance to fracture as well as the spatially varying tensorial stress field to which it is subjected. For example, price tags are often designed to fail cohesively to prevent tampering (i.e. the paper backing tears) instead of failing adhesively which could allow for price tag swapping. Clearly, the locus of failure in peel tests depends strongly on the properties of the bonded system, including the relative integrity of the cohesive properties of the component materials and the interfacial adhesion. These relative integrities can be rate and temperature dependent, so stick-slip behavior will often show different failure patterns. In addition, fracture resistance, for example, can vary spatially depending on the locus of failure, i.e. interfacial versus cohesive, as well as due to other inhomogeneities, including inherent stochastic variation and defects of various forms. This spatially, and sometimes directionally, varying resistance to failure often leads some to hypothesize weak-link explanations for failures. The concept that chains always break at the weakest link is a useful interpretation for discrete items in series (like a chain)

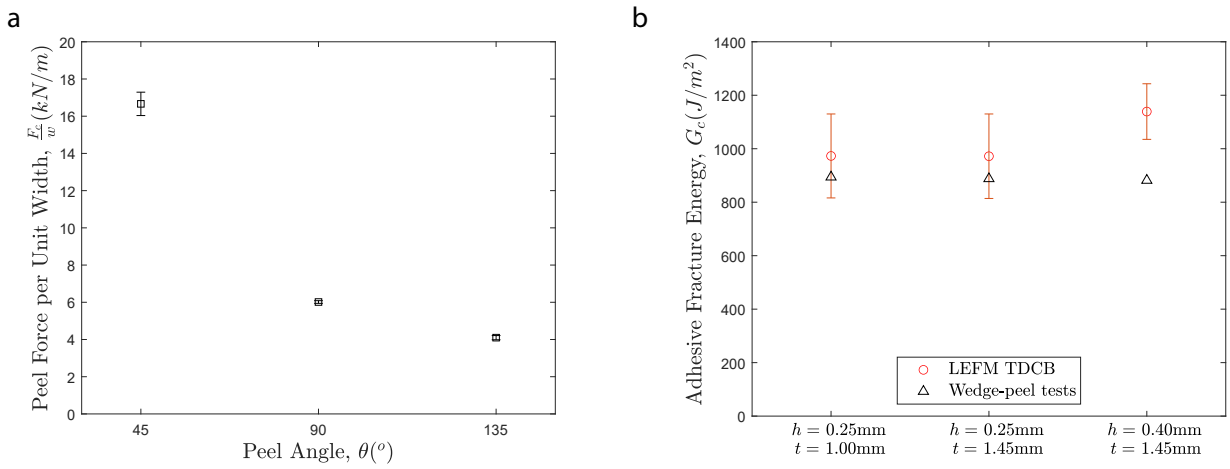

Figure 21: Peel force depends on peel angle, but resulting fracture energies are consistent. a) The measured peel force per unit width, F_c/w, as a function of the peel angle, θ, for fixed-arm peel tests consisting of an epoxy adhesive bonding aluminum-alloy substrates.[168] b) Values of G_c calculated from wedge-peel tests as a function of the thickness, h, of the adhesive layer and the thickness, t, of the peel arm for epoxy/aluminum-alloy joints.[168] (Results from LEFM TDCB tests are also shown where only the thickness, h, of the adhesive layer was varied.)

but become less appropriate for continua subjected to spatially varying and directionally dependent stress and strain fields. Instead, crack path selection and the resulting locus of failure ultimately depends on the complex interaction of the spatially dependent stress field imposed on and probing the directionally dependent resistance to failure. Implications on the resulting locus of failure thus motivates this section summarizing tendencies that may help explain observed failure modes and aid in forensic evaluation.

5.3.1 Dependence of peel resistance on locus of failure

For many adhesive suppliers, controlling the locus of failure is an essential attribute of their systems. Manufacturing firms using structural adhesives are reluctant to consider "adhesives that do not stick," so cohesive failure modes are often desired. Adhesive vendors may recommend appropriate substrate cleaning and surface treatment methods to their customers, but also may incorporate fillers or other ingredients in their formulations to encourage cohesive failures. As commented above, price tags for marking merchandise often utilizes weak paper backings so as to cause cohesive failure within the paper instead of adhesive failure at the merchandise interface.[225] Suppliers of products such as PSA tapes and medical products applied to the skin, on the other hand, often face the opposite challenge – i.e. how to obtain clean removal from a substrate, a problem that is addressed by ensuring superior adhesion to the backing, and appropriate crosslinking or multiphase morphologies to minimize residue left behind. Failure to wet and spread on a low energy surface can lead to interfacial failures, including for PSAs, which also often do not wet rough surfaces well.

5.3.2 Mode-mixity effect on locus of failure

As indicated in Section 5.2, mode-mixity can play a role in crack path selection, effectively "steering" or "encouraging" cracks to grow perpendicular to the largest tensile stress. The presence of shear stresses at bimaterial interfaces undoubtedly explains why cracks tend to veer away, into the adhesive layer, as opposed to propagate along an interface, even when the interface is "less tough" than the adhesive itself.[226,227] Similarly, cracks will tend to grow towards the peel arm exhibiting the higher tensile strain in a bonded joint with asymmetric thickness peel arms, e.g. the thinner peel arm in a tri-layer T-peel test, as predicted by mode-mixity. Mode-mixity, thus provides a tendency to steer cracks, though it does not guarantee the locus of failure, which depends on the spatially varying stress state probing the spatially, directionally dependent resistance to failure. Thus, mode-mixity may have less influence on the locus of failure for systems such as the example above regarding PSA to backing adhesion that is intentionally engineered to resist debonding. Furthermore, the influence of the mode-mixity on steering the crack can shift the fracture process zones and locus of failure towards either less tough or, in some cases, tougher regions within the bonded system[226] , thereby affecting the measured fracture energy, as noted in Section 5.2. In several reported cases, introducing relatively small amounts of Mode II can effectively steer cracks to less dissipative regions, such as out of a more dissipative adhesive layer to the interface[228–230] or to interlaminar failures in composite adherends.[231]

Altering the peel angle has some effect as well by moving debonding closer to one adherend than the other in otherwise symmetric geometries. Hence, in T-peel type geometries, varying the angle of the bonded "tail" can often change the locus of failure, as can sometimes be demonstrated when peeling apart a laminated film.[110] Without external support, this tail angle is primarily affected by the relative bending properties of the two adherends, though other factors such as the weight of a long tail can also influence the peel angle and mode-mixity, leading some standards, such as ASTM F88, to discuss tail angle control.

5.3.3 T-stress effect on locus of failure

In addition to mode-mixity effects, the T-stress, introduced in Williams' stress field expansion,[181] alters the propensity for growing cracks to alter their direction.[220,232,233] Residual interlayer stresses, such as induced in cooling from an elevated temperature cure, increase the T-stress, as do higher bending strains in peeled adherends.[230,234] Because peel tests often involve thinner adherends undergoing considerable elastic and even plastic bending, the in-plane tensile stress, and hence T-stress, within the interlayer are often significantly larger than might be encountered in a DCB specimen with thicker adherends. These higher T-stresses spatially destabilize the growing crack, leading to alternating failures[235] in less tough interlayers.[232,234] Figure 22 illustrates alternating failure modes in several brittle systems, which may be contrasted with a locus of failure of a more ductile system (22d), in which the failure visually appears dominantly at/near one interface. One mechanism to help explain this behavior is that when the crack grows along one adherend in a symmetric T-peel specimen, the other adherend plus interlayer effectively has a higher bending stiffness. This increases the moment arm, leading to a higher bending moment and when the bending stresses within the interlayer become sufficient, a crack will propagate through the interlayer

back to the other adherend, as also illustrated in the figure, resulting in a "wagging" action of the tail as the growing crack diverts back and forth between interfaces. Others have also considered the kinking of interfacial cracks away from an interface,[236–238] including when friction is involved,[239] as well as in functionally graded materials.[240]

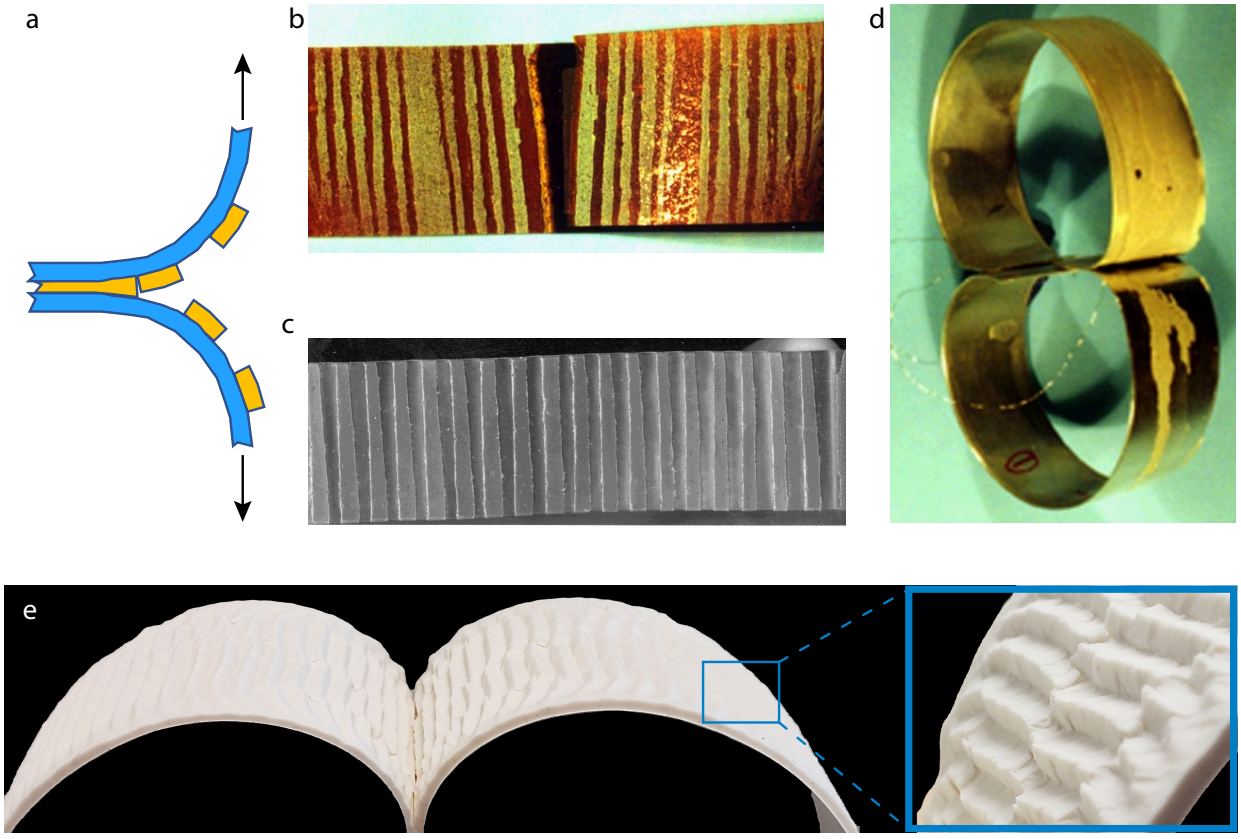

Figure 22: Illustration of T-peel test results. a) Illustration of how the stiffening effect of composite action (peel arm + adhesive) leads to a larger bending moment and higher stresses that can fracture the adhesive layer b) and c) Alternating locus of failure in two T-peel systems involving less tough adhesives. Adapted with permission from Ref. 110, Copyright 2012, John Wiley & Sons. d) A more consistent failure mode observed in a more ductile adhesive. e) Typical triangular failure pattern when testing T-peel specimens bonded with an elastomer.

5.4 Rate and temperature effects

Perhaps the most powerful accelerated testing technique for polymeric materials and glass-forming liquids has its basis in the time-temperature superposition principle. Therefore, it is not surprising that a number of researchers have used this technique to analyze (and attempt to accelerate) peel tests on adhesive joints. For example, Kaelble[43] used the 90° peel test to study the peel energy of cellophane bonded to cellophane with a polyisobutylene-based adhesive. These results are shown in Figure 23a. Note that, in addition to shifted data,

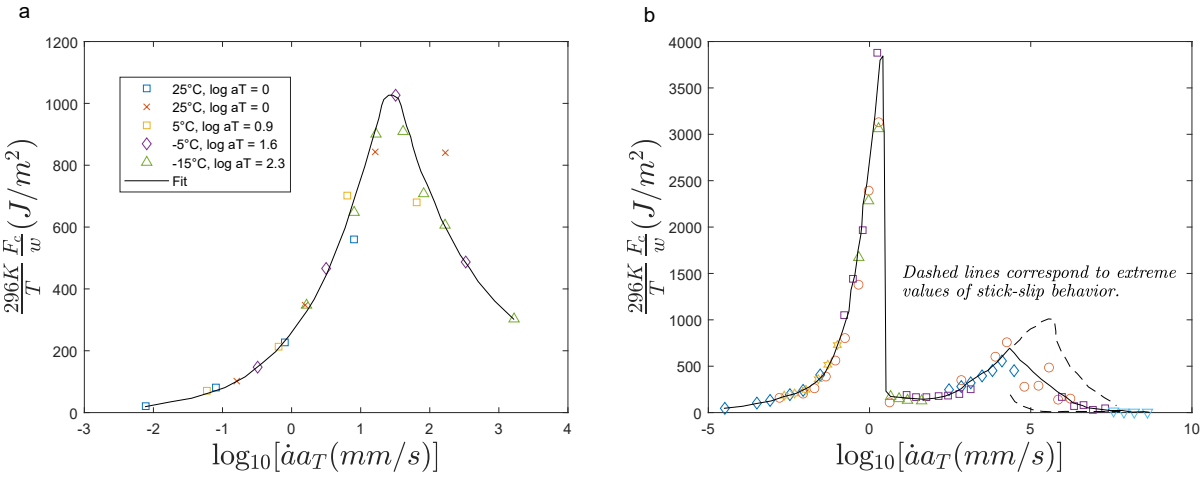

Figure 23: Time-temperature superposition of peel data. a) Kaelble's master curve of peel energy data for polyisobutylene-based adhesive reduced at a reference temperature of 25°C.[43] b) Master peel energy versus shifted rate plot for butadiene-styrene copolymer adhesive (Gent and Petrich polymer A) adhering to Mylar (i.e. PET).[41] **Note:** In both cases, the ordinate values have been scaled by the ratio of room temperature to the test temperature (the ratio $\frac{296K}{T}$).

this plot includes a number of measurements made at the 25°C reference temperature. In Kaelble's words, "comparison of the reduced data and direct test data indicates reasonably good agreement." He further noted that tests conducted in the region where the curve slope is negative exhibit stick-slip behavior where the peel force fluctuates markedly with time. This could contribute to the one outlying point. Kaelble used the same time-temperature approach to shift 180° peel data for cellulose acetate bonded to either cellophane or polyethylene using an acrylate copolymer. In this case, it is notable that the shifted data range extends over approximately six decades of rate. The time-temperature superposition principle is based on multiplying rates or dividing times by the shift factor, a_T, which accelerates results obtained at lower temperatures and decelerates lower temperature results to combine on a master curve at some reference temperature, resulting in simple shifts on logarithmic scales of time, frequency, strain rates, crack velocity, etc. (as shown in Figure 23).

Gent and Petrich also used time-temperature superposition to reduce T-peel data for two similar butadiene-styrene copolymers (labeled A and B) with similar number average molecular weights, adhering to a PET substrate.[41] Polymer B had a higher intrinsic viscosity and a broader distribution of molecular weight and was chosen to give a greater degree of rubber-like behavior at room temperature. The peel energy versus shifted rate data for polymer A exhibited a complicated behavior consisting of a steady increase in peel energy with rate of peel up to a critical rate, followed by an abrupt transition to much smaller peel forces (see Figure 23b). At the same time, the mode of failure changed from cohesive failure of the polymer layer to interfacial failure. Gent and Petrich explained this behavior in terms of the transition from liquid-like to rubber-like behavior of the polymer at the first peak and the transition from rubber-like to glass-like behavior at high rates. This was confirmed by comparing the peel energy/shifted rate plot with the plot of the Young's modulus and

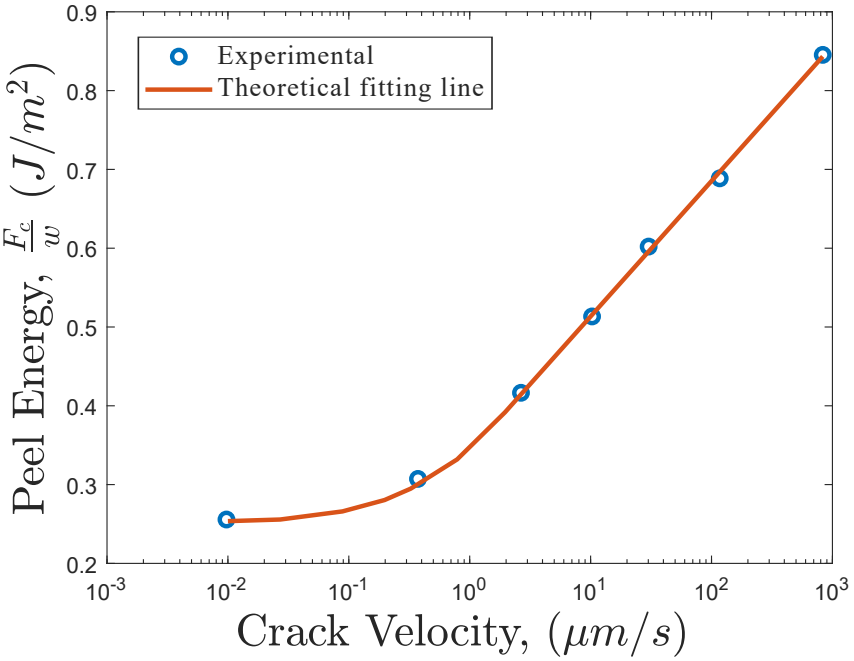

Figure 24: Crack velocity effects in peel. Peeling energy, F_c/w, increasing as the peel crack velocity is increased for a cellulose nitrate film adhering to glass [187,241].

rate of extension where the peaks did, in fact, align with the transitions. To confirm the hypothesis that the low-rate transition was associated with liquid-like flow, they crosslinked polymer A (resulting in polymer B) to prevent that flow from occurring. For the crosslinked material (i.e. polymer B), the first peak no longer appeared along with only interfacial failure. Interestingly, for polymer B only a single peak was observed. Again, this was explained in terms of the liquid-like flow which in this case was limited by the chemical crosslinking of the molecular chains in polymer B.

These examples (and others) illustrate that one can use temperature to effectively accelerate or decelerate the influence of loading rates and that by careful interpretation of the data, one can connect the observed behavior of the joint to the properties of the adhesive. Additionally, within limits, one can tailor the properties of the adhesive to control the behavior of the joints.

As discussed in Section 2.5, in order for $G_c = G_0 = W_{adh}$, assuming that only secondary intrinsic molecular adhesion bonds are acting, it is required that reversible peeling occurs, that is where energy is conserved, which is a process that requires vanishingly small crack speeds. As the peel crack travels faster, and viscoelastic and/or plastic energy is also dissipated around the peel front, so the peel force rises considerably as shown by the examples in Figure 24.

5.5 Stick-slip behavior

Figure 4a,b shows the peel force versus displacement curve associated with stable, steady crack propagation through the peel test. Here the crack grows in a steady, controlled manner with the rate of crack growth, $\dot{a}$, basically being dependent upon the crosshead speed, V, of the test machine and the peel angle selected. For such propagation, the peel geometry remains relatively unchanged, representing a nominally self-similar deformation configuration.

In contrast, temporally unstable, or stick-slip crack behavior, sometimes termed "shocky" or "zippy" behavior, is often observed during debond propagation, as shown in Figure 4d. This is a complex phenomenon dependent on multiple factors, including constitutive material properties, test rate, test temperature, specimen and load-train compliance, and system inertia. Figure 4d shows the peel force versus displacement curve associated with such unstable crack propagation in the peel test. Here the crack grows intermittently in a stick-slip manner.[57,176] As may be seen, this type of crack growth has a significant effect on the associated force versus displacement curve, which now has a characteristic saw-tooth shape, and also on the deformed shape and resulting moment arm(s), which vary as the ends displace at a constant rate but the debond propagates in an erratic manner. The values of F_{ci} and F_{ca} correspond to the forces at crack initiation and crack arrest, respectively. Assuming that the peel tests can be interpreted in terms of the fracture energy, G_c, then crack initiation and crack arrest values of G_c may be determined from the values of F_{ci} and F_{ca}. The fracture energy, G_{ci}, for the initiation of crack growth is considered to be a useful "material" or "bonded system" parameter, while the value of the fracture energy, G_{ca}, for crack arrest is considered to have no fundamental significance and its value is simply an artefact of the test.[242,243]

Reasons for the temporal instability of crack propagation often involve complex, multi-physics interactions, the details of which are beyond the scope of this paper.[244,245] In the preceding paragraph one recognizes that the fracture energy is not a constant when unstable crack growth occurs, but may possess rate dependence leading to a spatial (crack length) dependence. Spatial dependence can also involve a statistical variation of resistance to fracture due to inherent variability or local defects – perturbations than can trigger instabilities. The well-known temperature dependence of polymers may be evident via the test temperature, but also via local heating associated with dissipation in the peeling process, which becomes adiabatic at very high rates of crack propagation.[246] However, in addition to material time-dependence, which will be discussed in a more detail in following paragraphs, other factors are also involved, specifically, the evolution of the energy release rate available to continue driving the crack. Some of the commonly cited reasons for such stick-slip behavior are listed in Table 5, along with brief explanations or clarifications for these contributors. Additional details are provided in the following paragraphs, though due to coupling effects, multiple mechanisms are often involved. Aside from local variability and locus of failure, causes for stick-slip mechanisms can loosely be grouped into three underlying factors: system compliance, system inertia, and rate/temperature effects.

Table 5: Mechanisms potentially contributing to stick-slip instabilities in crack propagation.

Mechanism	**Brief explanation**
Evolving specimen compliance	Specimen compliance increases with crack propagation, contributing to system compliance that can stabilize or destabilize crack advance depending on several factors
Dependence of available G on crack length, a	Joint configuration and manner of loading affect $\partial G/\partial A$, making continued crack propagation more or less likely
System inertia	Higher inertias can lead to larger force oscillations
Test rate	Crack advance stability often depends on rate of testing
Rate-dependent material deformation	Viscoelastic/viscoplastic behavior affects local strains at crack tip, resulting in sharper or more blunted crack tips that affect local stress state
Rate-dependent resistance for crack propagation	Can result from material fracture behavior and may also relate to above crack tip blunting
Temperature effects	External temperature or localized heating affects viscoelastic nature of material
Manner of loading control	Whether constant force, constant displacement, or something else, the manner of loading plays an enormous role in stability, as load-control scenarios augment elastic stored energy with external work to increase the driving force for continued crack propagation.
Local variations in bond	Intentional or unintentional defects, internal architecture, crack stoppers, etc.
Variations in locus of failure	Propagating crack may vary, e.g. among cohesive, interfacial, alternating, etc.

5.5.1 Combined effect of system compliance and $\partial G/\partial A$

We begin first by considering the case of displacement control, where the input displacement is nominally controlled to be constant or vary in some controlled fashion. Under such conditions, a rapid advance of a crack (i.e. a slip event) is associated with little to no mechanical work being done on the system. Briefly, in a massless system, evolution of the available energy release rate, G, is governed by:[247,248]

$$\left(\frac{\partial G}{\partial A}\right)_{\Delta} = \left(\frac{\partial G}{\partial A}\right)_{F} - \left(\frac{\partial \delta}{\partial A}\right)_{F}^{2} \frac{1}{C_m + \left(\frac{\partial \delta}{\partial F}\right)_{A}} \tag{5.2}$$

where Δ represents the total displacement (e.g. crosshead displacement imposed on a test specimen during a test), δ is the specimen displacement, and C_m is the load-train compliance. This implies that, independent of the time dependence of the adhesive, the available energy release rate depends not only on the evolving compliance of the specimen but also on the compliance of the load-train, as both associated stored energies are available to rapidly advance a crack. C_m is typically small in well-designed load frames, so $\Delta \approx \delta$; for displacement-controlled frames, rapid debonding hence proceeds at nearly fixed specimen displacement and with minimal work input. Load control effectively means $C_m \to \infty$, which we will revisit in Section 5.5.5.

5.5.2 System inertia

One can understand the effective inertia of a system as further tempering crack acceleration and deceleration, but this also means a slowly growing crack resists acceleration (tending towards stick), and deceleration is resisted by the moving specimen (tending towards slip). As common peel specimens are often of thin gauge stock and are fairly lightweight, inertial effects might not be as pronounced as in more massive specimen configurations, such as in the DCB test.[249] System inertia for peeling, however, can be important, as Maugis and Barquins have reported the combined effects of spool inertia and time-dependent peeling of a PSA tape from a spool, described in terms of Hopf bifurcation instabilities, which are critical points where a system's stability switches and a periodic limit-cycle solution arises.[250]

5.5.3 Viscoelastic behavior and crack tip blunting

Although resulting from complex interactions of the dynamically evolving values of both G and G_c, the type of stick-slip crack growth observed in common peel tests is often associated with viscoelastic or viscoplastic deformation at the crack tip. Namely, upon initially loading the peel test at a relatively slow test rate,[†††] these conditions may lead to a relatively high extent of crack-tip blunting, and hence a relatively high value of G_{ci} at the initiation of crack growth. However, when the crack eventually propagates, with now a significantly

[†††]Here, as elsewhere, one should think of times and temporal rates in terms of reduced times and rates, in light of the time-temperature superposition principle. Other accelerants such as absorbed moisture can also play a similar role.

higher strain rate at the crack tip, the crack tip sharpens, since the yield stress will increase (decreasing extent of plastic zone) or there is less time to blunt if viscoelastic. Hence, the crack will now need less energy to propagate. Thus, the energy available (per unit area) to drive the debond will be greater than that required for stable crack growth, so this extra energy is expressed as kinetic energy. Hence, the crack will initially accelerate and unstable crack growth results, until the energy supply is insufficient and the crack arrests. This cycle of events is then repeated. The extent of crack acceleration, and hence the length of unstable crack growth, will obviously depend upon the excess energy available from the test specimen and any load-train compliance. Further, when stick-slip crack growth does result, the fracture surface(s) marks corresponding to the jump/arrest events are often visible as "beach-marks" in the form of fine lines across the width of the peel test, such as shown in Figure 25.[251] These "beach-marks" are often associated with the more ductile "stick" portion, where sustained loading can induce stress whitening and related phenomena associated with viscoelastic/plastic deformation.[251] Because the arm(s) of the test specimen are often thinner in peel tests than in other fracture tests, anticlastic bending effects tend to more localized, so the pronounced thumbnail-shaped "beach-marks" often seen in DCB tests become more muted, with more localized edge effects, still associated with anticlastic bending, plane-stress conditions near a free edge, and sometimes moisture or other environmental effects that first result near exposed edges. Finally, it is noteworthy, that researchers have demonstrated that intermittent propagation may also arise due to the insertion of crack stoppers, for example via the incorporation of ductile strips designed to arrest growing cracks, in the peel specimen or to the periodic variation of adhesive thickness or peel arm stiffness.[25,31] However, crack tip blunting followed by tip sharpening is often used to explain, conceptually at least, stick-slip phenomena in the common peel test.

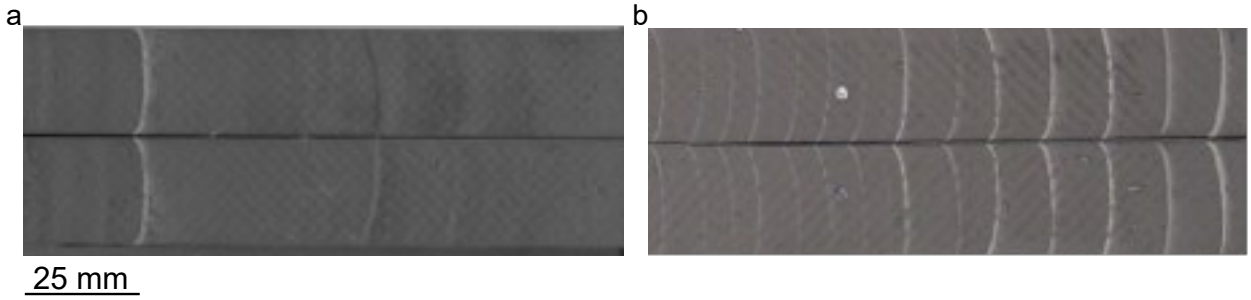

Figure 25: Images of stick-slip "beach-marks" in composite beam specimens a) DCB specimens, showing long slip regions between "beach-marks" because of the large specimen compliance. b) Driven wedge specimens provide more local loading (similar to an IWP test), thus reducing stored energy, extent of slip regions, and distance between "beach-marks". Adapted with permission from Ref. 243, Copyright 2011, Taylor & Francis.

5.5.4 Relation to dissipation peaks and loss tangent, tan δ

Mathematically, if crack tip sharpening decreases fracture resistance, the inherent crack growth behavior is such that $dG_c/d\dot{a}$ is negative in some part of the G_c versus $\dot{a}$ diagram,

and this negative-resistance branch cannot be accessed.[247] Further, since it corresponds to the crack resistance decreasing as the crack velocity increases, then a velocity jump, i.e. stick-slip crack growth, must be observed. These observations emphasize the importance of understanding the viscoelastic properties of the adhesive layer in interpreting and explaining stick-slip behavior, such as discussed by Maugis and Barquins.[247,250] Now every polymeric material is rate and temperature dependent, often exhibiting modulus plateaus and transition regions (e.g. α, or glass transition temperature, β-transition, etc.) Each of these transition regions is associated with enhanced dissipation, as evidenced by peaks in the loss modulus or loss tangent. Fracture energy enhancement can correlate with these transition regions, and in some circumstances, has been shown to correlate with the loss tangent, tan δ.[252,253] To illustrate this, the fracture energy, G_c, as a function of crack velocity, $\dot{a}$, is schematically shown in Figure 26, where the peak in this relationship corresponds, for simplicity, to the presence of a single (alpha) loss tangent transition for the adhesive. In essence, when one is climbing[‡‡‡] dissipative peaks, i.e. crack growth on the left or rubbery side of the transition, debonding is stable. Descending any dissipative peak, e.g. to the right or glassy side of the illustrated peak, crack advance is unstable and rapidly advances until slowed by inertial resistance, or as mentioned above, the lack of sufficient sustaining energy. This is often witnessed in displacement-controlled testing unless the system is highly compliant. At some point (i.e. the lower right in Figure 26), the crack abruptly decelerates and may arrest, in a process that repeats itself as debonding proceeds. Note that stable propagation occurs along the solid blue lines, but is unstable (rapid acceleration or deceleration) on the dashed blue lines. In light of the time-temperature correspondence, we note that we are speaking of reduced rate behavior that spans from the rubbery region, through the leathery transition, and into the glassy domain, giving rise to dramatic jumps and abrupt stops in debond propagation[§§§], i.e. stick-slip crack growth is observed. In addition to the often dominant glass (alpha) transition, similar instabilities can result near other transitions, e.g. at beta transition peaks.

5.5.5 Manner of loading

Notwithstanding, Maugis and Barquins and others have noted that the degree of stick-slip crack growth depends upon the specimen geometry and the apparatus used for the peel test, as implied in Equation 5.2 and discussed below.[254,255] For example, even complex geometric interfaces like gecko-inspired adhesives have shown stick-slip behavior.[256] Indeed, considering the effect of the load-train compliance, Andrews et al. have shown that, by inserting a spring in the load-train between the crosshead of the test machine and the peeling strip, they could stabilize stick-slip behavior.[257] In particular, when the fracture energy was plotted against the peel crack velocity, $\dot{a}$, the results from using a "soft machine," i.e. with the inserted

[‡‡‡]Climbing and descending are mentioned here as the phenomenon is analogous to pulling a trailer up a hill (stable) and descending on the other side (unstable), where slop in the hitch-pin of the car-trailer joining mechanism can result in repeated jerking behavior as car and trailer velocities diverge during descent.

[§§§]A simple classroom demonstration is to show that slow debonding of a PSA tape produces stable debonding whereas fast debonding results in "zippering". If one then suspends the roll above a cup of ice water for several minutes, such that half of the roll is immersed, and pulls at a moderate constant rate, one hears the zippering for the cold side because of the higher 'reduced rate' of testing.

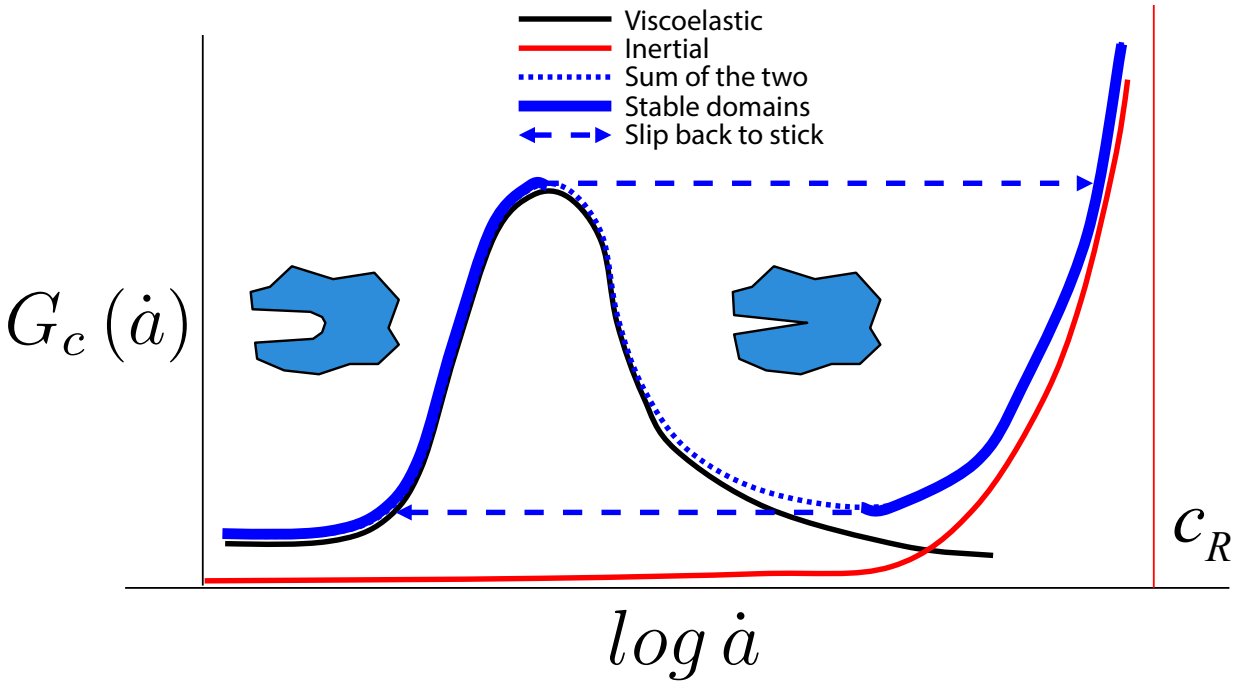

Figure 26: Schematic illustration of rate-dependent fracture energy versus reduced crack velocity. Showing a single viscoelastic transition peak (black line), an inertial wall at the Rayleigh wave speed (red line) c_R, and the addition of the two (blue line). On the left (rubbery) side of the viscoelastic peak, crack growth is stable. At the peak of the transition, the crack rapidly accelerates (on glassy side of the transition before slowing (potentially) due to inertial resistance and then abruptly arresting.

spring, revealed a regime of low energy peeling and a transition to the normal high energy peeling that could not be accessed and so observed in the absence of the spring. This transition behavior was studied as a function of adhesive thickness, crosshead speed, and spring stiffness. The phenomena revealed by soft-machine testing were interpreted in terms of variations in the radius of the peel crack tip caused by flow of the uncrosslinked rubbery PSA. Moreover, the practical implication was that far more information could be obtained from soft-machine tests than from conventional hard-machine tests since the problem of the oscillating peel forces associated with stick-slip peeling could also be eliminated. In Figure 27, Andrews et al. show results for deadload peel testing and also for traditional load-frame testing, along with those for compliant load-frame testing over a wide range of testing rates. There is of course considerable scatter in the debond rates for the deadload tests and for the force traces in the stiff load-frame tests. The compliant load-train results, however, stabilize the propagation and systematically bridge the gap between the force control and displacement-controlled testing. Because these are PSAs, the debonding occurs to the left of the glass transition temperature in Figure 26, the addition of load-train compliance tends to stabilize the debond rate rather than induce more dramatic stick-slip behavior, as would be expected if to the right of a polymer transition, and hence in the unstable region of debonding.

Finally, it is again important to remind ourselves that in addition to viscoelastic and/or

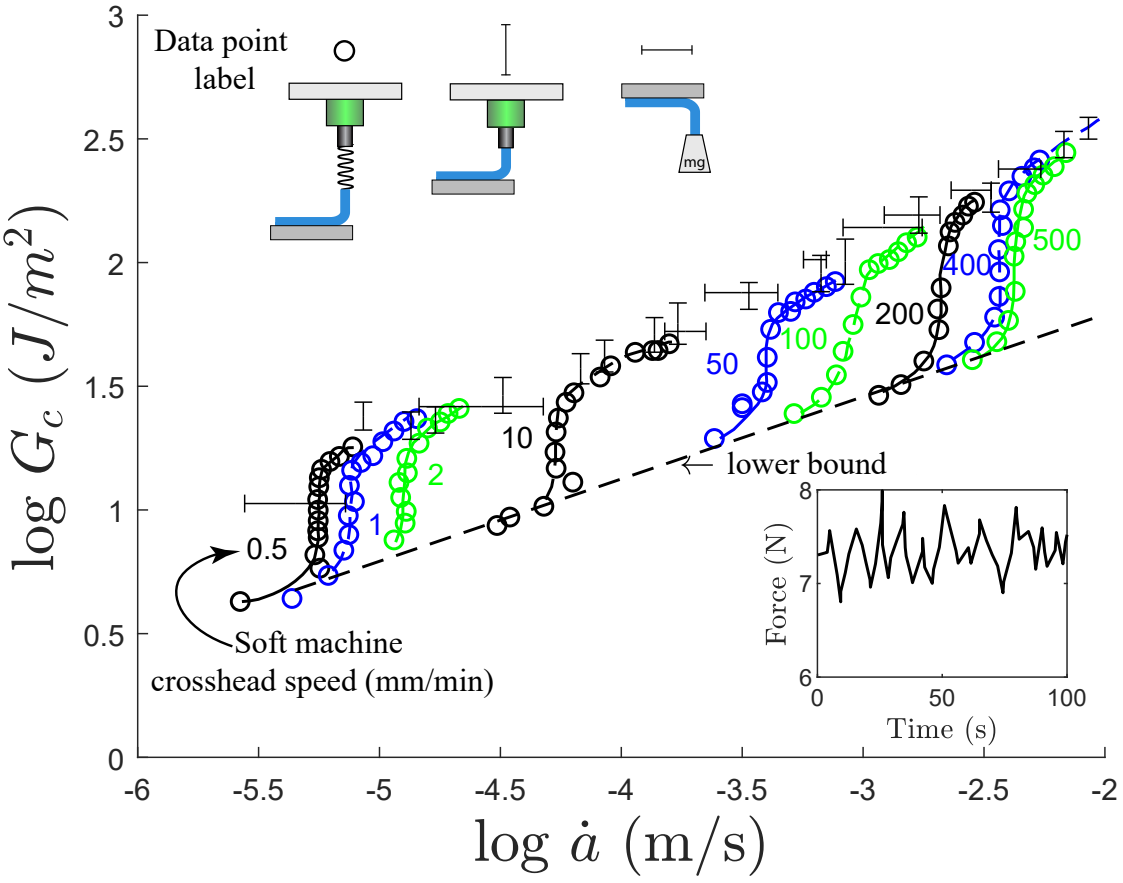

Figure 27: Fracture energy for surgical tape (uncrosslinked natural rubber + 7% sebum) to glass adhesion at 23°C to using three different loading scenarios for 90° peel. Schematics represent the test conditions and the horizontal error bars represent deadload peeling rates at various fixed load levels. The vertical error bars represent range of stick-slip force/width (e.g. lower inset) in a traditional (stiff) load frame undergoing constant crosshead rate testing. The data points and smooth, sigmoidal curves represent debonding results for similar tests conducted with a compliant spring incorporated in the load train resulting in consistent data that evolves from the suggested lower bound at the start of a test to the upper portion of each curve, agreeing well with the scatter bands for both deadload creep and conventional testing. Adapted from Ref. 257. (The crosshead speed for the soft machine in mm/min is given by the numbers. Also, being PSAs the results are on the stable rubbery (left) side of Figure 26

.)

plastic constitutive relationships for the adhesives or substrates, stick-slip behavior is also a geometric phenomenon, because the debond propagation rate ceases to correlate with the rate of crosshead displacement. The specimen geometry, including the effective moment arm length, may also affect the magnitude of the force required to re-initiate propagation. Other factors also affect the complex stick-slip process and the propagation distances during the slip stage, resulting in a complex interaction between the viscoelastic-plastic blunting, wave speeds in the specimens, the compliance of the system, and also in the system inertia, in what is often a very dynamic process.[242,243,258] For example, at sufficiently high propagation speeds, one cannot ignore adiabatic heating associated with dissipation mechanisms in the vicinity of the growing crack, which further complicates the fracture resistance landscape.[246]

Thus, in summary, stick-slip crack growth behavior is a very complex, multi-physics process and, whilst we do understand some of the underlying mechanisms and physics involved, we still cannot readily predict such behavior. Relatively modest changes in rate, temperature, and other factors can sometimes lead to systems moving between stable and unstable propagation modes. Interestingly, stick-slip behavior in PSA tape debonding can induce phenomena with physiological implications, such as nuisance noise from the characteristic chatter during this unzipping process and even emitting X-rays through triboluminescence,[259] reportedly at levels sufficient to perform X-ray imaging of finger bones, encouraging some to suggest this method for potential low-cost portable X-ray generators.[260]

6 Examples of peeling in biological systems

Numerous biological systems rely on the control of peeling to survive.[3,78,261–266] Controlling toe-pad adhesion for climbing organisms such as the gecko is essential for locomotion and clinging, specifically for how the gecko achieves reversible adhesion that is at one instant strong and in another instant weak for release. This can also be seen in wet adhesion in frog toe-pads and underwater adhesives. These biological systems will be discussed in the context of how peeling is used for survival and how the analysis of biological systems can be accomplished with methodologies discussed above for synthetic systems.

6.1 Climbing organisms: geckos, spiders, insects

Of particular interest is the use of adhesion in climbing or clinging organisms where their toe-pads capable of adhering, allowing for the organism to achieve perched locations for prey capture or rapid locomotion to evade predators.[267–271] This adaptation has arisen across a wide range of organisms, from small insects up to large geckos, where the mass of the climbing organism spans multiple orders of magnitude. These adhesives are typically called dry adhesives, as the adhesive contact is primarily dry and uses van der Waals forces to achieve adhesion,[3,272] although oils and other fluids can contribute to the adhesion.[273] On the toe-pads of these creatures, fibrillar features are often observed, where instead of a single large contact the interface is discretized into numerous smaller contacts. This feature has been shown to incorporate multiple benefits, including self-cleaning of the toe-pads, an ability to achieve strong yet rapidly releasable adhesion, and the ability to create contact on rough

surfaces.[274]

One of the primary interests in these fibrillar features in recent decades is the ability to control adhesion. An interesting observation in these systems is that the size of the fibrillar feature can vary. In some reports it has been found that when looking across organisms, as the mass of the organism increases, then the fibrillar features decrease in size.[6,275,276] However, when looking within taxa (i.e. looking within geckos), there is little correlation between mass and fibrillar feature size.[272] Results suggest that fibrillar features are not solely sufficient for climbing capabilities and that the morphology of natural features does not represent an inherently optimizing process.[272,277]

There are several outcomes for how the discretization of a contact can impact adhesion capacity during peeling. Consider a thin-film contact that is being peeled from a substrate at an angle θ, as shown in Figure 28. Based on the peeling of an inextensible elastic tape, we find that at high peel angles $F_c \propto w$, where w is the total contact width. However, if we break up that contact into multiple discrete contacts n, then the force capacity of that interface can be increased $F_c \propto nw$. This is often termed contact splitting,[6] and although it does not work in all adhesive scenarios,[275] breaking up a single, long peeling contact into multiple discrete contacts along the length can take advantage of the increased width to increase adhesion (Figure 28a,b) This is attributed to the fact that during peeling of long contacts, the force is not proportional to the overall length as the stress is localized near the peeling front. This results in long peeling contacts not utilizing the entire length to increase force capacity F_c. Therefore, breaking up the contact into smaller contacts where they can all contribute to F_c can be beneficial. There is also benefit to having to reinitiate a crack at each discontinuity.[278] For example, during the peeling of an elastomer with incisions, the crack can be trapped and then reinitiated at each incision to increase the force required to separate an interface.[279,280]

Varenberg et al. analyzed the morphology of biological attachments used for adhesion control.[276] They examined the total contact width for various climbing organisms ranging from small insects to arachnids and reptiles. They found that as the mass of an organism increased, the overall length of the peeling line also increased. This was particularly relevant in these systems as the terminal contact features, often termed spatula or spatulate structures, resemble thin film contacts. Although not all climbing organisms display the same climbing ability at the same mass, for example that of geckos and skinks may vary by tenfold, the correlation between contact line width and body mass suggests that adhesive peeling is an important component for biological adhesion control.

Although fibrillar features are common in nature, there are multiple insects that adhere with smooth adhesive pads. A more general adhesive framework that does not assume a contact geometry can also be utilized to describe adhesion in biological organisms. Bartlett et al. developed a reversible adhesion scaling theory which shows that the force capacity of a reversible adhesive interface scales as:[277]

$$F_c \sim \sqrt{G_c}\sqrt{\frac{A}{C}} \tag{6.1}$$

where C is the compliance in the loading direction, A is the contact area, and G_c is the fracture energy. As this equation does not specify a contacting geometry, it has been found

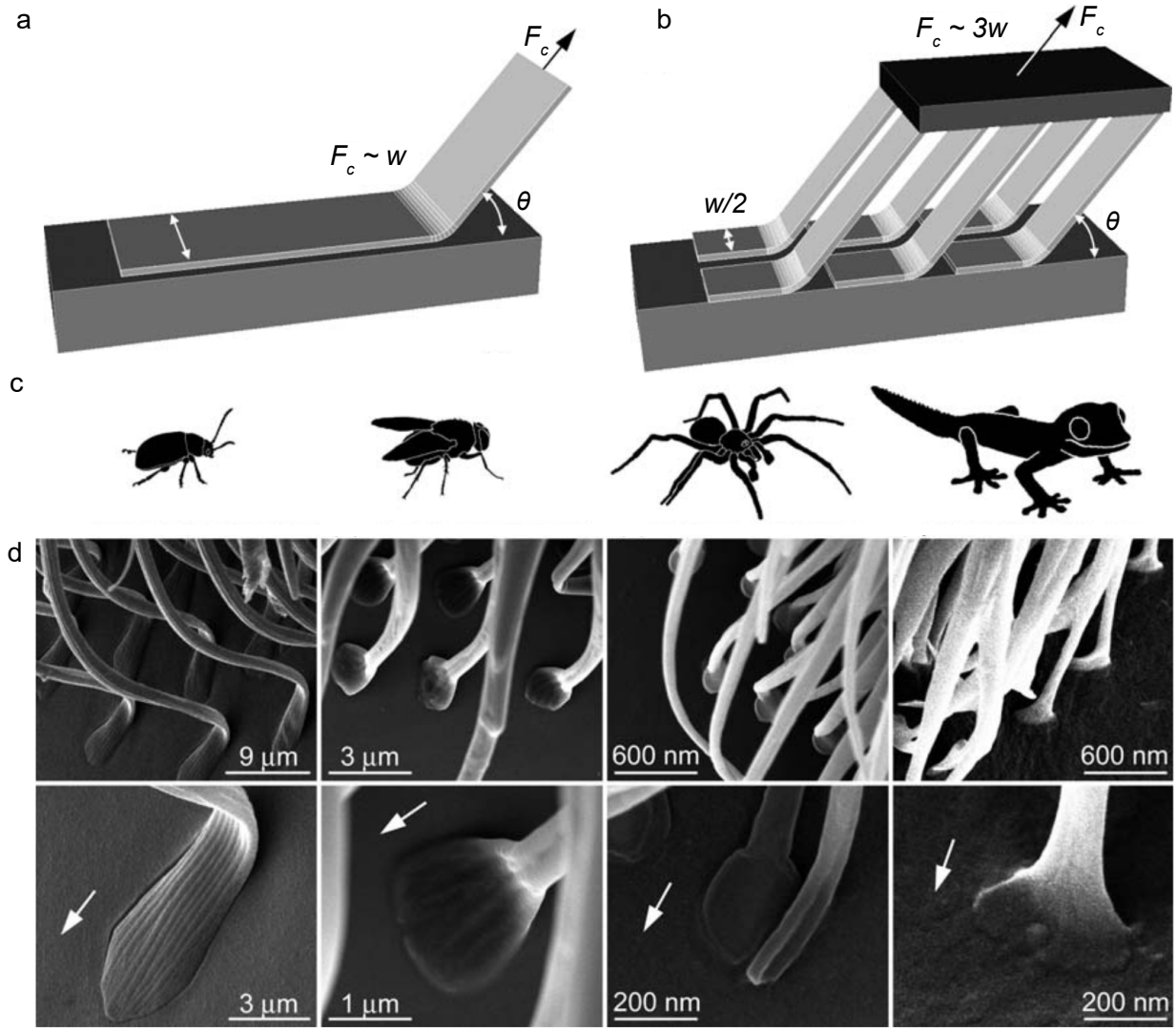

Figure 28: Adhesion in geckos, spiders, insects. a) Schematics demonstrating how the peel width changes by breaking up the length of a contact. b) Schematics of organisms such as a beetle, fly, spider, and a Tokay gecko. c) SEM micrographs showing the terminal contacts for the organisms where arrows are pointing in the distal direction. Adapted with permission from Ref. 276. Copyright 2010, RSC.

to be useful for a number of adhesives, size scales, and loading geometries.[281–285] It can also be used to describe diverse biological adhesion geometries, from full body gecko experiments to the individual levels of the gecko adhesion system including single seta and spatula, and other climbing organisms such as beetles, spiders, crickets, and flies (Figure 29). This equation works for both fibrillar features as well as smooth contact pads and shows the importance of creating contact area A without sacrificing C in reversible adhesion systems to control adhesive force capacity.

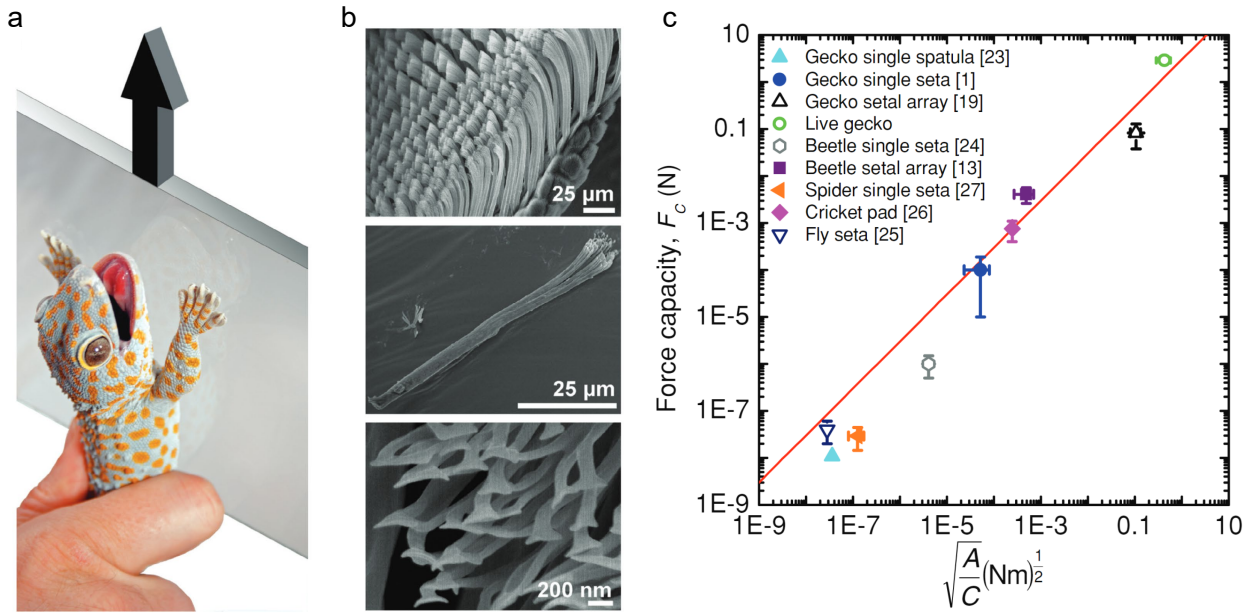

Figure 29: Scaling biological adhesive contacts. a) Full body adhesive experiments of a live gecko. b) SEM micrographs of various levels of the gecko's adhesive system, including setal arrays, single seta, and spatula. c) Adhesion force capacity, F_c, versus $\sqrt{A/C}$ for a variety of biological adhesive systems across multiple length scales. Adapted with permission from Ref. 277. Copyright 2012, John Wiley and Sons.

6.2 Wet and underwater adhesion: Frogs and mussels

There are several organisms that must control adhesion in wet and underwater environments.[286] Frogs for example must adhere not only in dry environments, but often live in environments where significant moisture and water are present.[287] Organisms like mussels often live in wet or submerged environments and must adhere completely underwater. These organisms display several mechanisms which are used to control adhesion in wet and underwater environments.

The toe-pads of tree frogs are soft and consist of a hexagonal microstructure that are approximately 10 μm in size with a finer microstructure of 0.1-0.4 μm peg-like features. These larger hexagonal features are separated by an approximately 1 μm channel. These toe-pads are permanently wetted by a mucus that is secreted from glands on the toe.[288] The separation of the toe-pad from the substrates occurs by peeling from the edge of contact. As the crack propagates across the surface in a peeling mode, the pull-off force is smaller than if the whole surface were required to separate at once. The primary mechanism for attachment is attributed to capillarity, with viscosity-dependent hydrodynamics (i.e. Stefan adhesion) likely playing a role.[289,290] It is also likely that the fluid will drain and that the toe-pad can create adhesive contact with the underlying substrate.[291,292] A variety of mimics have been created that focus on the multi-level structure with channels for fluid drainage.[293–296] This mechanism is critical for Stefan adhesion and akin to what tire patterns use to reduce hydroplaning.

Mussel adhesion has commonly been attributed to the chemistry produced by the mussel

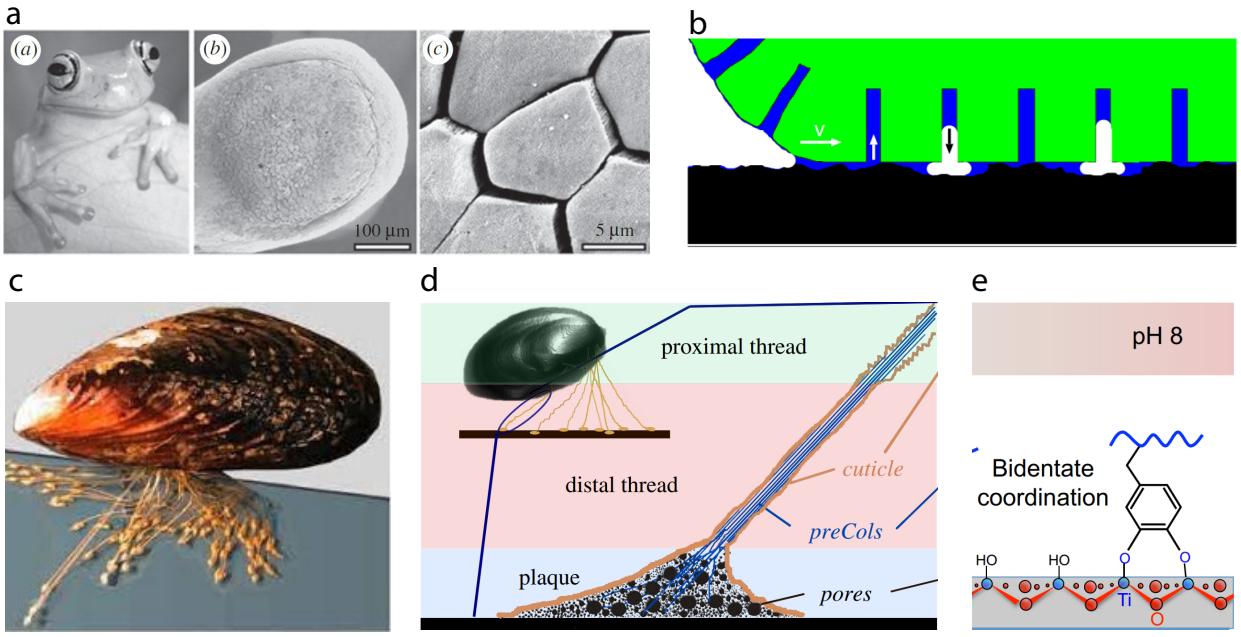

Figure 30: Biological attachment in wet and underwater environments. a) Images of a tree frog and their toe-pads. Adapted with permission from Ref. 288. Copyright 2006, The Royal Society. b) Schematic of the peeling of a frog toe-pad from a substrate. Adapted with permission from Ref. 291. Copyright 2007, IOP Publishing. c) Image of a mussel attached to a substrate. Adapted with permission from Ref. 297. Copyright 2017, Company of Biologists Ltd d) Structure of the mussel bysuss. d,e are adapted with permission from Ref. 298. Copyright 2019, The Royal Society. e) Example of a cathecol attachment to an oxide surface at pH 8. Adapted with permission from Ref. 297. Copyright 2017, Company of Biologists Ltd.

during attachment. This has been attributed to 3,4-dihydroxyphenyl-l-alanine (Dopa), which is an abundant catecholic amino acid found in mussel adhesive proteins.[297] This has inspired a wide range of underwater adhesives which have used catecholic-based chemistry to adhere underwater.[299–303] However, as discussed throughout this review, the interfacial chemistry is only one component to generate adhesion and the structure of the attachment features will play a significant role. The bysuss, which is a bundle of filaments secreted by many species of bivalve mollusc that function to attach the mollusc to a solid surface, consists of a bundle of threads and contains three components: spatulate adhesive plaque, a stiff distal portion and a more compliant proximal region, see Figure 30. The mussel plaque is an elliptical spatulate disc that is typically several mm in diameter with a 100 μm thickness.[298] It has been found that the detachment of the mussel plaque is a complex process. Desmond et al. pulled on adhered plaques in different directions while imaging the contact zone.[304] They found that the force-induced yielding of the mussel plaque improves bond strength by two orders of magnitude with an increasing probability of tearing at higher peeling angles and adhesive failure at an intermediate peel angle around 70-90°. These studies show how the mussel attachment in hostile conditions is a function of both the surface chemistry as well as the mechanical properties and loading conditions of the plaque.[304]

7 Examples of peel tests of non-biological systems - Tough and soft materials

Peeling has many uses as a tool to characterize material toughness and adhesion between materials. In this section we will give examples of tough and soft materials that commonly use peeling to characterize properties. This will include discussion of materials such as gels and elastomers, pressure sensitive adhesives, composites, as well as transfer printing and nanoscale peeling. We will also discuss the various microstructures of these materials that lead to the measured properties being used to design materials through peeling characterization.

7.1 Gels and elastomers

Peeling has emerged as an important technique to evaluate both the toughness of gels and elastomers and their adhesion to substrates.[305] For the case of material toughness, common geometries include the T-peel geometry and the trouser tear test. For adhesion measurements, the 90° peel experiments is commonly used. Both experiments allow for the evaluation of the role of adhesion to the substrate as well as identifying the mechanisms that toughen the gels and elastomers, see Figure 31.

Hydrogels are an important class of materials consisting of swollen polymer networks in water (i.e. roughly 60-90% water). Although hydrogels are traditionally brittle, materials science and chemistry have greatly improved their toughness over the past few decades. For example, Gong et al. demonstrated double network hydrogel concepts that greatly increased hydrogel toughness.[306] Here, heterogeneity is introduced by creating interpenetrating hydrogel networks by combining a tightly crosslinked network (first network) with a lightly crosslinked network (second network).[307] This microstructure creates a synergistic effect where the first network is rigid and brittle, such as a polyelectrolyte (poly(2-acrylamido,2-methyl, 1-propanesulfonic acid) or PAMPS for example), while the second network is a soft and ductile polymer, including neutral polymers such as gelatin or polyacrylamide (PAAm). This enhanced toughness in hydrogels has opened up significant research opportunities to make soft and tough materials. As such, multiple studies have utilized peeling as a means to evaluate the material and interfacial properties of gels. This has allowed for the evaluation of multiple network architectures and crosslink chemistries,[308] self-healing approaches,[309–311] and various composite compositions.[28,312–314] The toughening mechanisms of hydrogels are diverse and have been previously reviewed.[315,316]

7.1.1 Peeling for adhesion characterization

The adhesion of gels and elastomers is often evaluated using a 90° peel,[29,317] a 180° peel,[305] or a T-peel geometry.[318] In these experiments the hydrogel is often bonded to or incorporated into a stiff, yet flexible, backing to satisfy the inextensibility assumption in the elastic peeling models. The hydrogel/film composite can then be bonded to different substrates and the peeling experiments can measure G_c. One of the key characteristics to get strong, practical adhesion of hydrogels is to achieve both strong adhesion to a substrate, as well

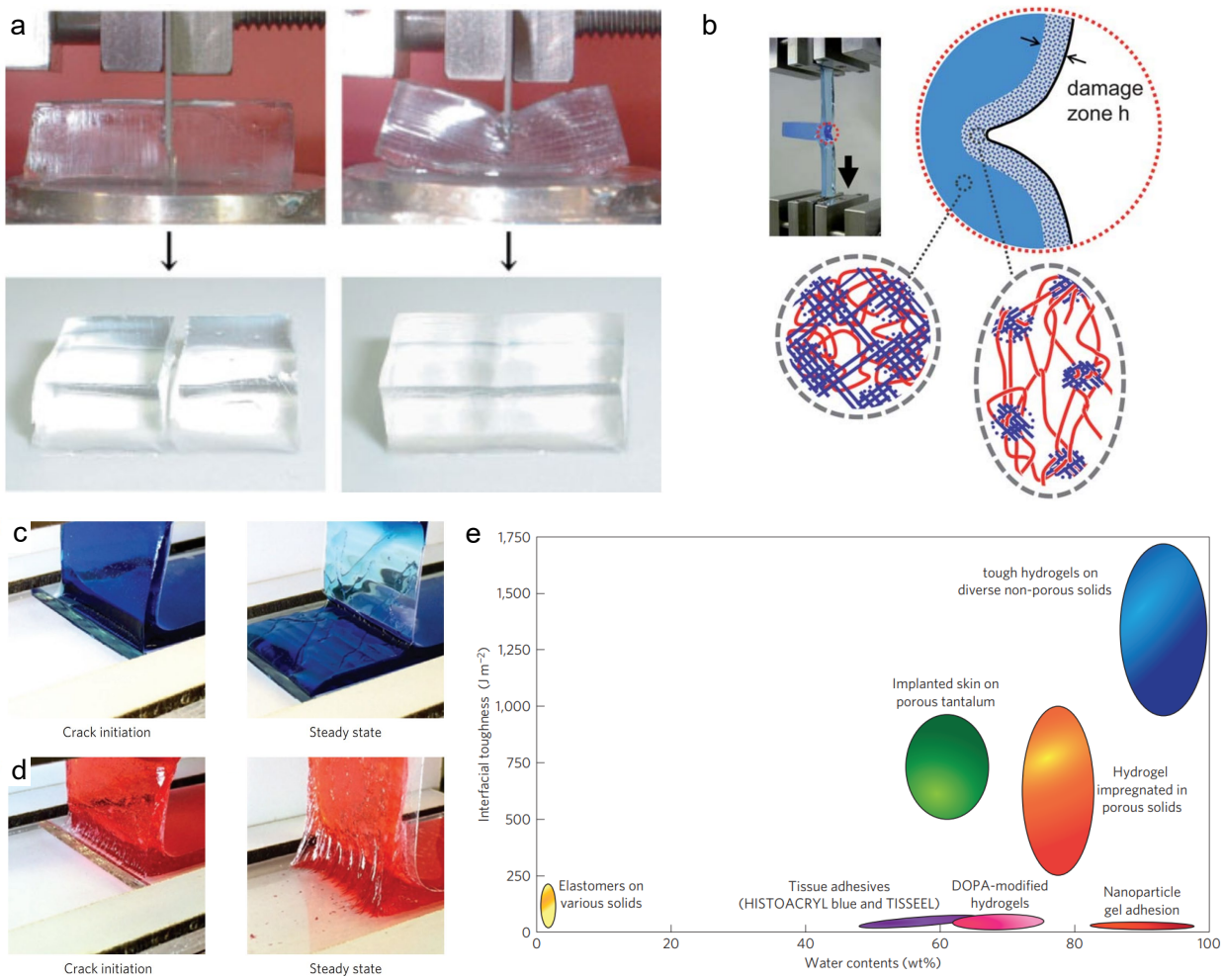

Figure 31: Hydrogels. a) Indentation of a blade into a traditional hydrogel (left) and a double network hydrogel.[306] Adapted with permission from Ref. 306. Copyright 2003, John Wiley and Sons. b) Illustration of the damage zone in a double network hydrogel during a T-peel experiment.[307] Adapted with permission from Ref. 307. Copyright 2010, RSC. c) Image of a common hydrogel chemically anchored on a glass substrate, showing cohesive failure during a 90° peel experiment. d) Image of a tough hydrogel with its long-chain network chemically anchored on a glass substrate, showing adhesive failure during a 90° peel experiment. e) Ashby-style plot showing interfacial toughness as a function of water content for hydrogels.[29] c-e are reprinted with permission from Ref. 29. Copyright 2016, Springer Nature.

as high toughness within the hydrogel.[29] Yuk et al. show that if common hydrogels are bonded to a substrate, or tough hydrogels with weak interfacial bonding (i.e. physically attached) are used, then G_c will be low. When tough hydrogels are chemically anchored to the substrate, then both the intrinsic fracture energy, G_0, and mechanical dissipation in the bulk hydrogel, G_D, can be utilized to give a relatively high $G_c = G_0 + G_D$, see Equations 2.11 and 2.12. In this case, the hydrogels are chemically anchored to the substrate through

an organosilane primer, which chemically bonds to the long-chain polymer network in the hydrogel (polyacrylamide). This combination allows for a hydrogel with 90% water content to achieve G_c values of over 1000 J/m^2 for interfacial failure, which is greater than the bond toughness of bone to tendon.[319] High intrinsic adhesion of hydrogels to substrates can be achieved through a variety of chemical and physical mechanisms. For example, bonding can also be achieved by topological adhesion, where uncrosslinked polymers form a stitch network between two polymers.[320] For a detailed explanation of hydrogel adhesion mechanisms, other excellent reviews are available.[321] In a similar manner, the fatigue of hydrogel adhesion has also been evaluated through 90° peel experiments, where crack extension versus number of cycles, can be measured in a cyclic peeling test.[322] Additionally, T-peel geometries have been used to measure hydrogel fatigue.[323]

7.1.2 Trouser tear for toughness characterization

The trouser tear experiment is also used to quantify toughness of gels, elastomers, and their composites.[28,324–326] The configuration is similar to a T-peel configuration, however, a notch is added to the plane of a material sheet and the two legs are pulled apart. The value of G_c is calculated as $G_c = 2F_c/t$ ¶¶¶ where the thickness, instead of the width for a T-peel configuration, is the relevant geometric parameter for normalization.[327] For both T-peel and trouser tear, the relevant geometric parameter for normalization is the width of the peel front. For example, King et al. created composites consisting of polyampholyte hydrogels and glass fiber woven fabrics, where high effective toughness (250 kJ/m^2) and high tear strength ($\sim$ 65 N/mm) are achieved through the deswelling-aided adhesion of the polyampholyte gel on the glass fabric, which dissipates energy in the polyampholyte matrix and through fiber pullout.[28] As King et al. note, the fiber pull out occurs largely through transverse fiber pullout, so the true surface created by tearing is greater than the crack thickness multiplied by the crack length (as assumed in their calculations). So the G_c value reported represents the effective G_c, not a true G_c, which is further demonstrated as the fracture energy increases with wider samples. Nonetheless, this fiber pullout mechanism produces extremely tough yet soft materials, representing an exciting area for future investigation.

7.2 Pressure sensitive adhesives (PSAs)

PSAs are used in many applications from Post-it Notes™ to duct tape to transdermal skin-patches, where their peel behavior plays a crucial role in product performance. Peel tests have long been a mainstay in the testing and evaluation of PSAs, as shown in Table 3. ASTM D3330, for example, includes both the 90° and 180° peel configurations for testing PSAs. What we refer to as a 0° peel test herein is also a common requirement for PSA tape characterization (Figure 32a), although it provides a very different metric for performance. Whereas higher peel angle test methods seek to quantify energy dissipation during peeling, at what become relatively high strain rates in the thin PSA layer at modest crosshead rates, 0° tests are understood to assess PSA tape durability. These static shear (sometimes referred to as 'shear holding power', an unfortunate misnomer) are typically conducted with a dead

¶¶¶The ASTM-D624 standard also has an extensibility correction, in contrast to peel tests they also report.

load applied, and times to failure are measured. As such, they quantify the resistance to shear deformation and slippage under nominally creep conditions, though the actual stress distributions are more complex.[328] Increases in time to failure for 0° tests are often associated with operating well out on elevated rubbery plateaus. In contrast, higher angle peel tests for PSAs lead to increased peel energies when operating in more dissipative regions of behavior, such as the toe of a transition (e.g. glass transition temperature of the elastomer or soft phase), where tan δ is larger. Hence, energy dissipation associated with peeling at these higher angles often show the opposite trend to 0° tests, which improve with material changes that increase resistance to shear deformation by moving farther from transition regions.[329,330]

A variety of tests to measure tack, the ability to resist removal after very brief and light contact, have been proposed, including the probe-tack test, the rolling ball test, and several peel-like configurations such as the loop-tack (ASTM D6195) and quick-stick test (PSTC 5) (Figure 32). For these tests, the tapes are lightly placed on top of a substrate without applying any significant pressure to adhere the PSA. Thus the weight of the tape and, more importantly, the compressive region (predicted by BoEF model) that precedes the tensile peel front upon peeling, provide sufficient contact pressure to secure the level of contact/wetting deemed appropriate for tack testing. After light contact is made, quick-stick tests are conducted by peeling in a 90° fashion to purportedly assess tack. For the loop-tack test illustrated in Figure 32c, two peel fronts, initially separated by 25 mm, propagate towards one another, each effectively approaching a 90° peel test as the debond tips near one another.

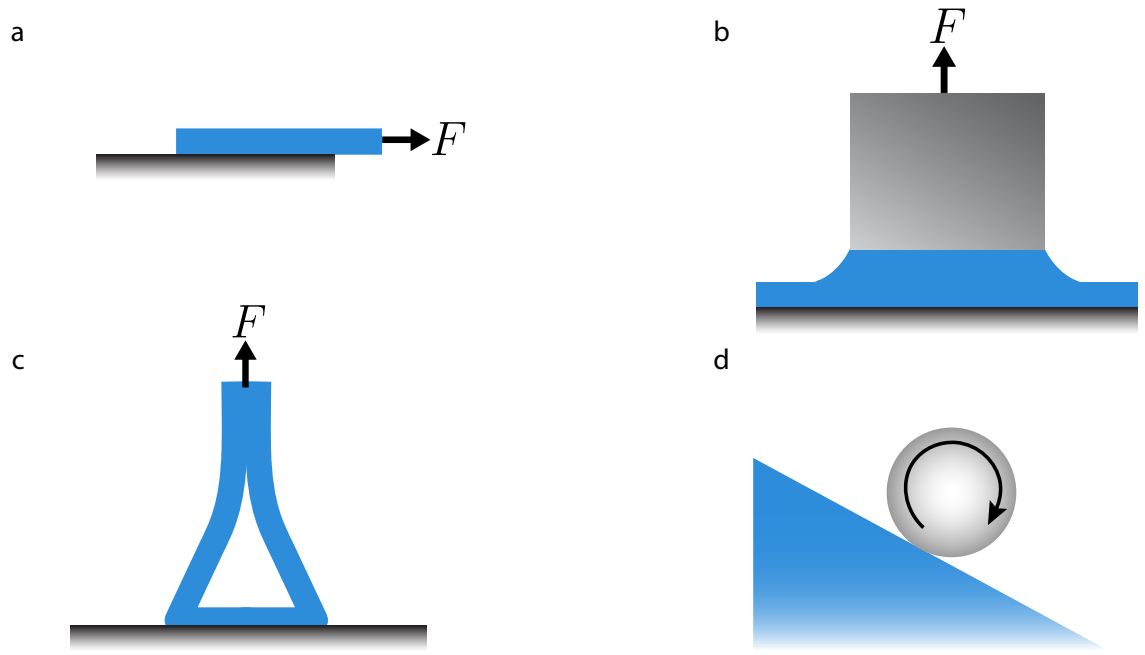

Figure 32: Common PSA tests. a) 0° peel test. b) Probe tack geometry. c) Loop tack peeling geometry. d) Rolling ball geometry. Source: Schematics ©M.D. Bartlett et al., CC BY-SA 4.0. Available at http://hdl.handle.net/10919/113716.

7.2.1 PSA performance and viscoelastic properties

For the design of PSAs, viscoelastic or rheological properties can be used to understand peel performance.[331–335] The viscoelastic properties of PSAs can be evaluated by using dynamic mechanical analysis, where the storage modulus, $G^{'}(\omega)$, and loss modulus, $G^{''}(\omega)$, are evaluated as a function of test frequency, ω, in a rheometer (Figure 33a). One useful approach is to separate PSA adhesion into bonding and debonding steps, where strong correlations between peel strength and $G^{'}$ and $G^{''}$ can be established. Essentially, a material's compliance, $\sim 1/G^{'}$, affects the ability to conform to and wet a surface during the bonding process, as Dahlquist noted in his criterion for PSA tack.[336–341] The parameter $G^{''}$ is associated with dissipation, and is important in the removal or debonding stage, when dissipative mechanisms can greatly enhance the peel resistance. Specifically, the peel energy shows strong correlation to the ratio of $G^{''}(\omega_{debonding})$ at a frequency correlating to the time scale of debonding, to $G^{'}(\omega_{bonding})$ at a frequency related to that of the bonding process (Figure 33b). This behavior is observed in a wide range of PSA products. As such, the adhesive properties of PSAs can be controlled by tuning $G^{'}$ and $G^{''}$ through basic polymer parameters such as molecular weight, molecular weight distribution, the glass transition temperature, and the entanglement molecular weight. Additionally, additives such as tackifying hydrocarbon resin, or rosin, and plasticizers or oil can influence rheological properties. For example, crosslinking polymer chains can significantly increase $G^{'}$ while showing minor increases to $G^{''}$, while adding hydrocarbon resin tends to decrease $G^{'}$ and increase $G^{''}$.[342] However, it should be noted that the values of $G^{'}$ and $G^{''}$ are mutually dependent on one another (through the Kramers-Kronig relationships[343]), hence complicating the formulation process. Work by both Tse and Yang initially proposed that PSA tack could be modeled as $Tack \sim W_{adh}BD$,[331,332] where the bonding term, $B \sim 1/G^{'}(\omega_{bonding})$ and $D \sim G^{''}(\omega_{debonding})$ reflect the roles cited above. The work of adhesion appears, reflecting the important role it plays to enhance the bonding process, but also amplifying energy dissipation by enabling the interface to sustain larger tractions, thus inducing more dissipation during debonding (see Section 2.5).[331] This was later extended from tack to peeling, as shown in Figure 33b.[342] A more recent paper has also explored the relationship between tack and peel.[344]

7.2.2 PSA fibrillation

Tack and peel resistance are both enhanced by fibrillation of the PSA, a topic widely studied.[333,335,339,345–353] Early on, Gent and coworkers explored how cavitation instability would occur when the hydrostatic stress state in an elastomer approaches $5/6E$,[354] reviewed its limitations,[355] and discussed the implications of elastomer fracture emanating from cavities.[356] These ideas continue to be explored and refined and applied to a range of soft or elastomeric materials.[357–359] In the case of peeling, fibrillation is a common mechanism that arises near the crack front during the peeling of PSAs (Figure 34a). These fibrils are the result of void growth which coalesce and then create the fibrillated morphology (Figure 34b).[360] Examples of fibrillation during the peeling of PSAs are shown at two different scales in Figure 34c,d, where the fibrils appear as highly elongated, string like features. These fibrils are akin to the Lake-Thomas model in that breakage of the discrete individual fibrils leads to nearly complete loss of any elastic energy stored therein. Therefore, fibrillation results in significant

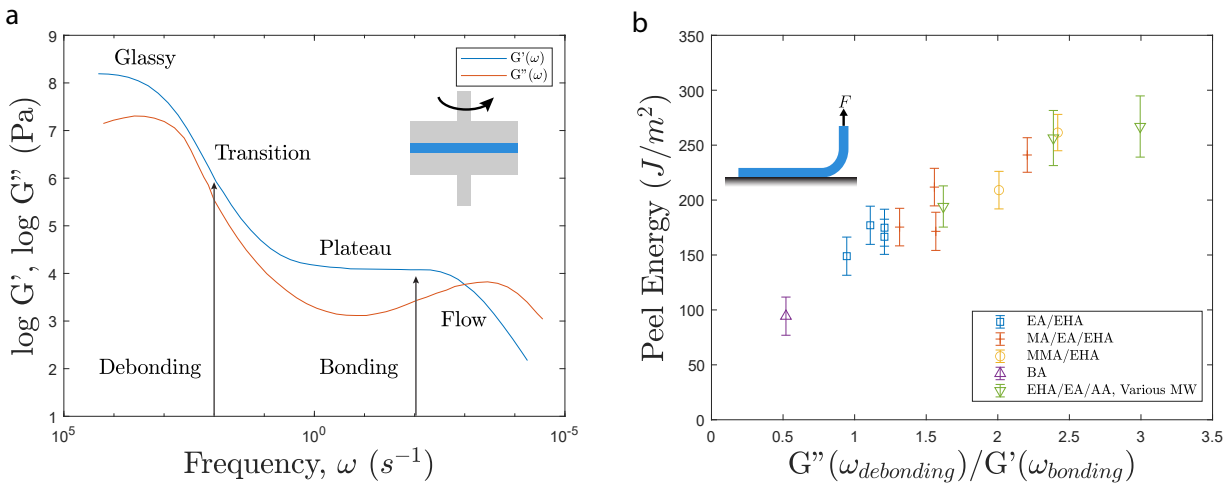

Figure 33: Pressure sensitive adhesive (PSA) analysis and correlation. a) Rheometry analysis of an idealized adhesive showing storage modulus, $G^{'}$, and loss modulus, $G^{''}$, as a function of frequency of the experiment. Adapted from Ref. 342. b) Correlation between peel strength and $G^{''}(\omega_1)/G^{'}(\omega_2)$ (as measured at the temperature of bonding and debonding processes). Polymers are based upon ethyl acrylate (EA), 2-ethylhexyl acrylate (EHA), methyl acrylate (MA), methyl methacrylate (MMA), butyl acrylate (BA), acrylic acid (AA); and (MW) is molecular weight. Adapted from Ref. 332.

energy dissipation and higher peeling forces as a result of the cavitation and new surface generation, rheological stretching of the fibrils (i.e. legging), and then their breakage.

7.2.3 Peeling in multifunctional PSA systems

As an example of PSAs as advanced, multifunctional materials, research conducted by Mohammed et al. and Rizi et al. was aimed at developing single-layer drug-in-adhesive patches specifically for the human nail with fungal infections.[346,361,362] Here, the PSA contains the drug which is sandwiched between an impermeable polyester backing-membrane and a release liner,[346,361–365] with the release liner being removed just prior to the patch being applied to the patient. The work presented in the earlier papers focused on testing and modeling a peel test at different speeds and with patches of increasing PSA thicknesses, which both directly relate to the pain level suffered by a patient upon removal of the patch.[346,361] In these studies the PSA contained no drug and was bonded to a high-density polyethylene substrate. (High-density polyethylene was selected as the substrate since it possesses a surface energy similar to that reported for the human fingernail plate). The effects of drug-loading and changing the interface to human nails on the peel force were reported in a subsequent publication.[362]

7.2.4 CZM Modeling of PSA systems

Fixed-arm peel tests were performed at various peel angles, at a constant rate of crack growth, and the peel forces needed to cause crack growth along the PSA-polyethylene sub-

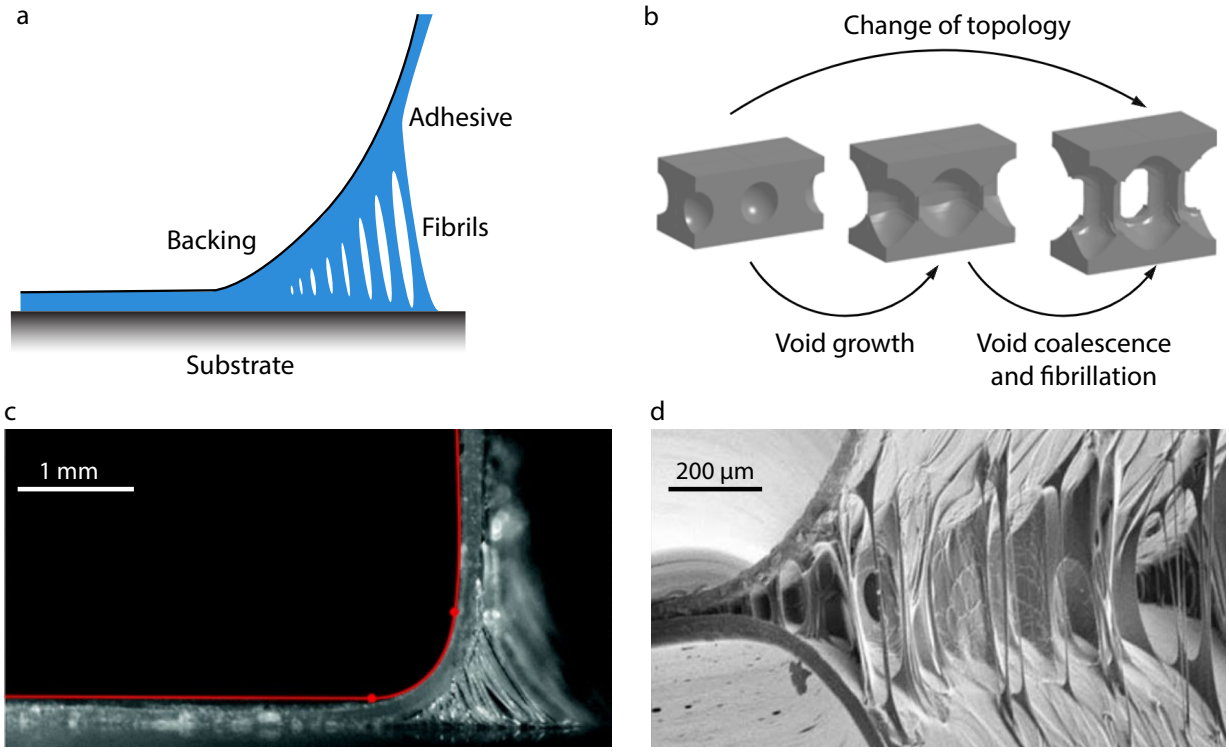

Figure 34: Fibrillation in pressure sensitive adhesives (PSAs). a) Schematic of a PSA undergoing fibrillation during peeling. b) Schematic showing the progression of topology that leads to fibrillation. Adapted with permission from Ref. 360. Copyright 2012, Elsevier. c) Representative image of fibrillation during peeling. Adapted with permission from Ref. 344. Copyright 2020, Royal Society of Chemistry. d) SEM micrograph showing a PSA under fibrillation during peeling. Adapted from and with permission of Ken Lewtas.

strate interface were measured.[346] FEA peeling simulations were conducted, modeling the backing membrane as an elasto-plastic power-law material and the adhesive as a visco-hyperelastic material. The material properties of the polyester backing membrane and the PSA were measured from tensile and stress-relaxation experiments. The properties of the PSA/polyethylene substrate interface were modeled using a CZM. The parameters required for the CZM, namely the critical stress, σ_{max}, and the fracture energy, G_c, were calculated analytically from a poker-chip probe-tack test. The latter method was found to give the more meaningful values of the CZM parameters. Thus, the values of σ_{max} and G_c from the poker-chip probe tack test, measured at the appropriate rate of test, were used to undertake predictions of the behavior of the peel tests using the FEA model. It was found that the numerically-predicted peel forces were in good agreement with the experimentally-measured peel forces over the range of peel angles studied. The accuracy of the FEA peeling model supported the poker-chip probe-tack method for determining independently, by direct measurement, the CZM parameters of σ_{max} and G_c. A second paper also demonstrated good agreement between the experimentally-measured and numerically-predicted peel forces for the different peel angles that were employed but now at various rates of test and for different values of the thickness of the PSA layer.[361] In addition, it was proven that the rate depen-

dence observed in the peel and probe-tack data was dominated by the rate dependence of the interface properties, i.e. the time dependence of the two CZM parameters of σ_{max} and G_c, rather than the time-dependent bulk viscoelasticity of the PSA. A final paper applied the results from these studies to assist in defining the best patch formulation, e.g. one that is occlusive, can be peeled off the nail plate cleanly and where the drug can be added to the PSA at a relatively high concentration and remains stable upon patch storage.[362] This work identified key structure-property relationships and a major finding was that the PSA possessing carboxylic groups exhibited greater drug solubility, possibly due to interactions with the amine moieties in the drugs, and gave the best peel behavior in terms of obtaining a clean interfacial failure at the PSA/nail interface. Therefore, these peel and drug modeling studies paved the way for a systematic and novel approach to the formulation of simple drug-in-adhesive fungal patches for the topical treatment of nail diseases.

7.2.5 Tape backing stiffness: insights from complementary energy

When debonding advances by an increment a in length during self-similar peeling, the force F_c is constant, and performs work as it moves through a distance $(1-\cos\theta)a$ due to the peel angle, plus an additional distance of εa due to extension, where ε is the peel arm strain. So, at a fixed value of G_c, peel arms with greater extensibility admit greater work input, and thus will generally debond at a smaller F_c than stiffer systems with the same G_c. As noted earlier, the difference between the input work (at constant force) and the strain energy is the complementary energy, which is the net energy that is available to drive fracture by an increment a. This complementary energy input into a debond increment of a (less any energy dissipated by bending and reversed bending) drives debonding, regardless of whether the peel arm extends in an elastic or inelastic manner – a somewhat surprising fact that results because tensile loading is not reversed during peeling, as seen in Section 3.2.2. (Note, however, that the complementary energy conceptually can be zero if all the extensional work goes into strain energy, e.g. if completely dissipated within the arm, as would be the case with perfectly plastic behavior.) The bending dissipation may also be negligible when the peel arm is very thin, or if peeling occurs at small peeling angles. Finally, if the peel arm is viscoelastic, the complementary energy should be based on the instantaneous response. Any additional deformation can be understood as creep, occurring at the constant force, F_c, and the work input during this subsequent time-dependent deformation goes into viscous dissipation and perhaps some stored energy that is only recoverable over time when unloaded, but is not available to drive debonding.

Returning to the extensional work, strain energy, and complementary energy for self-similar debonding, if linear elastic, the (elastic) strain energy and complementary energy are equal and each are half that of the input work, as is illustrated in Figure 35a. For a stiffening material Figure 35b, the larger complementary energy reduces the force required for debonding, whereas for a softening material (Figure 35c), more of the work input goes into strain energy, leaving less complementary energy available for crack propagation, hence requiring a higher force to debond. Consider the case of a more and less extensible peel arm illustrated schematically in Figure 35d. Thus, for a G_c, a stiffer material requires more force and deflects less than a more extensible material. Stretch-release adhesives, such as illustrated in Figure 35e take advantage of this by using highly extensible adhesive strips

(e.g. a removable wall hanger). Figure 35 shows the force-deflection curve for a stretch-release wall hanger adhesive strip of guage length $L = 50$ mm, showing the complementary and strain energy partitioning if stretched to five times its initial length.

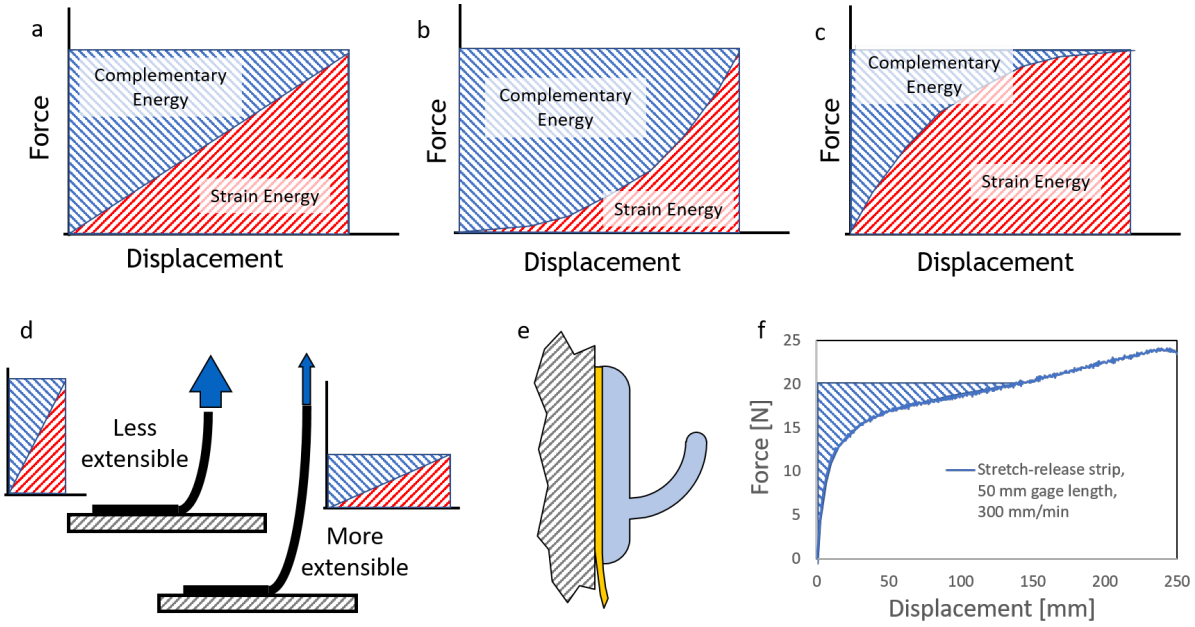

Figure 35: Complementary energy during self-similar debonding. For each of these images, we consider the case of the tensile load-deflection behavior of an increment, a, being debonded in a self-similar manner from the substrate at F_c. The diagrams all assume debonding occurs at a given G_c, and apply regardless of whether tensile deformation is elastic or inelastic, providing bending dissipation is negligible: a) For linear-elastic behavior; b) For a stiffening material; c) For a softening material; d) Illustration of consistent amounts of complementary energy for stiffer and softer peel arm debonding; e) Sketch of a stretch-release adhesive for commercially available wall hooks, f) Tensile load-deflection curve for a 50 mm long stretch-release double-sided adhesive tape strip. The shaded area is the complementary energy corresponding to a tensile force of 20 N. With the exception of any rate dependent extension on the time scale of 1 minute, this complementary energy would then be available to drive debonding for 50 mm along both the wall and hook interfaces, if debonding were to proceed at this force value. Source:

7.3 Composites

There are only a few papers where the peel arm has been a polymer-matrix continuous-fiber composite which is bonded to an underlying rigid substrate. Clearly, one problem is that such composite materials have a relatively high modulus, and thus would require long distance peel tests to achieve self-similar debonding configurations. A second problem is that such materials do not undergo significant plastic yielding. Thus, even when moderately thin peel arms are used, polymer-matrix continuous-fiber composites will not readily bend to

conform to the required angle; and if low peel angles, θ, are employed then the thin composite peel arm tends to fracture under the relatively high loads imposed. Indeed, these are the fundamental reasons why the LEFM DCB test is the common and standard[109] method for determining the fracture energy, G_c, of adhesively-bonded composite joints.

Nevertheless, de Freitas et al. have reported using the floating-roller peel test rig, which gives a peel angle of nominally 135°, see Figure 16a, where the peeling arm was a thin layer of unidirectional CFRP with an arm thickness of 0.37 mm.[366–368] They found that the measured peel force, F_c/w , per unit width for these tests was very significantly lower than that measured when a thin aluminum-alloy peel arm was used, even when the locus of failure was essentially cohesive in the adhesive layer in both types of test. This is, of course, due to the extra energy dissipated in the peel test by plastic deformation of the aluminum alloy, which leads to a relatively high value of F_c/w, as has been discussed above. Since, the effect of the type of composite and thickness used for the peeling arm was not quantitatively accounted for in such peel tests, it would appear that the use of the LEFM DCB test specimen,[109] which is an ISO Standard test method, would appear to be the better route by which to assess the toughness of adhesively-bonded composite joints.

On the other hand, Su et al. have developed a mandrel peel test to study the adhesion of a titanium-alloy bonded to a thermoplastic-matrix unidirectional continuous-carbon fibre composite.[369] The CFRP peel arm was a single-ply with a thickness of 0.15 mm and possessed sufficient flexibility and resistance to fracture to conform to the diameter of the mandrel used in the peel rig. Furthermore, these authors developed an analysis to derive the fracture energy, G_c, from their tests, which also included the effect of residual stresses in the joint and frictional effects in the mandrel peel test. They concluded that the mandrel peel test did indeed allow the ready characterisation of high toughness interfaces when a relatively thin, flexible and resistant to fracture CFRP could be used. The peeling of composites has also been performed to determine the degree of prepreg tack.[370–373] This allows for the prepreg to be bonded to and peeled from a substrate in a single continuous motion. Through this method the measured tack for carbon-fibre/epoxy prepregs can be evaluated as a function of different parameters, such as feed rate and temperature as well as surface conditions.

Finally, although not adhesive joints *per se*, it is noteworthy that mandrel peel tests and climbing drum peel tests, see Figure 16b and Figure 16c, have been used with some success to determine the interlaminar failure of polymer-matrix continuous-carbon fibre composites.[374–376] In these cases a thin, upper layer of the CFRP was peeled away from the underlying composite material and analyses were proposed to determine the interlaminar fracture energy, G_c, of the composite material.

7.4 Transfer printing

Peeling is often associated with the delamination of one or more thin materials, so extensions to the transfer of thin films and functional materials have recently received considerable attention. This has given rise to transfer printing techniques to assemble layered architectures of different materials, see Figure 36. Applications for these techniques include the assembly of thin film and flexible electronics, photovoltaics, and artificial skin.[377] Adhesion has played an important role in these processes, where the transfer of objects from one substrate to another can be controlled by modulating the adhesion force. The attraction forces on these

typically involve van der Waals and related mechanisms, where work of adhesion values up to several J/m^2 have been reported. Successful transfer printing, however, requires transfer of these films from the carrier layer to the desired substrate with very high reliability. One example of adhesion control has been demonstrated by controlling the pick and place velocity (i.e. kinetic control). Here, an elastomeric stamp rapidly peels objects off of one substrate ('donor'), giving high adhesion to the stamp for picking objects. Then the stamp is placed on a second substrate ('receiver') and slowly retracted, giving low adhesion to the elastomeric stamp, and transferring the objects to the receiver substrate.[378] Although kinetic control can be used to transfer print, many other mechanisms have also been utilized.[379] This includes a variety of triggers to activate and release adhesion, including pneumatic systems,[380–382] mechanically actuated systems,[383–389] phase change materials,[390–392] and electromagnetic approaches.[393–396] Other techniques can use subsurface features to push the object off of the substrate.[397]

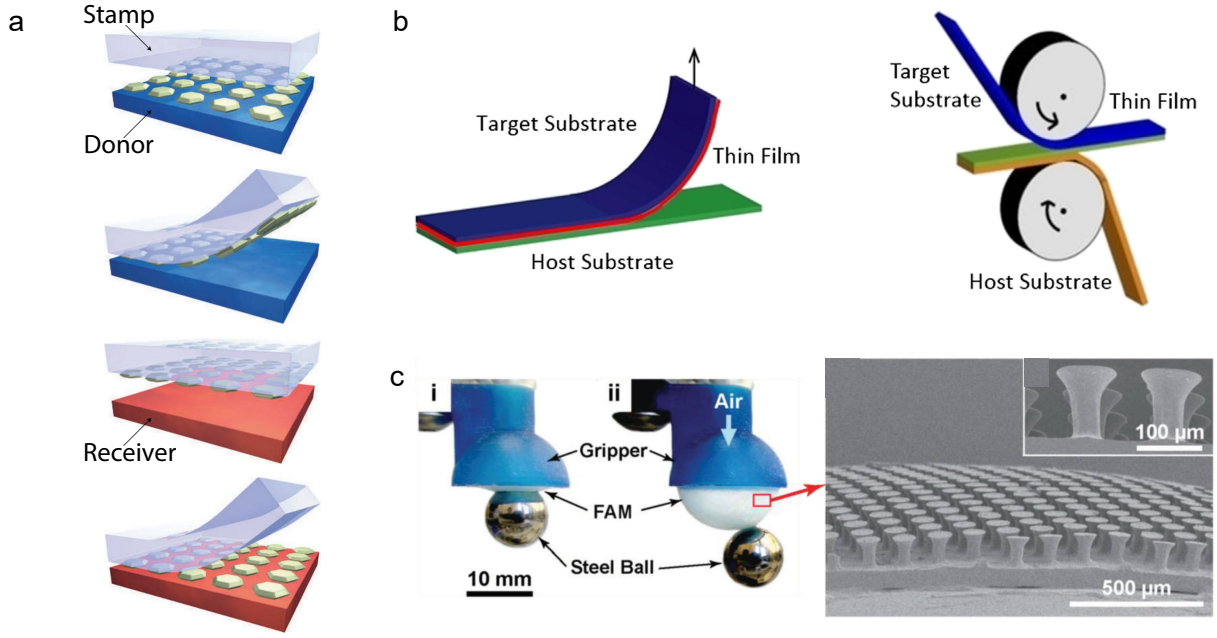

Figure 36: Peeling in transfer printing. a) Process diagram showing the transfer printing process, where an ink is pickup off of a donor substrate by a stamp and then printed into a receiver substrate. Adapted with permission from Ref. 378. Copyright 2006, Nature Publishing Group. b) Transfer printing process where a thin film is transferred from a host substrate to a target substrate. Adapted with permission from Ref. 377. Copyright 2019, AIP. c) Transfer printing with a micropatterned, pneumatically actuated stamp to pick and place steel balls. Adapted with permission from Ref. 382. Copyright 2014, John Wiley and Sons.

7.5 Nanoscale peeling

Having exceptional mechanical, electrical, and chemical properties, graphene offers unique promise for a number of applications, including flexible electronics, leading to efforts to

produce graphene sheets of large dimensions.[398] The rise of graphene was in part assisted by peeling, where a sticky tape was used to mechanically exfoliate by repeated peeling of pyrolytic graphite down to a few atomic layers, including single layer graphene.[399] An extensive review of graphene, including mechanics of adhesion and friction at interfaces, outlines their properties and opportunities.[400]

Graphene sheets have been grown on copper, nickel, and ruthenium foils using chemical vapor deposition processes.[401] Cao et al. have used deionized water to pressurize photoresist and graphene films suspended over a 1 mm diameter hole on polished copper plates to obtain work of adhesion values of 0.44 and 0.52 J/m^2, respectively.[401] By capturing interferometric images of blister height, they reported errors in simple plate models that were addressed by including residual stress and bending stiffness effects in the model. They have also examined mixed-mode fracture analysis of such graphene blister specimens.[402] Jain et al. developed a series of fracture maps by using cohesive zone models (with assumed fracture energies that were independent of mode-mixity) to predict interface selection delamination while parametrically varying moduli, peak tractions, fracture energies, and initial crack length.[377] Based on over one hundred simulations, they found the clearest correlation in predicting interface selection at the desired interface, as required for successful transfer printing, by determining which interface had the lowest mode-mix angle. They subsequently applied similar methods to graphene transfer.[403]

Peeling has also be extended to one-dimensional geometries including carbon nanotubes (CNT) that are peeled away from themselves or from flat surfaces. Plaut et al. analyzed carbon nanotubes and graphene nanoribbons folded into tennis racket shapes,[404] where van der Waals adhesion is balanced with bending energy in a geometry earlier considered by Gent as a possible method to characterize peel adhesion.[405] Using an elastic continuum analysis, they reviewed prior work and corrected the resulting contact lengths reported by others. Peeling of single-walled CNT (SWCNT) has been been conducted, examining peeling, stick-slip frictional behavior, and buckling,[406] and of SWCNT bundles.[407] Nanowire and SWCNT and multi-walled CNT (MWCNT) peeling has been addressed using the Kendall model of the continuum mechanics.[408] Chen, et al have used a nanomanipulator to peel a bundled CNT from a calibrated atomic force microscope tip.[409] Peel testing has also been conducted on spinnable CNT webs.[410]

In addition to carbon-based materials, nanoscale peeling has been utilized in a variety of thin films including inorganic materials,[378,411] metals,[412–414] organic materials,[415–417] and biological materials.[418–420] For example, germanium nanowires with diameters of ∼30 nm can be assembled on 100 mm silicon wafers by transfer printing.[421] Additionally, organic semiconductors such as pentacene can be assembled with PDMS stamps directly onto transparent conductors such as indium tin oxide.[422] In some cases, multiple types of materials need to be assembled together to create integrated devices, such as organic thin-film transistors, which require metals, polymers, and organic semiconductor layers.[423] Nanoscale films of biological materials such as proteins can also be utilized to strongly adhere to wet surfaces such as hydrogels and tissues.[424]

7.6 Peeling in additive manufacturing

Additive manufacturing (AM) has gained widespread interest, not only for prototyping, but increasingly for fabrication of engineered components and products across a wide range of length scales.[425,426] Successful printing, dimensional stability, and structural integrity of these products revolve around adhesion at the myriad interfaces that result from the various AM processes. In some methods, including powder bed fusion of polymers and metals, and fused filament fabrication (FFF) of thermoplastic polymers, adhesion results from a sintering-like fusion of entities ranging from fine particles to polymer filaments. In multi-jet printing, stereolithography (SLA), and digital light projection (DLP) printing of photo-polymers, a liquid monomer or oligomer is photo-cured onto the preceding print layer. In all of these and other AM processes, satisfactory printing and subsequent performance relies on the quality of each internal interface. Characterizing these interfaces has proven to be a challenge, and initial efforts have largely focused on measurements of stiffness, strength, and hardness. Increasingly, however, researchers are turning to fracture tests, including peeling, to characterize print interface quality. For example, He et al. have used an essential work of fracture (EWF) method to evaluate the fusion bonding between the filaments by determining the value of the specific essential work of fracture, W_e, and the associated experimental reproducibility from test specimens printed using a FFF manufacturing route.[427,428] These authors considered that the EWF test method was more suited to the specimen geometries that they were able to 3D print than a peel test. However, on the other hand, Vu et al. explored the use of several DCB configurations to quantify the fracture resistance of UV-cure acrylic specimens consisting of an elastomeric interlayer between glassy arms as a function of build direction, and used T-peel configurations showing intriguing preliminary data that hierarchical interfaces between glassy and rubbery layers can significantly increase adhesion in AM products.[429] Butt et al.[430] explored the peel resistance of aluminum/copper laminates produced by a process they refer to as "Composite Metal Foil Manufacturing". Seppala et al.,[431,432] Davis et al.,[433] and Gilmer et al.,[434] for example, have utilized peel testing to characterize the interfacial adhesion of FFF specimens consisting of a wall of single-road specimens, in what appears to resemble a tear test.[327] Parandoush et al.[435] utilized a laser assisted AM technique for the creation of continuous fiber reinforced thermoplastic polymer composites and utilized lap shear strength and peel strength testing to evaluate bond strength. These and other peeling configurations are likely to be employed as AM processes and characterization methods continue to evolve.

7.7 Peeling control through geometry and active materials

As we noted previously, the stiffness of the peel arms can significantly impact the peeling behavior. An interesting experiment illustrating purely elastic crack-stopping was carried out by Kendall.[108] Using smooth elastic rubber healed back onto a glass surface, an elastic peeling film under steady force at constant velocity was made to hit a film of the same thickness but reinforced with fibers to raise its Young's modulus. The peel crack was arrested or considerably slowed, but once the crack moved past the region with the change in modulus, the peeling sped up back to its original value, even though the film was now much stiffer. The elastic modulus or bending stiffness does not enter the 90° peel equation $F/w = G_c$,

but the peel force is strongly influenced by a local change in elastic modulus that can cause crack stopping. At this discontinuity, the adhesive force can be changed by:

$$\frac{F_{c,s}}{F_{c,c}} = \frac{E_s I_s}{E_c I_c} \tag{7.1}$$

where the subscripts s and c denote the stiff and compliant terms, respectively. A sudden increase in thickness of the peeling film gives the same effect: the crack tends to stop at the change, but speeds up again once it has fully passed the thickness change. This is understood in that at an abrupt change in bending stiffness, propagation ceases to be self-similar. Thus, in the local vicinity of such perturbations, there is a transition from self-similar (independent of bending stiffness) to locally-controlled debonding, which is dictated by the bending stiffness contrast.

Additionally, directional geometric or material features can be incorporated into film adhesives.[436–441] Kirigami approaches have also been shown to be effective to control peel adhesion, see Figure 37. Here, an adhesive film is laser patterned to create cut structures. These cut structures in the films define stiff and compliant regions that can be used to control local bending rigidity and contact area. This allows for the spatial control of adhesion as well as a mechanism to enhance adhesion and provide different peeling characteristics in different directions for anisotropic adhesive response.[31] The kirigami structure can also manipulate the local stress fields and delamination behavior, which can be used to enhance adhesion to underlying, deformable substrates.[442]

Another approach is to incorporate active materials to control peeling. For example, electroadhesion can be utilized in manipulation tasks with soft grippers to control adhesion.[445] For example, the electrostatics technique can be used to manipulate different objects by applying voltages in carbon electrodes within silicone adhesives.[443] Additionally, granular jamming, where granular materials lock together to become stiffer, has been used to control bending rigidity across an adhesive strip. Here, granular jamming through pneumatic control allows the control of crack initiation, propagation, and arrest by integrating a granular jamming layer into adhesive films.[25] Electromagnetic stimuli such as light can be introduced to give peeling control. For example, when using azobenzene-containing crosslinked liquid crystalline elastomers (LCEs), the adhesion can be activated and released through the application of UV light.[444]

8 Conclusions and future work

The peeling apart of materials and interfaces is ubiquitous. Although peeling is often a simple experiment, the analysis method strongly depends on the materials, geometry, and loading conditions of the experiment. Thus, the analysis method must be carefully chosen and properly applied to extract the relevant adhesion and material properties of interest. As such, the microstructure and processing of the adhesive materials must also be considered, as properties such as modulus, toughness, and heterogeneity can influence the evaluation method and analysis. Peeling impacts multiple current and emerging technologies, not only as a tool for evaluation of key properties, but as a mechanism for the control of adhesion to

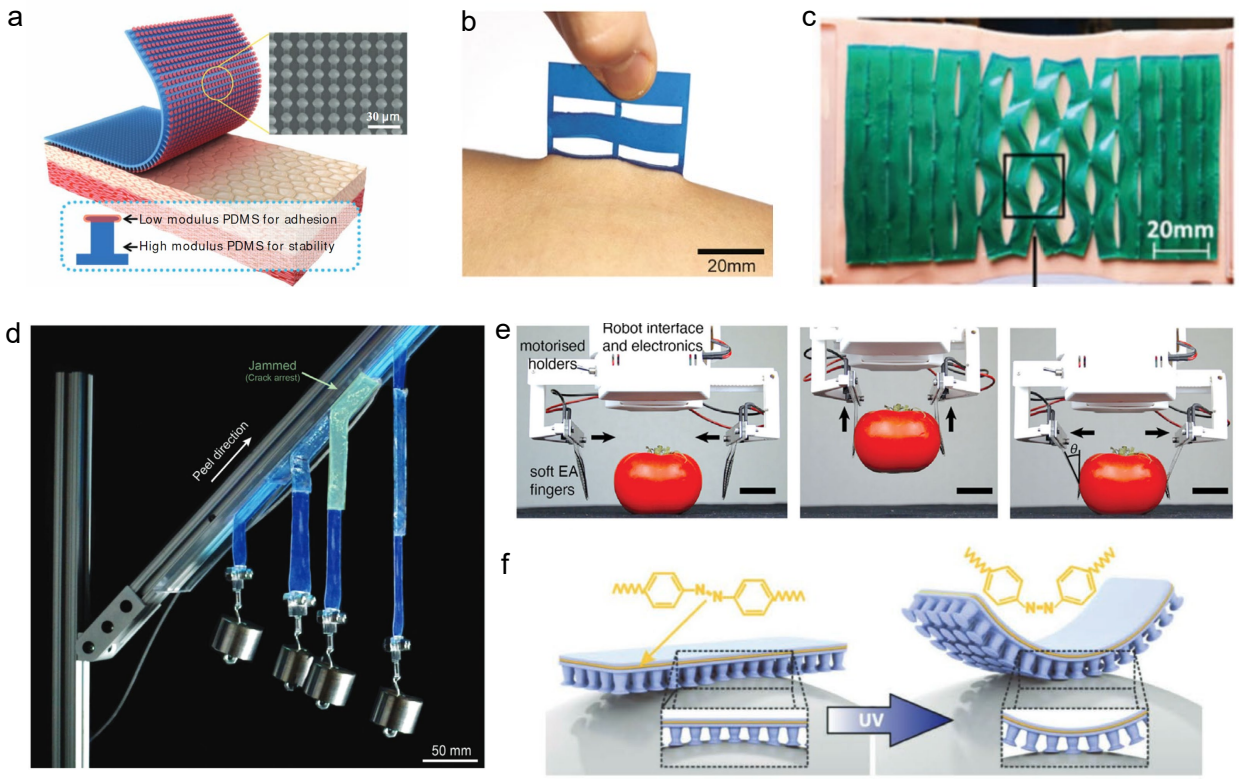

Figure 37: Peeling control through geometry and active materials. a) Micropatterned adhesive film for enhanced skin adhesion. Adapted with permission from Ref. 438. Copyright 2013, John Wiley and Sons. b) Kirigami-inspired adhesive film for enhanced and anisotropic adhesion control. Adapted with permission from Ref. 31. Copyright 2018, ACS. c) Kirigami enhanced film adhesion for bonding to non-homogeneous substrates. Adapted with permission from Ref. 442. Copyright 2018, RSC. d) Control of peel crack initiation and propagation through jamming based switchable adhesives. Adapted with permission from Ref. 25. Copyright 2021, RSC. e) Electrostatic control of peel adhesion. Adapted with permission from Ref. 443. Copyright 2022, Elsevier. f) Light control of film adhesion. Adapted with permission from Ref. 444. Copyright 2017, AAAS.

impact advanced functionality. Moving forward, we anticipate several future possibilities for investigation, including:

1. Reversible adhesives represent an intriguing area for future work to develop strong adhesives that can be easily removed and reused. Two broad categories of reversible adhesives are 1) passively reversible, where no additional energy input or mechanisms are required to reverse adhesion, and 2) actively reversible adhesives which are commonly referred to as switchable adhesives, where additional energy input or mechanics are required to reverse adhesion. Both approaches rely on manipulating how cracks move at the interface, where strong adhesion is achieved by preventing crack propagation and adhesion release requires cracks to propagate easily. Although this control has been demonstrated in several examples and is an active area of research, new materials and geometries should be developed to better achieve more dramatic and controllable

changes in adhesion strength. Such adhesives have large potential for applications in medical use, manufacturing, recycling and advertising and camouflage, where you could remove a large sheet very readily (and intact for use another day) and then bond on a new large sheet onto an advertising board (or onto a plane, ship or tank to change its camouflage).

2. Improving the ability to accurately calculate the energy for plastic bending for peel tests, where this is a very dominant feature, such as in toughened epoxy/aluminum peel joints and to more accurately extract values of G_c using the combination of test results and modeling. This is attractive from an experimental viewpoint because peel tests are often easier and are less costly to conduct than DCB or TDCB tests. Additionally, peel tests are attractive for accelerated testing, where the temperature is controlled or cycled because the samples generally have lower thermal mass than DCB or TDCB samples (e.g. Ref. 446).

3. As noted in the text, both the relevance and importance of mode-mixity for peeling remains an active research area with contrasting viewpoints being presented. Classic methods to determine mode-mixity are likely inappropriate for many practical bonded systems. On the other hand, modeling capabilities, such as those provided by CZM/FEA approaches, seem relevant for improving our understanding of the roles that opening and shearing actions have on the resistance to fracture, the resulting locus of failure, and their inextricable connection. However, these approaches have yet to fulfil their initial promise, possibly since the CZM concept is empirical and a choice must be made *a priori* on the presence, or not, of mode-mixity effects in the CZM. Nevertheless, these and other methods may offer potential to better understand and model their effects, especially if simplifications can be made to make such solutions tractable for practitioners.

4. We need to be able to predict the peel behavior more accurately. As discussed, stick-slip behavior is a complex, multiphysics problem that remains complicated to model and understand, and yet precipitous drops in peel energy can be frightening in concept. The rate dependence of debonding, coupled with the system compliance and inertia, all play important roles in the transition from stable to stick-slip (and reverse) transitions, confounding our efforts to reliably predict system behavior and performance. The gecko adhesive system utilizes stick-slip like processes combined with a large number of contacts to make reliable attachment during slipping events. Such examples from nature can be harnessed to rapidly and reliable control adhesion as we gain a better understanding of underlying phenomena.

5. Although significant progress has been to understand and mimic adhesives found in nature, there are still many opportunities to further this work. Many organisms have unique needs and are equipped with certain material assets, which often leads to impressive performance in a specific environment. For example, geckos excel in dry environments while mussels thrive in wet environments. Synthetic adhesives inspired by these systems have opportunities to combine promising characteristics of both systems through materials design and chemistry. A notable example of this approach is the

"Geckle" adhesive which combines gecko-like fibrils with mussell-inspired chemistry.[299] Further, developing synergistic combinations of natural adhesive mechanisms into engineered systems could create adhesives suitable for multiple environments or adhesives that excel in environments not typically observed in biological organisms (i.e. high temperature, low temperature, vacuum).

6. Adhesives for biomedical applications also represent a significant need. From adhesives for bandages and long term-use adhesives for health monitoring to sealing tissues rapidly and temporary attachment during surgery, adhesives are a critical component in the biomedical space. Continued progress in this area requires adhesives that provide the desired response – secure adhesion when desired yet the ability to be removed without tissue damage – as well as the functionality required for biomedical use. This includes being bio-compatible, adhesives capable of delivering drugs, and adhesives that degrade over relevant timescales. Peeling will play a major role in these developments both as a tool for characterization of new materials as well as a mechanism to create adhesives that can be strong, reversible, or have specific adhesion characteristics across different areas of a biomedical film.

Acknowledgements

We acknowledge thoughtful conversations with Kevin Kendall. MDB acknowledges support from the National Science Foundation under the DMREF program (award number: 2119105). We are also grateful for figure help from D. Albacarys.

Appendix A

The generalized Irwin-Kies relationship has the form:[71]

$$G = \frac{n}{n+1} P^{\frac{n+1}{n}} \frac{dC}{dA}$$

Below are examples for different values of n.

1. $n = 1$, typically involving linear extension, bending, torsion, or highly pre-tensioned stretching:
   (a) the 0° peel configuration and related in-plane stretching tests[10,61,120]
   (b) bending-dominated tests, such as the double cantilever beam and double encastred beam
   (c) torsional geometries[4]
   (d) shallow angle peel and blister tests involving out-of-plane stretching that is dominated by large residual tensile stresses present[154]
2. $n = 3$, which often arises with out of plane stretching for constrained membranes or peel arms:

(a) Gent and Kaang's pull-off test, where stiffness results from out of plane stretching[131]

(b) extensions of this from uniaxial stretching to biaxial out-of-plane stretching in blister-like configurations[146,154]

3. $n = \infty$ is an idealization that the structure is perfectly rigid in stretching and combined with no stiffness in bending. For such cases, $dU_E = 0$, so energy is supplied solely by the work input of the external force(s)[‡]:

   (a) Rivlin's peel relationship ignoring possibility of stored energy[60]

4. Combinations of n are also common, including:

   (a) Where compliances for deformation modes are uncoupled, so add easily and allow the generalized Irwin-Kies relationship to apply:

      i. Lindley's extension of Rivlin's solution to include peel arm stretching which combines $n = 1$ and $n = \infty$ forms[61]

   (b) Where compliances are coupled, so direct use of the Irwin-Kies is more involved:

      i. Examples include situations in which both bending ($n = 1$) and out-of-plane stretching ($n = 3$) relationships contribute to the overall stiffness, resulting in complex transition regions that have been analytically approximated for linear,[132] axisymmetric punch adhesion,[447] and circular configurations (subjected to pressurization or central loading).[149,157,448] Numerical methods have also been used for these more complex transition relationships.[135,137,149,448]

[‡]For such idealized cases, 'strain energy release rate' may be semantically less appropriate than 'energy release rate', used in the Griffith sense including all potential energy (work and elastic) of the system. This distinction disappears for real systems, however, where even the smallest amounts of stored elastic energy are sufficient to supply energy for a virtual crack advance in the absence of external work.

9 References

[1] S. P. Timoshenko, *History of Strength of Materials*. New York, USA: McGraw-Hill, 1953.

[2] H. Yuk, C. E. Varela, C. S. Nabzdyk, X. Mao, R. F. Padera, E. T. Roche, and X. Zhao, "Dry double-sided tape for adhesion of wet tissues and devices," *Nature*, vol. 575, no. 7781, pp. 169–174, 2019.

[3] K. Autumn, Y. A. Liang, S. T. Hsieh, W. Zesch, W. P. Chan, T. W. Kenny, R. Fearing, and R. J. Full, "Adhesive force of a single gecko foot-hair," *Nature*, vol. 405, no. 6787, pp. 681–685, 2000.

[4] J. O. Outwater and D. J. Gerry, "On the fracture energy, rehealing velocity and refracture energy of cast epoxy resin," *The Journal of Adhesion*, vol. 1, no. 4, pp. 290–298, 1969.

[5] G. Spies, "The peeling test on redux-bonded joints: A theoretical analysis of the test devised by Aero Research Limited," *Aircraft Engineering and Aerospace Technology*, vol. 25, no. 3, pp. 64–70, 1953.

[6] E. Arzt, S. Gorb, and R. Spolenak, "From micro to nano contacts in biological attachment devices," *Proceedings of the National Academy of Sciences*, vol. 100, no. 19, pp. 10603–10606, 2003.

[7] L. Afferrante, G. Carbone, G. Demelio, and N. Pugno, "Adhesion of elastic thin films: double peeling of tapes versus axisymmetric peeling of membranes," *Tribology Letters*, vol. 52, no. 3, pp. 439–447, 2013.

[8] C. Creton and S. Gorb, "Sticky feet: from animals to materials," *MRS Bulletin*, vol. 32, no. 6, pp. 466–472, 2007.

[9] A. A. Griffith, "The phenomena of rupture and flow in solids," *Philosophical Transactions of the Royal Society*, vol. A221, pp. 163–198, 1921.

[10] K. Kendall, "Thin-film peeling-the elastic term," *Journal of Physics D: Applied Physics*, vol. 8, no. 13, p. 1449, 1975.

[11] D. A. Dillard, B. Mukherjee, P. Karnal, R. C. Batra, and J. Frechette, "A review of Winkler's foundation and its profound influence on adhesion and soft matter applications," *Soft Matter*, vol. 14, no. 19, pp. 3669–3683, 2018.

[12] ASTM-D1876, *Peel Resistance for Adhesives, T-peel Test*. West Conshohocken, PA: American Society for Testing and Materials.

[13] K. Kendall, "A cracking approach to inventing new tough materials: fracture stranger than friction," *Philosophical Transactions of the Royal Society A: Mathematical, Physical and Engineering Sciences*, vol. 379, no. 2203, p. 20200286, 2021.

[14] J. d. De Munck, K. Van Landuyt, M. Peumans, A. Poitevin, P. Lambrechts, M. Braem, and B. Van Meerbeek, "A critical review of the durability of adhesion to tooth tissue: methods and results," *Journal of Dental Research*, vol. 84, no. 2, pp. 118–132, 2005.

[15] K. Bundy, U. Schlegel, B. Rahn, V. Geret, and S. Perren, "An improved peel test method for measurement of adhesion to biomaterials," *Journal of Materials Science: Materials in Medicine*, vol. 11, no. 8, pp. 517–521, 2000.

[16] A. E. Larose, A. Dakiw-Piaceski, M. A. Barbier, D. Larouche, R. Gauvin, M. Caruso, E. Pope, and L. Germain, "Peel test to assess the adhesion strength of the dermal–epidermal junction in tissue-engineered skin," *Tissue Engineering Part C: Methods*, vol. 26, no. 3, pp. 180–189, 2020.

[17] W. Thiedmanu, F. Tolan, P. Pearce, and C. Morris, "Silane coupling agents as adhesion promoters for aerospace structural film adhesives," *The Journal of Adhesion*, vol. 22, no. 3, pp. 197–210, 1987.

[18] A. L. Santos, E. C. Botelho, K. G. Kostov, M. Ueda, and L. L. G. da Silva, "Carbon fiber surface modification by plasma treatment for interface adhesion improvements of aerospace composites," in *Advanced Materials Research*, vol. 1135, pp. 75–87, Trans Tech Publ, 2016.

[19] L.-G. Tang and J. L. Kardos, "A review of methods for improving the interfacial adhesion between carbon fiber and polymer matrix," *Polymer Composites*, vol. 18, no. 1, pp. 100–113, 1997.

[20] M. D. Thouless, J. L. Adams, M. S. Kafkalidis, S. M. Ward, R. A. Dickie, and G. L. Westerbeek, "Determining the toughness of plastically deforming joints," *Journal of Materials Science*, vol. 33, no. 1, pp. 189–197, 1998.

[21] J. L. Gardon, "Peel adhesion. i. some phenomenological aspects of the test," *Journal of Applied Polymer Science*, vol. 7, no. 2, pp. 625–641, 1963.

[22] K. S. Kim and N. Aravas, "Elastoplastic analysis of the peel test," *International Journal of Solids and Structures*, vol. 24, no. 4, pp. 417–435, 1988.

[23] K.-S. Kim and J. Kim, "Elasto-plastic analysis of the peel test for thin film adhesion," *Journal of Engineering Materials and Technology*, vol. 110, no. 3, pp. 266–273, 1988.

[24] A. J. Kinloch, C. Lau, and J. G. Williams, "The peeling of flexible laminates," *International Journal of Fracture*, vol. 66, no. 1, pp. 45–70, 1994.

[25] C. B. Haverkamp, D. Hwang, C. Lee, and M. D. Bartlett, "Deterministic control of adhesive crack propagation through jamming based switchable adhesives," *Soft Matter*, vol. 17, no. 7, pp. 1731–1737, 2021.

[26] D.-H. Kim, N. Lu, R. Ma, Y.-S. Kim, R.-H. Kim, S. Wang, J. Wu, S. M. Won, H. Tao, A. Islam, *et al.*, "Epidermal electronics," *Science*, vol. 333, no. 6044, pp. 838–843, 2011.

[27] Y. Tang, Q. Zhang, G. Lin, and J. Yin, "Switchable adhesion actuator for amphibious climbing soft robot," *Soft Robotics*, vol. 5, no. 5, pp. 592–600, 2018.

[28] D. R. King, T. L. Sun, Y. Huang, T. Kurokawa, T. Nonoyama, A. J. Crosby, and J. P. Gong, "Extremely tough composites from fabric reinforced polyampholyte hydrogels," *Materials Horizons*, vol. 2, no. 6, pp. 584–591, 2015.

[29] H. Yuk, T. Zhang, S. Lin, G. A. Parada, and X. Zhao, "Tough bonding of hydrogels to diverse non-porous surfaces," *Nature Materials*, vol. 15, no. 2, pp. 190–196, 2016.

[30] C. Creton, "Pressure-sensitive adhesives: an introductory course," *MRS Bulletin*, vol. 28, no. 6, pp. 434–439, 2003.

[31] D.-G. Hwang, K. Trent, and M. D. Bartlett, "Kirigami-inspired structures for smart adhesion," *ACS Applied Materials & Interfaces*, vol. 10, no. 7, pp. 6747–6754, 2018.

[32] V. Sariola and M. Sitti, "Mechanically switchable elastomeric microfibrillar adhesive surfaces for transfer printing," *Advanced Materials Interfaces*, vol. 1, no. 4, pp. 1–5, 2014.

[33] H. Yi, M. Seong, K. Sun, I. Hwang, K. Lee, C. Cha, T.-i. Kim, and H. E. Jeong, "Wet-Responsive, reconfigurable, and biocompatible hydrogel adhesive films for transfer printing of nanomembranes," *Advanced Functional Materials*, vol. 1706498, p. 1706498, 2018.

[34] D. Brodoceanu, C. Bauer, E. Kroner, E. Arzt, and T. Kraus, "Hierarchical bioinspired adhesive surfaces—a review," *Bioinspiration & Biomimetics*, vol. 11, no. 5, p. 051001, 2016.

[35] A. B. Croll, N. Hosseini, and M. D. Bartlett, "Switchable adhesives for multifunctional interfaces," *Advanced Materials Technologies*, vol. 4, no. 8, 2019.

[36] M. D. Bartlett, E. J. Markvicka, and C. Majidi, "Rapid fabrication of soft, multilayered electronics for wearable biomonitoring," *Advanced Functional Materials*, vol. 26, no. 46, pp. 8496–8504, 2016.

[37] B. Van Meerbeek, J. Perdigao, P. Lambrechts, and G. Vanherle, "The clinical performance of adhesives," *Journal of Dentistry*, vol. 26, no. 1, pp. 1–20, 1998.

[38] S. Nam and D. Mooney, "Polymeric tissue adhesives," *Chemical Reviews*, vol. 121, no. 18, pp. 11336–11384, 2021.

[39] T. A. Pozarycki, D. Hwang, E. J. Barron III, B. T. Wilcox, R. Tutika, and M. D. Bartlett, "Tough bonding of liquid metal-elastomer composites for multifunctional adhesives," *Small*, vol. 18, no. 41, p. 2203700, 2022.

[40] J. W. Hutchinson and Z. Suo, "Mixed mode cracking in layered materials," *Advances in Applied Mechanics*, vol. 29, pp. 63–191, 1991.

[41] A. N. Gent and R. P. Petrich, "Adhesion of viscoelastic materials to rigid substrates," *Proceedings of the Royal Society of London. A. Mathematical and Physical Sciences*, vol. 310, no. 1502, pp. 433–448, 1969.

[42] D. H. Kaelble, "Peel adhesion: Influence of surface energies and adhesive rheology," *The Journal of Adhesion*, vol. 1, no. 2, pp. 102–123, 1969.

[43] D. Kaelble, "Theory and analysis of peel adhesion: Rate-temperature dependence of viscoelastic interlayers," *Journal of Colloid Science*, vol. 19, no. 5, pp. 413–424, 1964.

[44] Q. Li, R. C. Batra, I. Graham, and D. A. Dillard, "Examining T-peel specimen bond length effects: Experimental and numerical explorations of transitions to steady-state debonding," *International Journal of Solids and Structures*, vol. 180, pp. 72–83, 2019.

[45] Q. Yang, M. D. Thouless, and S. Ward, "Numerical simulations of adhesively-bonded beams failing with extensive plastic deformation," *Journal of the Mechanics and Physics of Solids*, vol. 47, no. 6, pp. 1337–1353, 1999.

[46] Q. Yang, M. D. Thouless, and S. Ward, "Analysis of the symmetrical 90-peel test with extensive plastic deformation," *The Journal of Adhesion*, vol. 72, no. 2, pp. 115–132, 2000.

[47] N. M. Pugno, "The theory of multiple peeling," *International Journal of Fracture*, vol. 171, no. 2, pp. 185–193, 2011.

[48] J. Gohl, T. Thiele-Sardina, M. Rencheck, K. Erk, and C. Davis, "A modular peel fixture for tape peel tests on immovable substrates," *Experimental Mechanics*, vol. 61, no. 7, pp. 1209–1213, 2021.

[49] M. Ciavarella, S. Chen, and H. Gao, "A general expression for the maximum force in peeling a tape from a rigid substrate with an initial crack," *The Journal of Adhesion*, vol. In press, pp. 1–13, 2022.

[50] T. Elder, T. Twohig, H. Singh, and A. B. Croll, "Adhesion of a tape loop," *Soft Matter*, vol. 16, no. 47, pp. 10611–10619, 2020.

[51] P.-G. de Gennes, "Soft adhesives," *Langmuir*, vol. 12, no. 19, pp. 4497–4500, 1996.

[52] D. Kaelble, "Theory and analysis of peel adhesion: adhesive thickness effects," *The Journal of Adhesion*, vol. 37, no. 1-3, pp. 205–214, 1992.

[53] M. Kothari, Z. Lemon, C. Roth, and T. Cohen, "Controlled propagation and jamming of a delamination front," *Soft Matter*, vol. 16, no. 43, pp. 9838–9843, 2020.

[54] ASTM D5045-99, *Standard test methods for plane-strain fracture toughness and strain energy release rate of plastic materials*. West Conshohocken, PA: American Society for Testing and Materials.

[55] ASTM-D6862, *Standard Test Method for 90 Degree Peel Resistance of Adhesives*. West Conshohocken, PA: American Society for Testing and Materials.

[56] A. N. Gent and G. R. Hamed, "Peel mechanics of adhesive joints," *Polymer Engineering & Science*, vol. 17, no. 7, pp. 462–466, 1977.

[57] A. J. Kinloch, *Adhesion and adhesives: science and technology*. UK: Springer Science & Business Media, 1987.

[58] L. D. R. Grant, R. D. Adams, and L. F. M. da Silva, "Experimental and numerical analysis of T-peel joints for the automotive industry," *Journal of Adhesion Science and Technology*, vol. 23, pp. 317–38, 2009.

[59] B. Blackman, H. Hadavinia, A. J. Kinloch, and J. Williams, "The use of a cohesive zone model to study the fracture of fibre composites and adhesively-bonded joints," *International Journal of Fracture*, vol. 119, no. 1, pp. 25–46, 2003.

[60] R. S. Rivlin, "The effective work of adhesion," *Paint Technology*, vol. IX, no. 106, pp. 215–216, 1944.

[61] P. Lindley, "Ozone attack at a rubber-metal bond," *Journal of the Institution of the Rubber Industry*, vol. 5, pp. 243–249, 1971.

[62] J. Bikerman, "Theory of peeling through a Hookean solid," *Journal of Applied Physics*, vol. 28, no. 12, pp. 1484–1485, 1957.

[63] E. Winkler, *Die Lehre von der Elasticitaet und Festigkeit: mit besonderer Rücksicht auf ihre Anwendung in der Technik, für polytechnische Schulen, Bauakademien, Ingenieure, Maschinenbauer, Architecten, etc.* H. Dominicus, 1867.

[64] K. L. Johnson, K. Kendall, and A. D. Roberts, "Surface energy and the contact of elastic solids," *Proceedings of the Royal Society of London. A. Mathematical and Physical Sciences*, vol. 324, pp. 301–313, 1971.

[65] A. J. Kinloch and M. Yuen, "The mechanical behaviour of polyimide-copper laminates," *Journal of Materials Science*, vol. 24, no. 6, pp. 2183–2190, 1989.

[66] D. H. Kaelble, "Theory and analysis of peel adhesion: bond stresses and distributions," *Transactions of the Society of Rheology*, vol. 4, no. 1, pp. 45–73, 1960.

[67] C. E. Inglis, "Stresses in plates due to the presence of cracks and sharp corners," *Transactions of the Institute of Naval Architects*, vol. 55, pp. 219–241, 1913.

[68] D. Broek, *Elementary engineering fracture mechanics*. Springer Science & Business Media, 1982.

[69] G. R. Irwin and J. Kies, "Critical energy rate analysis of fracture strength," *SPIE Milestone Series MS*, vol. 137, no. 136-141, p. 29, 1997.

[70] G. R. Irwin and J. Kies, "Critical energy rate analysis of fracture strength," *Welding J. Res. Suppl.*, vol. 33, no. 4, pp. 193–198, 1954.

[71] J. G. Williams, "Fracture mechanics of polymers," *Halsted Press, UK*, 1984.

[72] E. Andrews and A. J. Kinloch, "Mechanics of adhesive failure. 2," *Proceedings of the Royal Society of London. A. Mathematical and Physical Sciences*, vol. 332, no. 1590, pp. 401–414, 1973.

[73] A. N. Gent and J. Schultz, "Effect of wetting liquids on the strength of adhesion of viscoelastic material," *The Journal of Adhesion*, vol. 3, no. 4, pp. 281–294, 1972.

[74] F. Saulnier, T. Ondarçuhu, A. Aradian, and E. Raphaël, "Adhesion between a viscoelastic material and a solid surface," *Macromolecules*, vol. 37, no. 3, pp. 1067–1075, 2004.

[75] F. Brochard-Wyart, P. De Gennes, L. Leger, Y. Marciano, and E. Raphael, "Adhesion promoters," *The Journal of Physical Chemistry*, vol. 98, no. 38, pp. 9405–9410, 1994.

[76] G. Lake and A. Thomas, "The strength of highly elastic materials," *Proceedings of the Royal Society of London. Series A. Mathematical and Physical Sciences*, vol. 300, no. 1460, pp. 108–119, 1967.

[77] A. Ghatak, K. Vorvolakos, H. She, D. L. Malotky, and M. K. Chaudhury, "Interfacial rate processes in adhesion and friction," *The Journal of Physical Chemistry B*, vol. 104, no. 17, pp. 4018–4030, 2000.

[78] K. Autumn, M. Sitti, Y. A. Liang, A. M. Peattie, W. R. Hansen, S. Sponberg, T. W. Kenny, R. Fearing, J. N. Israelachvili, and R. J. Full, "Evidence for van der waals adhesion in gecko setae," *Proceedings of the National Academy of Sciences*, vol. 99, no. 19, pp. 12252–12256, 2002.

[79] K. Kendall, "The effects of shrinkage on interfacial cracking in a bonded laminate," *Journal of Physics D: Applied Physics*, vol. 8, no. 15, pp. 1722–1732, 1975.

[80] X. Wan, Y. He, and C. Yang, "Simulation of the peel of hydrogels with stiff backing," *Soft Matter*, vol. 18, no. 2, pp. 272–281, 2022.

[81] T. Yin, G. Zhang, S. Qu, and Z. Suo, "Peel of elastomers of various thicknesses and widths," *Extreme Mechanics Letters*, vol. 46, p. 101325, 2021.

[82] R. Rivlin and A. G. Thomas, "Rupture of rubber. I. Characteristic energy for tearing," *Journal of Polymer Science*, vol. 10, no. 3, pp. 291–318, 1953.

[83] R. J. Farris, J. Goldfarb, and M. A. Maden, "The correlation between residual stresses and delamination behavior of polymer coatings," in *Makromolekulare Chemie. Macromolecular Symposia*, vol. 68, pp. 57–67, Wiley Online Library, 1993.

[84] R. J. Farris and J. L. Goldfarb, "An experimental partitioning of the mechanical energy expended during peel testing," *Journal of Adhesion Science and Technology*, vol. 7, no. 8, pp. 853–868, 1993.

[85] N. Aravas, K.-S. Kim, and M. Loukis, "On the mechanics of adhesion testing of flexible films," *Materials Science and Engineering: A*, vol. 107, pp. 159–168, 1989.

[86] J. Kim, K. S. Kim, and Y. H. Kim, "Mechanical effects in peel adhesion test," *Journal of Adhesion Science and Technology*, vol. 3, no. 1, pp. 175–187, 1989.

[87] J. G. Williams, "Root rotation and plastic work effects in the peel test," *The Journal of Adhesion*, vol. 41, no. 1-4, pp. 225–239, 1993.

[88] A. J. Kinloch and J. G. Williams, *The Mechanics of Peel Tests*, vol. 1 of *Adhesion Science and Engineering*, pp. 273–302. Amsterdam: Elsevier, 2002.

[89] A. N. Gent and G. R. Hamed, "Peel mechanics," *The Journal of Adhesion*, vol. 7, no. 2, pp. 91–95, 1975.

[90] A. N. Gent and G. R. Hamed, "Peel mechanics for an elastic-plastic adherend," *Journal of Applied Polymer Science*, vol. 21, no. 10, pp. 2817–2831, 1977.

[91] M. Kanninen, "A dynamic analysis of unstable crack propagation and arrest in the DCB test specimen," *International Journal of Fracture*, vol. 10, no. 3, pp. 415–430, 1974.

[92] S. Hashemi, A. J. Kinloch, and J. G. Williams, "The analysis of interlaminar fracture in uniaxial fibre-polymer composites," *Proceedings of the Royal Society of London. A. Mathematical and Physical Sciences*, vol. 427, no. 1872, pp. 173–199, 1990.

[93] "Imperial College London, 'IC Peel'." https://www.imperial.ac.uk/mechanical-engineering/research/mechanics-of-materials/composites-adhesives-and-soft-solids/adhesion/test-protocols/. Accessed: 2021-11-23.

[94] A. J. Kinloch, H. Koay, S. Lee, and L. Ng, "Using the simple peel test to measure the adhesive fracture energy, G_A," https://www.researchgate.net/publication/318099667, accessed 7/16/2022, Presented at Euradh Conference, at: Friedrichshaven, Germany, Sept. 2012.

[95] A. J. Kinloch, H. Hadavinia, L. Kawashita, D. R. Moore, and J. G. Williams, "A numerical analysis of the elastic-plastic peel test," *Engineering Fracture Mechanics*, vol. 73, pp. 2324–35, 2006.

[96] A. K. Moidu, A. N. Sinclair, and J. K. Spelt, "On the determination of fracture energy using the peel test," *Journal of Testing and Evaluation*, vol. 26, no. 3, pp. 247–254, 1998.

[97] A. K. Moidu, A. N. Sinclair, and J. K. Spelt, "Analysis of the peel test - prediction of adherend plastic dissipation and extraction of fracture energy in metal-to-metal adhesive joints," *Journal of Testing and Evaluation*, vol. 23, no. 4, pp. 241–253, 1995.

[98] E. Simlissi, M. Martiny, S. Mercier, S. Bahi, and L. Bodin, "Elastic–plastic analysis of the peel test for ductile thin film presenting a saturation of the yield stress," *International Journal of Fracture*, vol. 220, no. 1, pp. 1–16, 2019.

[99] Q. Yang and M. D. Thouless, "Mixed-mode fracture analyses of plastically-deforming adhesive joints," *International Journal of Fracture*, vol. 110, pp. 175–187, 2001.

[100] M. Alfano, F. Furgiuele, G. Lubineau, and G. H. Paulino, "Simulation of debonding in Al/epoxy T-peel joints using a potential-based cohesive zone model," *Procedia Engineering*, vol. 10, pp. 1760–1765, 2011.

[101] X. Yang, Y. Xia, Q. Zhou, P.-C. Wang, and K. Wang, "Modeling of high strength steel joints bonded with toughened adhesive for vehicle crash simulations," *International Journal of Adhesion and Adhesives*, vol. 39, pp. 21–32, 2012.

[102] V. Tvergaard and J. W. Hutchinson, "The relation between crack growth resistance and fracture process parameters in elastic-plastic solids," *Journal of the Mechanics and Physics of Solids*, vol. 40, no. 6, pp. 1377–1397, 1992.

[103] V. Tvergaard and J. W. Hutchinson, "The influence of plasticity on mixed mode interface toughness," *Journal of the Mechanics and Physics of Solids*, vol. 41, no. 6, pp. 1119–1135, 1993.

[104] V. Tvergaard and J. W. Hutchinson, "Toughness of an interface along a thin ductile layer joining elastic solids," *Philosophical Magazine A*, vol. 70, no. 4, pp. 641–656, 1994.

[105] V. Tvergaard and J. W. Hutchinson, "On the toughness of ductile adhesive joints," *Journal of the Mechanics and Physics of Solids*, vol. 44, no. 5, pp. 789–800, 1996.

[106] H. Bruce and C. Holmqvist, "Modelling adhesion in packaging materials: Physical tests and virtual tests in abaqus," Master's thesis, 2013, Lund University, Sweden.

[107] E. P. Chan, D. Ahn, and A. J. Crosby, "Adhesion of patterned reactive interfaces," *The Journal of Adhesion*, vol. 83, no. 5, pp. 473–489, 2007.

[108] K. Kendall, "Control of cracks by interfaces in composites," *Proceedings of the Royal Society of London. A. Mathematical and Physical Sciences*, vol. 341, no. 1627, pp. 409–428, 1975.

[109] ISO-25217, "Adhesives — determination of the mode 1 adhesive fracture energy of structural adhesive joints using double cantilever beam and tapered double cantilever beam specimens," Geneva, CH, 2009.

[110] D. A. Dillard, "The T-peel test," in *Testing Adhesive Joints: Best Practices*, pp. 229–244, John Wiley & Sons, 2012.

[111] Q. Li, *Finite Deformations of Fiber-Reinforced Rubberlike Solids, and of Adhesively Bonded T-peel Joints*. PhD thesis, Virginia Tech, USA, 2018.

[112] M. D. Thouless and Q. D. Yang, *Measurement and Analysis of the Fracture Properties of Adhesive Joints*, vol. 1 of *Adhesion Science and Engineering*, pp. 235–272. Amsterdam: Elsevier, 2002.

[113] Q. D. Yang, M. D. Thouless, and S. M. Ward, "Elastic-plastic mode-II fracture of adhesive joints," *International Journal of Solids and Structures*, vol. 38, no. 18, pp. 3251–3262, 2001.

[114] M. S. Kafkalidis, M. D. Thouless, Q. D. Yang, and S. M. Ward, "Deformation and fracture of adhesive layers constrained by plastically-deforming adherends," *Journal of Adhesion Science and Technology*, vol. 14, no. 13, pp. 1593–1607, 2000.

[115] F. B. Seely and J. O. Smith, *Advanced mechanics of materials*. Wiley, 1952.

[116] R. H. Plaut, D. Hwang, C. Lee, M. D. Bartlett, and D. A. Dillard, "Peeling of finite-length elastica on Winkler foundation until complete detachment," *International Journal of Solids and Structures*, vol. 256, p. 111944, 2022.

[117] R. H. Plaut and D. A. Dillard, "Peeling of finite-length 1-D plates on elastomeric foundation," *In review*, 2022.

[118] D. A. Dillard, "Bending of plates on thin elastomeric foundations," *Journal of Applied Mechanics-Transactions of the ASME*, vol. 56, no. 2, pp. 382–386, 1989.

[119] A. Ghatak and M. K. Chaudhury, "Adhesion-induced instability patterns in thin confined elastic film," *Langmuir*, vol. 19, no. 7, pp. 2621–2631, 2003.

[120] T. R. Brussat, S. T. Chiu, and S. Mostovoy, "Fracture mechanics for structural adhesive bonds," Report AFNL-TR-77-163, Air Force Materials Laboratory, USA, 1977.

[121] W. S. Johnson, "Stress-analysis of the cracked-lap-shear specimen - an ASTM round-robin," *Journal of Testing and Evaluation*, vol. 15, no. 6, pp. 303–324, 1987.

[122] Y. Lai, M. Rakestraw, and D. Dillard, "The cracked lap shear specimen revisited - a closed form solution," *International Journal of Solids and Structures*, vol. 33, no. 12, pp. 1725–1743, 1996.

[123] R. B. Barros, R. D. Campilho, I. J. Sánchez-Arce, J. M. Dionísio, and K. Madani, "Evaluation of the cracked lap shear test for mixed-mode fracture toughness estimation of adhesive joints," *Proceedings of the Institution of Mechanical Engineers, Part L: Journal of Materials: Design and Applications*, p. 14644207221140296, 2022.

[124] L. J. Hart-Smith, "Designing to minimize peel stresses in adhesive bonded joints," *ASTM STP*, vol. 876, pp. 238– 266, 1985.

[125] L. J. Hart-Smith, *The Design of Adhesively Bonded Joints*, vol. 1 of *Adhesion Science and Engineering I: The Mechanics of Adhesion*. Amsterdam: Elsevier, 2002.

[126] T. Chang, E. A. Sproat, Y. H. Lai, N. E. Shephard, and D. A. Dillard, "A test method for accelerated humidity conditioning and estimation of adhesive bond durability," *Journal of Adhesion*, vol. 60, no. 1-4, pp. 153–162, 1997.

[127] D. Dillard, B. Chen, T. Chang, and Y. Lai, "Analysis of the notched coating adhesion test," *Journal of Adhesion*, vol. 69, no. 1-2, pp. 99–120, 1999.

[128] O. Orell, J. Jokinen, M. Kallio, and M. Kanerva, "Revised notched coating adhesion test to account for plasticity and 3D behaviour," *Polymer Testing*, vol. 102, p. 107319, 2021.

[129] H.-h. Yu and J. W. Hutchinson, "Delamination of thin film strips," *Thin Solid Films*, vol. 423, no. 1, pp. 54–63, 2003.

[130] R. Farris and C. Bauer, "A self-delamination method of measuring the surface energy of adhesion of coatings," *The Journal of Adhesion*, vol. 26, no. 4, pp. 293–300, 1988.

[131] A. N. Gent and S. Kaang, "Pull-off forces for adhesive tapes," *Journal of Applied Polymer Science*, vol. 32, no. 4, pp. 4689–4700, 1986.

[132] K.-T. Wan, "Fracture mechanics of a v-peel adhesion test–transition from a bending plate to a stretching membrane," *The Journal of Adhesion*, vol. 70, no. 3-4, pp. 197–207, 1999.

[133] D. Dillard, K. Liechti, C. Lin, J. Thornton, and H. Brinson, "Development of alternative techniques for measuring the fracture toughness of rubber-to-metal bonds in harsh environments," *ASTM STP*, vol. 981, pp. 83–97, 1988.

[134] K. Liechti and Y.-M. Liang, "The interfacial fracture characteristics of bimaterial and sandwich blister specimens," *International Journal of Fracture*, vol. 55, no. 2, pp. 95–114, 1992.

[135] K. Liechti, E. Becker, C. Lin, and T. Miller, "A fracture analysis of cathodic delamination in rubber to metal bonds," *International Journal of Fracture*, vol. 39, no. 1, pp. 217–234, 1989.

[136] R. Hamadeh, D. Dillard, K. Liechti, and J. Thornton, "A mechanistic evaluation of cathodic debonding of elastomer to metal bonds," *Journal of Adhesion Science and Technology*, vol. 3, no. 1, pp. 421–440, 1989.

[137] Z. Sun, K.-T. Wan, and D. A. Dillard, "A theoretical and numerical study of thin film delamination using the pull-off test," *International Journal of Solids and Structures*, vol. 41, no. 3-4, pp. 717–730, 2004.

[138] M. Gunda, P. Kumar, and M. Katiyar, "Review of mechanical characterization techniques for thin films used in flexible electronics," *Critical Reviews in Solid State and Materials Sciences*, vol. 42, no. 2, pp. 129–152, 2017.

[139] M. Rabold, A. Doll, F. Goldschmidtboing, and P. Woias, "Non-destructive strength characterization of full-wafer bonds using a modified blister test method," in *19th IEEE International Conference on Micro Electro Mechanical Systems*, pp. 338–341, IEEE, 2006.

[140] M. Berdova, J. Lyytinen, K. Grigoras, A. Baby, L. Kilpi, H. Ronkainen, S. Franssila, and J. Koskinen, "Characterization of thin film adhesion by mems shaft-loading blister testing," *Journal of Vacuum Science & Technology A: Vacuum, Surfaces, and Films*, vol. 31, no. 3, p. 031102, 2013.

[141] G. Margaritis, S. Sikorski, and F. McGarry, "Elastic-plastic finite element method analysis and application of the island blister test," *Journal of Adhesion Science and Technology*, vol. 8, no. 3, pp. 273–287, 1994.

[142] H. Dannenberg, "Measurement of adhesion by a blister method," *Journal of Applied Polymer Science*, vol. 5, no. 14, pp. 125–134, 1961.

[143] H. Dannenberg, "Measurement of adhesion by a blister method," *Journal of Polymer Science*, vol. 33, no. 126, pp. 509–510, 1958.

[144] Y.-H. Lai and D. A. Dillard, "A study of the fracture efficiency parameter of blister tests for films and coatings," *Journal of Adhesion Science and Technology*, vol. 8, no. 6, pp. 663–678, 1994.

[145] M. Williams, "The relation of continuum mechanics to adhesive fracture," *The Journal of Adhesion*, vol. 4, no. 4, pp. 307–332, 1972.

[146] A. N. Gent and L. H. Lewandowski, "Blow-off pressures for adhering layers.," *Journal of Applied Polymer Science*, vol. 33, pp. 1567–1577, 1987.

[147] J. G. Williams, "Energy release rates for the peeling of flexible membranes and the analysis of blister tests," *International Journal of Fracture*, vol. 87, no. 3, pp. 265–288, 1997.

[148] K.-T. Wan and S.-C. Lim, "The bending to stretching transition of a pressurized blister test," *International Journal of Fracture*, vol. 92, no. 4, pp. 43–47, 1998.

[149] K.-T. Wan, S. Guo, and D. A. Dillard, "A theoretical and numerical study of a thin clamped circular film under an external load in the presence of a tensile residual stress," *Thin Solid Films*, vol. 425, no. 1-2, pp. 150–162, 2003.

[150] M. G. Allen and S. D. Senturia, "Analysis of critical debonding pressures of stressed thin films in the blister test," *The Journal of Adhesion*, vol. 25, no. 4, pp. 303–315, 1988.

[151] M. G. Allen and S. D. Senturia, "Application of the island blister test for thin film adhesion measurement," *The Journal of Adhesion*, vol. 29, no. 1-4, pp. 219–231, 1989.

[152] M. Napolitano, A. Chudnovsky, and A. Moet, "The constrained blister test for the energy of interfacial adhesion," *Journal of Adhesion Science and Technology*, vol. 2, no. 1, pp. 311–323, 1988.

[153] Y.-S. Chang, Y.-H. Lai, and D. A. Dillard, "The constrained blister—a nearly constant strain energy release rate test for adhesives," *The Journal of Adhesion*, vol. 27, no. 4, pp. 197–211, 1989.

[154] D. A. Dillard and Y. Bao, "The peninsula blister test: a high and constant strain energy release rate fracture specimen for adhesives," *The Journal of Adhesion*, vol. 33, no. 4, pp. 253–271, 1991.

[155] D. Xu, K. M. Liechti, and T. H. de Lumley-Woodyear, "Closed form nonlinear analysis of the peninsula blister test," *The Journal of Adhesion*, vol. 82, no. 8, pp. 831–866, 2006.

[156] S. Roy, Y. Wang, S. Park, D. Xu, and K. M. Liechti, "A three-dimensional viscoelastic analysis of thin film delamination in a peninsula blister specimen," *Mechanics of Advanced Materials and Structures*, vol. 14, no. 5, pp. 379–390, 2007.

[157] K.-T. Wan and Y.-W. Mai, "Fracture mechanics of a shaft-loaded blister of thin flexible membrane on rigid substrate," *International Journal of Fracture*, vol. 74, no. 2, pp. 181–197, 1996.

[158] E. O'Brien, T. Ward, S. Guo, and D. Dillard, "Strain energy release rates of a pressure sensitive adhesive measured by the shaft-loaded blister test," *The Journal of Adhesion*, vol. 79, no. 1, pp. 69–97, 2003.

[159] ASTM D3167, *Peel resistance of (structural) adhesive bonds*. West Conshohocken, PA: American Society for Testing and Materials.

[160] ASTM D1781, *For flexible to rigid adhesion.* West Conshohocken, PA: American Society for Testing and Materials.

[161] L. Kawashita, D. Moore, and J. G. Williams, "The development of a mandrel peel test for the measurement of adhesive fracture toughness of epoxy–metal laminates," *The Journal of Adhesion*, vol. 80, no. 3, pp. 147–167, 2004.

[162] L. Kawashita, A. J. Kinloch, D. Moore, and J. G. Williams, "A critical investigation of the use of a mandrel peel method for the determination of adhesive fracture toughness of metal-polymer laminates," *Engineering Fracture Mechanics*, vol. 73, no. 16, pp. 2304–2323, 2006.

[163] L. Kawashita, A. J. Kinloch, D. R. Moore, and J. G. Williams, "The influence of bond line thickness and peel arm thickness on adhesive fracture toughness of rubber toughened epoxy–aluminium alloy laminates," *International Journal of Adhesion and Adhesives*, vol. 28, no. 4-5, pp. 199–210, 2008.

[164] A. J. Kinloch and M. Yuen, "The mechanical behaviour of polyimide/copper laminates Part 2: peel energy measurements," *The Journal of Adhesion*, vol. 30, no. 1-4, pp. 151–170, 1989.

[165] ISO-11343: 1993 modified, "Structural adhesives - determination of dynamic resistance to cleavage of high strength adhesive bonds under impact conditions - wedge impact method," 2002, Geneva, CH.

[166] B. Blackman, A. J. Kinloch, A. Taylor, and Y. Wang, "The impact wedge-peel performance of structural adhesives," *Journal of Materials Science*, vol. 35, no. 8, pp. 1867–1884, 2000.

[167] A. J. Kinloch and J. G. Williams, "Comments on" Determining the toughness of plastically deforming joints"," *Journal of Materials Science Letters*, vol. 17, no. 10, pp. 813–814, 1998.

[168] P. Martiny, F. Lani, A. J. Kinloch, and T. Pardoen, "Numerical analysis of the energy contributions in peel tests: A steady-state multilevel finite element approach," *International Journal of Adhesion and Adhesives*, vol. 28, no. 4-5, pp. 222–236, 2008.

[169] P. Martiny, F. Lani, A. J. Kinloch, and T. Pardoen, "A multiscale parametric study of mode I fracture in metal-to-metal low-toughness adhesive joints," *International journal of Fracture*, vol. 173, no. 2, pp. 105–133, 2012.

[170] P. Martiny, F. Lani, A. J. Kinloch, and T. Pardoen, "A maximum stress at a distance criterion for the prediction of crack propagation in adhesively-bonded joints," *Engineering Fracture Mechanics*, vol. 97, pp. 105–135, 2013.

[171] T. Ferracin, C. Landis, F. Delannay, and T. Pardoen, "On the determination of the cohesive zone properties of an adhesive layer from the analysis of the wedge-peel test," *International Journal of Solids and Structures*, vol. 40, no. 11, pp. 2889–2904, 2003.

[172] J. P. Hoefnagels, J. Neggers, P. H. Timmermans, O. van der Sluis, and M. G. Geers, "Copper–rubber interface delamination in stretchable electronics," *Scripta Materialia*, vol. 63, no. 8, pp. 875–878, 2010.

[173] J. Neggers, J. P. Hoefnagels, O. Van Der Sluis, and M. G. Geers, "Multi-scale experimental analysis of rate dependent metal–elastomer interface mechanics," *Journal of the Mechanics and Physics of Solids*, vol. 80, pp. 26–36, 2015.

[174] R. O. Ritchie, J. F. Knott, and J. Rice, "On the relationship between critical tensile stress and fracture toughness in mild steel," *Journal of the Mechanics and Physics of Solids*, vol. 21, no. 6, pp. 395–410, 1973.

[175] J. M. Whitney and R. J. Nuismer, "Stress fracture criteria for laminated composites containing stress concentrations," *Journal of Composite Materials*, vol. 8, no. 3, pp. 253–265, 1974.

[176] A. J. Kinloch and J. G. Williams, "Crack blunting mechanisms in polymers," *Journal of Materials Science*, vol. 15, no. 4, pp. 987–996, 1980.

[177] J. Clark and I. McGregor, "Ultimate tensile stress over a zone: a new failure criterion for adhesive joints," *The Journal of Adhesion*, vol. 42, no. 4, pp. 227–245, 1993.

[178] D. Taylor, "The theory of critical distances," *Engineering Fracture Mechanics*, vol. 75, no. 7, pp. 1696–1705, 2008.

[179] D. Dillard, "Stress distribution: mode of failure," *Handbook of Adhesion, 2nd ed. John Wiley & Sons, Bath, UK*, pp. 496–499, 2005.

[180] H. Chai, "Shear fracture," *International Journal of Fracture*, vol. 37, no. 2, pp. 137–159, 1988.

[181] M. L. Williams, "On the stress distribution at the base of a stationary crack," *Journal of Applied Mechanics*, vol. 24, pp. 109–114, 1957.

[182] T. L. Anderson, *Fracture mechanics: fundamentals and applications*. Boca Raton, USA: CRC press, 2017.

[183] E. F. Rybicki and M. F. Kanninen, "A finite element calculation of stress intensity factors by a modified crack closure integral," *Engineering Fracture Mechanics*, vol. 9, no. 4, pp. 931–938, 1977.

[184] D. Xie, A. M. Waas, K. W. Shahwan, J. A. Schroeder, and R. G. Boeman, "Computation of energy release rates for kinking cracks based on virtual crack closure technique," *Computer Modeling in Engineering & Sciences*, vol. 6, no. 6, pp. 515–524, 2004.

[185] T. Becker Jr, J. McNaney, R. Cannon, and R. Ritchie, "Limitations on the use of the mixed-mode delaminating beam test specimen: Effects of the size of the region of k-dominance," *Mechanics of Materials*, vol. 25, no. 4, pp. 291–308, 1997.

[186] S. Hashemi, A. J. Kinloch, and J. G. Williams, "Mixed-mode fracture in fiber-polymer composite laminates," *ASTM STP*, vol. 1110, pp. 143–168, 1991.

[187] K. Kendall, *Crack control: Using fracture theory to create tough new materials*. Oxford, UK: Elsevier, 2020.

[188] Y.-M. Liang and K. Liechti, "Toughening mechanisms in mixed-mode interfacial fracture," *International Journal of Solids and Structures*, vol. 32, no. 6-7, pp. 957–978, 1995.

[189] J. Swadener and K. Liechti, "Asymmetric shielding mechanisms in the mixed-mode fracture of a glass/epoxy interface," *Journal of Applied Mechanics*, vol. 65, no. 1, pp. 25–29, 1998.

[190] K. Liechti and Y. Chai, "Asymmetric shielding in interfacial fracture under in-plane shear," *Journal of Applied Mechanics*, vol. 59, no. 2, pp. 295–304, 1992.

[191] H. Chai, "Experimental evaluation of mixed-mode fracture in adhesive bonds," *Experimental Mechanics*, vol. 32, no. 4, pp. 296–303, 1992.

[192] G. Fernlund and J. Spelt, "Mixed-mode fracture characterization of adhesive joints," *Composites Science and Technology*, vol. 50, no. 4, pp. 441–449, 1994.

[193] G. Fernlund and J. Spelt, "Mixed mode energy release rates for adhesively bonded beam specimens," *Journal of Composites, Technology and Research*, vol. 16, no. 3, pp. 234–243, 1994.

[194] M. Charalambides, A. J. Kinloch, Y. Wang, and J. G. Williams, "On the analysis of mixed-mode failure," *International Journal of Fracture*, vol. 54, no. 3, pp. 269–291, 1992.

[195] T. K. O'Brien *et al.*, "Composite interlaminar shear fracture toughness, G_{IIc}: Shear measurement or sheer myth?," *ASTM STP*, vol. 1330, pp. 3–18, 1998.

[196] W. Shakespeare, "Much adoe about nothing," *First Folio*, 1623.

[197] R. Krueger and T. O'Brien, "A shell/3D modeling technique for the analysis of delaminated composite laminates," *Composites Part A: Applied Science and Manufacturing*, vol. 32, no. 1, pp. 25–44, 2001.

[198] R. Krueger, M. K. Cvitkovich, T. K. O'Brien, and P. J. Minguet, "Testing and analysis of composite skin/stringer debonding under multi-axial loading," *Journal of composite Materials*, vol. 34, no. 15, pp. 1263–1300, 2000.

[199] R. Krueger, P. J. Minguet, and T. K. O'Brien, "Implementation of interlaminar fracture mechanics in design: an overview," Presented at 14th International Conference on Composite Materials (ICCM-14), San Diego, July 14-18, 2003.

[200] I. Paris, P. Minguet, and T. O'Brien, "Comparison of delamination characterization for IM7/8552 composite woven and tape laminates," *ASTM STP*, vol. 1436, pp. 372–390, 2003.

[201] J. Rice, "Elastic fracture mechanics concepts for interfacial cracks," *Journal of Applied Mechanics*, vol. 55, no. 1, pp. 98–103, 1988.

[202] Z. Suo and J. W. Hutchinson, "Interface crack between two elastic layers," *International Journal of Fracture*, vol. 43, pp. 1–18, 1990.

[203] W.-L. Yin and J. Wang, "The energy-release rate in the growth of a one-dimensional delamination," *Journal of Applied Mechanics*, vol. 51, no. 4, pp. 939–941, 1984.

[204] J. G. Williams, "On the calculation of energy release rates for cracked laminates," *International Journal of Fracture*, vol. 36, no. 2, pp. 101–119, 1988.

[205] M. Conroy, A. J. Kinloch, J. G. Williams, and A. Ivankovic, "Mixed mode partitioning of beam-like geometries: A damage dependent solution," *Engineering Fracture Mechanics*, vol. 149, pp. 351–367, 2015.

[206] B. D. Davidson, P. L. Fariello, R. C. Hudson, and V. Sundararaman, "Accuracy assessment of the singular-field-based mode-mix decomposition procedure for the prediction of delamination," *ASTM STP*, vol. 1242, pp. 109–128, 1997.

[207] M. D. Thouless and H. Jensen, "Elastic fracture mechanics of the peel-test geometry," *The Journal of Adhesion*, vol. 38, no. 3-4, pp. 185–197, 1992.

[208] J. Dundurs and I. Jasiuk, "Effective elastic moduli of composite materials: reduced parameter dependence," *Applied Mechanics Reviews*, vol. 50, no. 11s, pp. S39–S43, 1997.

[209] Y. Wei and J. W. Hutchinson, "Interface strength, work of adhesion and plasticity in the peel test," *International Journal of Fracture*, pp. 315–333, 1998.

[210] S. Li, J. Wang, and M. D. Thouless, "The effects of shear on delamination in layered materials," *Journal of the Mechanics and Physics of Solids*, vol. 52, no. 1, pp. 193–214, 2004.

[211] M. D. Thouless, "Shear forces, root rotations, phase angles and delamination of layered materials," *Engineering Fracture Mechanics*, vol. 191, pp. 153–167, 2018.

[212] S. Wang, J. Mandell, and F. McGarry, "An analysis of the crack tip stress field in DCB adhesive fracture specimens," *International Journal of Fracture*, vol. 14, no. 1, pp. 39–58, 1978.

[213] R. Duer, D. Katevatis, A. J. Kinloch, and J. G. Williams, "Comments on mixed-mode fracture in adhesive joints," *International Journal of Fracture*, vol. 75, no. 2, pp. 157–162, 1996.

[214] D. Hunston, A. J. Kinloch, and S. Wang, "Micromechanics of fracture in structural adhesive bonds," *The Journal of Adhesion*, vol. 28, no. 2-3, pp. 103–114, 1989.

[215] H. Chai and M. Y. Chiang, "A crack propagation criterion based on local shear strain in adhesive bonds subjected to shear," *Journal of the Mechanics and Physics of Solids*, vol. 44, no. 10, pp. 1669–1689, 1996.

[216] V. N. Burlayenko and T. Sadowski, "Fe modeling of delamination growth in interlaminar fracture specimens," *Budownictwo i Architektura*, vol. 2, pp. 95–109, 2008.

[217] F. Erdogan and G. Sih, "On the crack extension in plates under plane loading and transverse shear," *Journal of Fluids Engineering*, vol. 85, no. 4, pp. 519–525, 1963.

[218] K. Palaniswamy and W. Knauss, *Mechanics Today*. Pergamon Press, New York, 1978.

[219] R. Goldstein and R. Salganik, "Brittle fracture of solids with arbitrary cracks," *International Journal of Fracture*, vol. 10, p. 507, 1974.

[220] B. Cotterell and J. Rice, "Slightly curved or kinked cracks," *International Journal of Fracture*, vol. 16, no. 2, pp. 155–169, 1980.

[221] B. Cotterell, "Notes on the paths and stability of cracks," *International Journal of Fracture Mechanics*, vol. 2, no. 3, pp. 526–533, 1966.

[222] B. Blackman, A. J. Kinloch, and M. Paraschi, "The determination of the mode II adhesive fracture resistance, G_{IIC}, of structural adhesive joints: an effective crack length approach," *Engineering Fracture Mechanics*, vol. 72, no. 6, pp. 877–897, 2005.

[223] S. M. Lee, "Mode II delamination failure mechanisms of polymer matrix composites," *Journal of Materials Science*, vol. 32, no. 5, pp. 1287–1295, 1997.

[224] "ISO 25217:2009 - adhesives - determination of the mode I adhesive fracture energy of structural adhesive joints using double cantilever beam and tapered double cantilever beam specimens," Testing standard, International Organization for Standardization, Geneva, CH, 2009.

[225] R. Ashley, M. Cochran, and K. Allen, "Adhesives in packaging," *International Journal of Adhesion and Adhesives*, vol. 15, no. 2, pp. 101–108, 1995.

[226] S. R. Ranade, Y. Guan, R. B. Moore, J. G. Dillard, R. C. Batra, and D. A. Dillard, "Characterizing fracture performance and the interaction of propagating cracks with locally weakened interfaces in adhesive joints," *International Journal of Adhesion and Adhesives*, vol. 82, pp. 196–205, 2018.

[227] A. J. Kinloch, E. Thrusabanjong, and J. G. Williams, "Fracture at bimaterial interfaces: the role of residual stresses," *Journal of Materials Science*, vol. 26, no. 23, pp. 6260–6270, 1991.

[228] M. D. Thouless, "Fracture resistance of an adhesive interface," *Scripta metallurgica et materialia*, vol. 26, no. 6, pp. 949–951, 1992.

[229] H. Parvatareddy and D. A. Dillard, "Effect of mode-mixity on the fracture toughness of Ti-6Al-4V/FM-5 adhesive joints," *International Journal of Fracture*, vol. 96, no. 3, pp. 215–228, 1999.

[230] B. Chen, D. A. Dillard, J. G. Dillard, and R. L. Clark, "Crack path selection in adhesively bonded joints: the roles of external loads and speciment geometry," *International Journal of Fracture*, vol. 114, no. 2, pp. 167–190, 2002.

[231] D. A. Dillard, H. K. Singh, D. J. Pohlit, and J. M. Starbuck, "Observations of decreased fracture toughness for mixed mode fracture testing of adhesively bonded joints," *Journal of Adhesion Science and Technology*, vol. 23, no. 10-11, pp. 1515–1530, 2009.

[232] N. A. Fleck, J. W. Hutchinson, and S. Zhigang, "Crack path selection in a brittle adhesive layer," *International Journal of Solids and Structures*, vol. 27, no. 13, pp. 1683–1703, 1991.

[233] M. Mirsayar, M. Aliha, and A. Samaei, "On fracture initiation angle near bi-material notches–effects of first non-singular stress term," *Engineering Fracture Mechanics*, vol. 119, pp. 124–131, 2014.

[234] B. Chen and D. A. Dillard, "The effect of the t-stress on crack path selection in adhesively bonded joints," *International Journal of Adhesion and Adhesives*, vol. 21, no. 5, pp. 357–368, 2001.

[235] H. Chai, "A note on crack trajectory in an elastic strip bounded by rigid substrates," *International Journal of Fracture*, vol. 32, no. 3, pp. 211–213, 1986.

[236] J.-B. Leblond and J. Frelat, "Crack kinking from an initially closed interface crack," *Comptes Rendus de l'Académie des Sciences-Series IIB-Mechanics-Physics-Astronomy*, vol. 327, no. 13, pp. 1311–1318, 1999.

[237] D. Xie, A. M. Waas, K. W. Shahwan, J. A. Schroeder, and R. G. Boeman, "Fracture criterion for kinking cracks in a tri-material adhesively bonded joint under mixed mode loading," *Engineering Fracture Mechanics*, vol. 72, no. 16, pp. 2487–2504, 2005.

[238] M.-Y. He, A. Bartlett, A. G. Evans, and J. W. Hutchinson, "Kinking of a crack out of an interface: role of in-plane stress," *Journal of the American Ceramic Society*, vol. 74, no. 4, pp. 767–771, 1991.

[239] J. Frelat and J.-B. Leblond, "Crack kinking from an initially closed interface crack in the presence of friction," in *IUTAM Symposium on Analytical and Computational Fracture Mechanics of Non-Homogeneous Materials*, pp. 223–232, Springer, 2002.

[240] T. Becker Jr, R. Cannon, and R. Ritchie, "Finite crack kinking and T-stresses in functionally graded materials," *International Journal of Solids and Structures*, vol. 38, no. 32-33, pp. 5545–5563, 2001.

[241] K. Kendall, "The dynamics of slow peeling," *International Journal of Fracture*, vol. 11, no. 1, pp. 3–12, 1975.

[242] D. J. Macon and G. L. Anderson, "Kinetic energy corrections for slip-stick behavior in brittle adhesives," *Journal of Applied Polymer Science*, vol. 86, no. 8, pp. 1821–1828, 2002.

[243] D. A. Dillard, D. J. Pohlit, G. C. Jacob, J. M. Starbuck, and R. K. Kapania, "On the use of a driven wedge test to acquire dynamic fracture energies of bonded beam specimens," *The Journal of Adhesion*, vol. 87, no. 4, pp. 395–423, 2011.

[244] M. Kanninen, "Applications of dynamic fracture mechanics for the prediction of crack arrest in engineering structures," *International journal of fracture*, vol. 27, pp. 299–312, 1985.

[245] B. Blackman, A. J. Kinloch, F. R. Sanchez, W. Teo, and J. G. Williams, "The fracture behaviour of structural adhesives under high rates of testing," *Engineering Fracture Mechanics*, vol. 76, no. 18, pp. 2868–2889, 2009.

[246] A. Karac, B. Blackman, V. Cooper, A. J. Kinloch, S. R. Sanchez, W. Teo, and A. Ivankovic, "Modelling the fracture behaviour of adhesively-bonded joints as a function of test rate," *Engineering Fracture Mechanics*, vol. 78, no. 6, pp. 973–989, 2011.

[247] D. Maugis, "Subcritical crack growth, surface energy, fracture toughness, stick-slip and embrittlement," *Journal of Materials Science*, vol. 20, no. 9, pp. 3041–3073, 1985.

[248] J. Hutchinson and P. Paris, "Stability of analysis of J controlled crack growth," *ASTM STP*, vol. 668, pp. 37–64, 1979.

[249] B. Blackman, J. Dear, A. J. Kinloch, H. Macgillivray, Y. Wang, J. G. Williams, and P. Yayla, "The failure of fibre composites and adhesively bonded fibre composites under high rates of test," *Journal of Materials Science*, vol. 30, no. 23, pp. 5885–5900, 1995.

[250] D. Maugis and M. Barquins, "Stick-slip and peeling of adhesive tapes," in *Adhesion 12*, pp. 205–222, Springer, 1988.

[251] S. Yamini and R. J. Young, "The mechanical properties of epoxy resins," *Journal of Materials Science*, vol. 15, no. 7, pp. 1823–1831, 1980.

[252] D. Pohlit, D. Dillard, G. Jacob, and J. Starbuck, "Evaluating the rate-dependent fracture toughness of an automotive adhesive," *The Journal of Adhesion*, vol. 84, no. 2, pp. 143–163, 2008.

[253] S. Xu and D. A. Dillard, "Determining the impact resistance of electrically conductive adhesives using a falling wedge test," *IEEE Transactions on Components and Packaging Technologies*, vol. 26, no. 3, pp. 554–562, 2003.

[254] M. Ciccotti, B. Giorgini, and M. Barquins, "Stick-slip in the peeling of an adhesive tape: evolution of theoretical model," *International Journal of Adhesion and Adhesives*, vol. 18, no. 1, pp. 35–40, 1998.

[255] M.-J. Dalbe, R. Villey, M. Ciccotti, S. Santucci, P.-P. Cortet, and L. Vanel, "Inertial and stick-slip regimes of unstable adhesive tape peeling," *Soft Matter*, vol. 12, no. 20, pp. 4537–4548, 2016.

[256] S. Das, N. Cadirov, S. Chary, Y. Kaufman, J. Hogan, K. L. Turner, and J. N. Israelachvili, "Stick–slip friction of gecko-mimetic flaps on smooth and rough surfaces," *Journal of The Royal Society Interface*, vol. 12, no. 104, p. 20141346, 2015.

[257] E. Andrews, T. Khan, and H. Majid, "Adhesion to skin: Part 1 peel tests with hard and soft machines," *Journal of Materials Science*, vol. 20, no. 10, pp. 3621–3630, 1985.

[258] J. C. Simón, E. Johnson, and D. A. Dillard, "Characterizing dynamic fracture behavior of adhesive joints under quasi-static and impact loading," *Journal of ASTM International*, vol. 2, no. 7, p. 53, 2005.

[259] S. T. Thoroddsen, H. Nguyen, K. Takehara, and T. Etoh, "Stick-slip substructure in rapid tape peeling," *Physical Review E*, vol. 82, no. 4, p. 046107, 2010.

[260] C. G. Camara, J. V. Escobar, J. R. Hird, and S. J. Putterman, "Correlation between nanosecond x-ray flashes and stick–slip friction in peeling tape," *Nature*, vol. 455, no. 7216, pp. 1089–1092, 2008.

[261] D. J. Irschick, C. C. Austin, K. Petren, R. N. Fisher, J. B. Losos, and O. Ellers, "A comparative analysis of clinging ability among pad-bearing lizards," *Biological Journal of the Linnean Society*, vol. 59, no. 1, pp. 21–35, 1996.

[262] S. Gorb, *Attachment devices of insect cuticle*. Dordrecht, Netherlands: Springer Science & Business Media, 2001.

[263] R. Spolenak, S. Gorb, H. Gao, and E. Arzt, "Effects of contact shape on the scaling of biological attachments," *Proceedings of the Royal Society A: Mathematical, Physical and Engineering Sciences*, vol. 461, no. 2054, pp. 305–319, 2005.

[264] A. Y. Stark, I. Badge, N. A. Wucinich, T. W. Sullivan, P. H. Niewiarowski, and A. Dhinojwala, "Surface wettability plays a significant role in gecko adhesion underwater," *Proceedings of the National Academy of Sciences*, vol. 110, no. 16, pp. 6340–6345, 2013.

[265] V. Sahni, T. A. Blackledge, and A. Dhinojwala, "A review on spider silk adhesion," *The Journal of Adhesion*, vol. 87, no. 6, pp. 595–614, 2011.

[266] I. Badge, A. Y. Stark, E. L. Paoloni, P. H. Niewiarowski, and A. Dhinojwala, "The role of surface chemistry in adhesion and wetting of gecko toe pads," *Scientific Reports*, vol. 4, no. 1, pp. 1–8, 2014.

[267] N. Glassmaker, A. Jagota, C.-Y. Hui, and J. Kim, "Design of biomimetic fibrillar interfaces: 1. making contact," *Journal of the Royal Society Interface*, vol. 1, no. 1, pp. 23–33, 2004.

[268] C.-Y. Hui, N. Glassmaker, T. Tang, and A. Jagota, "Design of biomimetic fibrillar interfaces: 2. mechanics of enhanced adhesion," *Journal of the Royal Society Interface*, vol. 1, no. 1, pp. 35–48, 2004.

[269] C. A. Gilman, M. J. Imburgia, M. D. Bartlett, D. R. King, A. J. Crosby, and D. J. Irschick, "Geckos as springs: Mechanics explain across-species scaling of adhesion," *PLOS ONE*, vol. 10, no. 9, p. e0134604, 2015.

[270] S. Reddy, E. Arzt, and A. del Campo, "Bioinspired surfaces with switchable adhesion," *Advanced Materials*, vol. 19, no. 22, pp. 3833–3837, 2007.

[271] K. Autumn and N. Gravish, "Gecko adhesion: evolutionary nanotechnology," *Philosophical Transactions of the Royal Society A: Mathematical, Physical and Engineering Sciences*, vol. 366, no. 1870, pp. 1575–1590, 2008.

[272] A. Peattie and R. Full, "Phylogenetic analysis of the scaling of wet and dry biological fibrillar adhesives," *Proceedings of the National Academy of Sciences*, vol. 104, no. 47, pp. 18595–18600, 2007.

[273] P. Y. Hsu, L. Ge, X. Li, A. Y. Stark, C. Wesdemiotis, P. H. Niewiarowski, and A. Dhinojwala, "Direct evidence of phospholipids in gecko footprints and spatula–substrate contact interface detected using surface-sensitive spectroscopy," *Journal of the Royal Society Interface*, vol. 9, no. 69, pp. 657–664, 2012.

[274] L. F. Boesel, C. Greiner, E. Arzt, and A. Del Campo, "Gecko-inspired surfaces: a path to strong and reversible dry adhesives," *Advanced Materials*, vol. 22, no. 19, pp. 2125–2137, 2010.

[275] M. Varenberg, B. Murarash, Y. Kligerman, and S. N. Gorb, "Geometry-controlled adhesion: revisiting the contact splitting hypothesis," *Applied Physics A*, vol. 103, pp. 933–938, 2011.

[276] M. Varenberg, N. M. Pugno, and S. N. Gorb, "Spatulate structures in biological fibrillar adhesion," *Soft Matter*, vol. 6, p. 3269, 2010.

[277] M. D. Bartlett, A. B. Croll, D. R. King, B. M. Paret, D. J. Irschick, and A. J. Crosby, "Looking beyond fibrillar features to scale gecko-like adhesion," *Advanced Materials*, vol. 24, no. 8, pp. 1078–1083, 2012.

[278] N. J. Glassmaker, A. Jagota, C.-Y. Hui, W. L. Noderer, and M. K. Chaudhury, "Biologically inspired crack trapping for enhanced adhesion.," *Proceedings of the National Academy of Sciences*, vol. 104, no. 26, pp. 10786–10791, 2007.

[279] A. Ghatak, L. Mahadevan, J. Y. Chung, M. K. Chaudhury, and V. Shenoy, "Peeling from a biomimetically patterned thin elastic film," *Proceedings of the Royal Society of London. Series A: Mathematical, Physical and Engineering Sciences*, vol. 460, no. 2049, pp. 2725–2735, 2004.

[280] J. Y. Chung and M. K. Chaudhury, "Roles of discontinuities in bio-inspired adhesive pads.," *Journal of the Royal Society Interface*, vol. 2, no. 2, pp. 55–61, 2005.

[281] D. R. King, M. D. Bartlett, C. A. Gilman, D. J. Irschick, and A. J. Crosby, "Creating gecko-like adhesives for "real world" surfaces," *Advanced Materials*, vol. 26, no. 25, pp. 4345–4351, 2014.

[282] M. D. Bartlett and A. J. Crosby, "High capacity, easy release adhesives from renewable materials," *Advanced Materials*, vol. 26, no. 21, pp. 3405–3409, 2014.

[283] M. D. Bartlett and A. J. Crosby, "Scaling normal adhesion force capacity with a generalized parameter," *Langmuir*, vol. 29, no. 35, pp. 11022–11027, 2013.

[284] M. D. Bartlett, A. B. Croll, and A. J. Crosby, "Designing bio-inspired adhesives for shear loading: From simple structures to complex patterns," *Advanced Functional Materials*, vol. 22, no. 23, pp. 4985–4992, 2012.

[285] J. Risan, A. B. Croll, and F. Azarmi, "Compliance switching for adhesion control," *Journal of Polymer Science Part B: Polymer Physics*, vol. 53, no. 1, pp. 48–57, 2015.

[286] S. T. Frey, A. B. M. T. Haque, R. Tutika, E. V. Krotz, C. Lee, C. B. Haverkamp, E. J. Markvicka, and M. D. Bartlett, "Octopus-inspired adhesive skins for intelligent and rapidly switchable underwater adhesion," *Science Advances*, vol. 8, no. 28, p. eabq1905, 2022.

[287] Z. Gu, S. Li, F. Zhang, and S. Wang, "Understanding surface adhesion in nature: A peeling model," *Advanced Science*, vol. 3, no. 7, p. 1500327, 2016.

[288] W. Federle, W. Barnes, W. Baumgartner, P. Drechsler, and J. Smith, "Wet but not slippery: boundary friction in tree frog adhesive toe pads," *Journal of the Royal Society Interface*, vol. 3, no. 10, pp. 689–697, 2006.

[289] W. J. Barnes, C. Oines, J. M. Smith, *et al.*, "Whole animal measurements of shear and adhesive forces in adult tree frogs: insights into underlying mechanisms of adhesion obtained from studying the effects of size and scale," *Journal of Comparative Physiology A*, vol. 192, no. 11, pp. 1179–1191, 2006.

[290] G. Hanna, W. Jon, and W. J. Barnes, "Adhesion and detachment of the toe pads of tree frogs," *Journal of Experimental Biology*, vol. 155, no. 1, pp. 103–125, 1991.

[291] B. Persson, "Wet adhesion with application to tree frog adhesive toe pads and tires," *Journal of Physics: Condensed Matter*, vol. 19, no. 37, p. 376110, 2007.

[292] F. Meng, Q. Liu, X. Wang, D. Tan, L. Xue, and W. J. P. Barnes, "Tree frog adhesion biomimetics: opportunities for the development of new, smart adhesives that adhere under wet conditions," *Philosophical Transactions of the Royal Society A*, vol. 377, no. 2150, p. 20190131, 2019.

[293] J. K. Langowski, D. Dodou, M. Kamperman, and J. L. van Leeuwen, "Tree frog attachment: mechanisms, challenges, and perspectives," *Frontiers in Zoology*, vol. 15, no. 1, pp. 1–21, 2018.

[294] Q. Liu, D. Tan, F. Meng, B. Yang, Z. Shi, X. Wang, Q. Li, C. Nie, S. Liu, and L. Xue, "Adhesion enhancement of micropillar array by combining the adhesive design from gecko and tree frog," *Small*, vol. 17, no. 4, p. 2005493, 2021.

[295] Z. Shi, D. Tan, Q. Liu, F. Meng, B. Zhu, and L. Xue, "Tree frog-inspired nanopillar arrays for enhancement of adhesion and friction," *Biointerphases*, vol. 16, no. 2, p. 021001, 2021.

[296] Y. Chen, J. Meng, Z. Gu, X. Wan, L. Jiang, and S. Wang, "Bioinspired multiscale wet adhesive surfaces: structures and controlled adhesion," *Advanced Functional Materials*, vol. 30, no. 5, p. 1905287, 2020.

[297] J. H. Waite, "Mussel adhesion–essential footwork," *Journal of Experimental Biology*, vol. 220, no. 4, pp. 517–530, 2017.

[298] N. Cohen, J. H. Waite, R. M. McMeeking, and M. T. Valentine, "Force distribution and multiscale mechanics in the mussel byssus," *Philosophical Transactions of the Royal Society B*, vol. 374, no. 1784, p. 20190202, 2019.

[299] H. Lee, B. P. Lee, and P. B. Messersmith, "A reversible wet/dry adhesive inspired by mussels and geckos," *Nature*, vol. 448, no. 7151, pp. 338–341, 2007.

[300] B. P. Lee, P. B. Messersmith, J. N. Israelachvili, and J. H. Waite, "Mussel-inspired adhesives and coatings," *Annual Review of Materials Research*, vol. 41, pp. 99–132, 2011.

[301] P. Kord Forooshani and B. P. Lee, "Recent approaches in designing bioadhesive materials inspired by mussel adhesive protein," *Journal of Polymer Science Part A: Polymer Chemistry*, vol. 55, no. 1, pp. 9–33, 2017.

[302] M. S. Akram Bhuiyan, J. D. Roland, B. Liu, M. Reaume, Z. Zhang, J. D. Kelley, and B. P. Lee, "In situ deactivation of catechol-containing adhesive using electrochemistry," *Journal of the American Chemical Society*, vol. 142, no. 10, pp. 4631–4638, 2020.

[303] N. Bandara, H. Zeng, and J. Wu, "Marine mussel adhesion: biochemistry, mechanisms, and biomimetics," *Journal of Adhesion Science and Technology*, vol. 27, no. 18-19, pp. 2139–2162, 2013.

[304] K. W. Desmond, N. A. Zacchia, J. H. Waite, and M. T. Valentine, "Dynamics of mussel plaque detachment," *Soft Matter*, vol. 11, no. 34, pp. 6832–6839, 2015.

[305] J. Li, A. Celiz, J. Yang, Q. Yang, I. Wamala, W. Whyte, B. Seo, N. Vasilyev, J. Vlassak, Z. Suo, *et al.*, "Tough adhesives for diverse wet surfaces," *Science*, vol. 357, no. 6349, pp. 378–381, 2017.

[306] J. P. Gong, Y. Katsuyama, T. Kurokawa, and Y. Osada, "Double-network hydrogels with extremely high mechanical strength," *Advanced Materials*, vol. 15, no. 14, pp. 1155–1158, 2003.

[307] J. P. Gong, "Why are double network hydrogels so tough?," *Soft Matter*, vol. 6, no. 12, pp. 2583–2590, 2010.

[308] Y. S. Zhang and A. Khademhosseini, "Advances in engineering hydrogels," *Science*, vol. 356, no. 6337, p. eaaf3627, 2017.

[309] A. Phadke, C. Zhang, B. Arman, C.-C. Hsu, R. A. Mashelkar, A. K. Lele, M. J. Tauber, G. Arya, and S. Varghese, "Rapid self-healing hydrogels," *Proceedings of the National Academy of Sciences*, vol. 109, no. 12, pp. 4383–4388, 2012.

[310] Z. Wei, J. H. Yang, J. Zhou, F. Xu, M. Zrínyi, P. H. Dussault, Y. Osada, and Y. M. Chen, "Self-healing gels based on constitutional dynamic chemistry and their potential applications," *Chemical Society Reviews*, vol. 43, no. 23, pp. 8114–8131, 2014.

[311] I. Jeon, J. Cui, W. R. Illeperuma, J. Aizenberg, and J. J. Vlassak, "Extremely stretchable and fast self-healing hydrogels," *Advanced Materials*, vol. 28, no. 23, pp. 4678–4683, 2016.

[312] D. R. King, T. Okumura, R. Takahashi, T. Kurokawa, and J. P. Gong, "Macroscale double networks: design criteria for optimizing strength and toughness," *ACS Applied Materials & Interfaces*, vol. 11, no. 38, pp. 35343–35353, 2019.

[313] X. Feng, Z. Ma, J. V. MacArthur, C. J. Giuffre, A. F. Bastawros, and W. Hong, "A highly stretchable double-network composite," *Soft Matter*, vol. 12, no. 44, pp. 8999–9006, 2016.

[314] L. Han, X. Lu, K. Liu, K. Wang, L. Fang, L.-T. Weng, H. Zhang, Y. Tang, F. Ren, C. Zhao, *et al.*, "Mussel-inspired adhesive and tough hydrogel based on nanoclay confined dopamine polymerization," *ACS Nano*, vol. 11, no. 3, pp. 2561–2574, 2017.

[315] X. Zhao, "Multi-scale multi-mechanism design of tough hydrogels: building dissipation into stretchy networks," *Soft Matter*, vol. 10, no. 5, pp. 672–687, 2014.

[316] C. Creton and M. Ciccotti, "Fracture and adhesion of soft materials: a review," *Reports on Progress in Physics*, vol. 79, no. 4, p. 046601, 2016.

[317] R. Takahashi, K. Shimano, H. Okazaki, T. Kurokawa, T. Nakajima, T. Nonoyama, D. R. King, and J. P. Gong, "Tough particle-based double network hydrogels for functional solid surface coatings," *Advanced Materials Interfaces*, vol. 5, no. 23, p. 1801018, 2018.

[318] C. Cui, B. Liu, T. Wu, Y. Liu, C. Fan, Z. Xu, Y. Yao, and W. Liu, "A hyperbranched polymer elastomer-based pressure sensitive adhesive," *Journal of Materials Chemistry A*, 2022.

[319] J. Bobyn, G. Wilson, D. MacGregor, R. Pilliar, and G. Weatherly, "Effect of pore size on the peel strength of attachment of fibrous tissue to porous-surfaced implants," *Journal of Biomedical Materials Research*, vol. 16, no. 5, pp. 571–584, 1982.

[320] J. Steck, J. Kim, J. Yang, S. Hassan, and Z. Suo, "Topological adhesion. I. rapid and strong topohesives," *Extreme Mechanics Letters*, vol. 39, p. 100803, 2020.

[321] J. Yang, R. Bai, B. Chen, and Z. Suo, "Hydrogel adhesion: A supramolecular synergy of chemistry, topology, and mechanics," *Advanced Functional Materials*, vol. 30, no. 2, p. 1901693, 2020.

[322] J. Liu, S. Lin, X. Liu, Z. Qin, Y. Yang, J. Zang, and X. Zhao, "Fatigue-resistant adhesion of hydrogels," *Nature Communications*, vol. 11, no. 1, pp. 1–9, 2020.

[323] W. Zhang, Y. Gao, H. Yang, Z. Suo, and T. Lu, "Fatigue-resistant adhesion I. long-chain polymers as elastic dissipaters," *Extreme Mechanics Letters*, vol. 39, p. 100813, 2020.

[324] K. Sawyers and R. Rivlin, "The trousers test for rupture," *Engineering Fracture Mechanics*, vol. 6, no. 3, pp. 557–562, 1974.

[325] A. M. Hubbard, W. Cui, Y. Huang, R. Takahashi, M. D. Dickey, J. Genzer, D. R. King, and J. P. Gong, "Hydrogel/elastomer laminates bonded via fabric interphases for stimuli-responsive actuators," *Matter*, vol. 1, no. 3, pp. 674–689, 2019.

[326] M. Wang, P. Zhang, M. Shamsi, J. L. Thelen, W. Qian, V. K. Truong, J. Ma, J. Hu, and M. D. Dickey, "Tough and stretchable ionogels by in situ phase separation," *Nature Materials*, vol. 21, no. 3, pp. 359–365, 2022.

[327] ASTM D624-00, *Standard Test Method for Tear Strength of Conventional Vulcanized Rubber and Thermoplastic Elastomers*. West Conshohocken, PA: American Society for Testing and Materials.

[328] A. R. Mojdehi, D. P. Holmes, and D. A. Dillard, "Revisiting the generalized scaling law for adhesion: role of compliance and extension to progressive failure," *Soft Matter*, vol. 13, no. 41, pp. 7529–7536, 2017.

[329] D. Satas, *Handbook of pressure sensitive adhesive technology*, vol. 1. Springer, 1989.

[330] R. Milker and Z. Czech, "New trends in the development of solvent-free acrylic psa systems," *RadTech Europe*, vol. 5, pp. 573–582, 2005.

[331] M. F. Tse, "Studies of triblock copolymer-tackifying resin interactions by viscoelasticity and adhesive performance," *Journal of Adhesion Science and Technology*, vol. 3, no. 1, pp. 551–570, 1989.

[332] H. W. Yang, "Water-based polymers as pressure-sensitive adhesives—viscoelastic guidelines," *Journal of Applied Polymer Science*, vol. 55, no. 4, pp. 645–652, 1995.

[333] R. Villey, C. Creton, P.-P. Cortet, M.-J. Dalbe, T. Jet, B. Saintyves, S. Santucci, L. Vanel, D. J. Yarusso, and M. Ciccotti, "Rate-dependent elastic hysteresis during the peeling of pressure sensitive adhesives," *Soft Matter*, vol. 11, no. 17, pp. 3480–3491, 2015.

[334] J. Chopin, R. Villey, D. Yarusso, E. Barthel, C. Creton, and M. Ciccotti, "Nonlinear viscoelastic modeling of adhesive failure for polyacrylate pressure-sensitive adhesives," *Macromolecules*, vol. 51, no. 21, pp. 8605–8610, 2018.

[335] D. J. Yarusso, "Quantifying the relationship between peel and rheology for pressure sensitive adhesives," *The Journal of Adhesion*, vol. 70, no. 3-4, pp. 299–320, 1999.

[336] C. Dahlquist, "Pressure-sensitive adhesives" in "Treatise on Adhesion and Adhesives," *edited by R. L. Patrick, CRC Press*, vol. 2, pp. 219–260, 1969.

[337] B. E. Gdalin, E. V. Bermesheva, G. A. Shandryuk, and M. M. Feldstein, "Effect of temperature on probe tack adhesion: Extension of the dahlquist criterion of tack," *The Journal of Adhesion*, vol. 87, no. 2, pp. 111–138, 2011.

[338] K. Autumn, C. Majidi, R. Groff, A. Dittmore, and R. Fearing, "Effective elastic modulus of isolated gecko setal arrays," *Journal of Experimental Biology*, vol. 209, no. 18, pp. 3558–3568, 2006.

[339] C. Creton and H. Lakrout, "Micromechanics of flat-probe adhesion tests of soft viscoelastic polymer films," *Journal of Polymer Science Part B: Polymer Physics*, vol. 38, no. 7, pp. 965–979, 2000.

[340] B. Persson, O. Albohr, C. Creton, and V. Peveri, "Contact area between a viscoelastic solid and a hard, randomly rough, substrate," *The Journal of Chemical Physics*, vol. 120, no. 18, pp. 8779–8793, 2004.

[341] F. Deplace, C. Carelli, S. Mariot, H. Retsos, A. Chateauminois, K. Ouzineb, and C. Creton, "Fine tuning the adhesive properties of a soft nanostructured adhesive with rheological measurements," *The Journal of Adhesion*, vol. 85, no. 1, pp. 18–54, 2009.

[342] H. W. Yang and E.-P. Chang, "The role of viscoelastic properties in the design of pressure-sensitive adhesives," *Trends in Polymer Science*, vol. 11, no. 5, pp. 380–384, 1997.

[343] J. D. Ferry, *Viscoelastic Properties of Polymers*. New York, USA: Wiley, 1980.

[344] V. Pandey, A. Fleury, R. Villey, C. Creton, and M. Ciccotti, "Linking peel and tack performances of pressure sensitive adhesives," *Soft Matter*, vol. 16, no. 13, pp. 3267–3275, 2020.

[345] A. Zosel, "The effect of fibrilation on the tack of pressure sensitive adhesives," *International Journal of Adhesion and Adhesives*, vol. 18, no. 4, pp. 265–271, 1998.

[346] I. Mohammed, M. Charalambides, and A. J. Kinloch, "Modelling the interfacial peeling of pressure-sensitive adhesives," *Journal of Non-Newtonian Fluid Mechanics*, vol. 222, pp. 141–150, 2015.

[347] K. Takahashi, R. Oda, K. Inaba, and K. Kishimoto, "Scaling effect on the detachment of pressure-sensitive adhesives through fibrillation characterized by a probe-tack test," *Soft Matter*, vol. 16, no. 28, pp. 6493–6500, 2020.

[348] J. Du, D. Lindeman, and D. Yarusso, "Modeling the peel performance of pressure-sensitive adhesives," *The Journal of Adhesion*, vol. 80, no. 7, pp. 601–612, 2004.

[349] H. Lakrout, P. Sergot, and C. Creton, "Direct observation of cavitation and fibrillation in a probe tack experiment on model acrylic pressure-sensitive-adhesives," *The Journal of Adhesion*, vol. 69, no. 3-4, pp. 307–359, 1999.

[350] G. Lamanna and A. Basile, "Mechanics of soft PSAs (pressure sensitive adhesives)," *The Open Materials Science Journal*, vol. 7, no. 1, pp. 23–28, 2013.

[351] B. G. Vossen, P. J. Schreurs, O. van der Sluis, and M. Geers, "Multi-scale modeling of delamination through fibrillation," *Journal of the Mechanics and Physics of Solids*, vol. 66, pp. 117–132, 2014.

[352] L. Zhang and J. Wang, "A generalized cohesive zone model of the peel test for pressure-sensitive adhesives," *International Journal of Adhesion and Adhesives*, vol. 29, no. 3, pp. 217–224, 2009.

[353] Y.-Y. Lin, C. Hui, and Y. Wang, "Modeling the failure of an adhesive layer in a peel test," *Journal of Polymer Science Part B: Polymer Physics*, vol. 40, no. 19, pp. 2277–2291, 2002.

[354] A. N. Gent and P. Lindley, "Internal rupture of bonded rubber cylinders in tension," *Proceedings of the Royal Society of London. Series A. Mathematical and Physical Sciences*, vol. 249, no. 1257, pp. 195–205, 1959.

[355] A. N. Gent, "Cavitation in rubber: a cautionary tale," *Rubber Chemistry and Technology*, vol. 63, no. 3, pp. 49–53, 1990.

[356] A. N. Gent and C. Wang, "Fracture mechanics and cavitation in rubber-like solids," *Journal of Materials Science*, vol. 26, no. 12, pp. 3392–3395, 1991.

[357] C. Creton, G. Hu, F. Deplace, L. Morgret, and K. R. Shull, "Large-strain mechanical behavior of model block copolymer adhesives," *Macromolecules*, vol. 42, no. 20, pp. 7605–7615, 2009.

[358] A. J. Crosby and J. McManus, "Blowing bubbles to study living material," *Physics Today*, vol. 64, no. 2, pp. 62–63, 2011.

[359] J. A. Zimberlin, J. J. McManus, and A. J. Crosby, "Cavitation rheology of the vitreous: mechanical properties of biological tissue," *Soft Matter*, vol. 6, no. 15, pp. 3632–3635, 2010.

[360] M. Helbig and T. Seelig, "Micro-mechanical modeling of fibrillation in amorphous polymers," *Computational Materials Science*, vol. 52, no. 1, pp. 118–122, 2012.

[361] I. Mohammed, M. Charalambides, and A. J. Kinloch, "Modelling the interfacial peeling of pressure-sensitive adhesives," *Journal of Non-Newtonian Fluid Mechanics*, vol. 233, pp. 85–94, 2016.

[362] K. Rizi, I. Mohammed, K. Xu, A. J. Kinloch, M. Charalambides, and S. Murdan, "A systematic approach to the formulation of anti-onychomycotic nail patches," *European Journal of Pharmaceutics and Biopharmaceutics*, vol. 127, pp. 355–365, 2018.

[363] S. Venkatraman and R. Gale, "Skin adhesives and skin adhesion: 1. transdermal drug delivery systems," *Biomaterials*, vol. 19, no. 13, pp. 1119–1136, 1998.

[364] H. S. Tan and W. R. Pfister, "Pressure-sensitive adhesives for transdermal drug delivery systems," *Pharmaceutical Science & Technology Today*, vol. 2, no. 2, pp. 60–69, 1999.

[365] R. H. Plaut, "Two-dimensional analysis of peeling adhesive tape from human skin," *The Journal of Adhesion*, vol. 86, no. 11, pp. 1086–1110, 2010.

[366] S. T. de Freitas and J. Sinke, "Adhesion properties of bonded composite-to-aluminium joints using peel tests," *The Journal of Adhesion*, vol. 90, no. 5-6, pp. 511–525, 2014.

[367] S. T. de Freitas and J. Sinke, "Test method to assess interface adhesion in composite bonding," *Applied Adhesion Science*, vol. 3, no. 1, pp. 1–13, 2015.

[368] S. T. de Freitas, M. Banea, S. Budhe, and S. De Barros, "Interface adhesion assessment of composite-to-metal bonded joints under salt spray conditions using peel tests," *Composite Structures*, vol. 164, pp. 68–75, 2017.

[369] Y. Su, M. de Rooij, W. Grouve, and L. Warnet, "Characterisation of metal–thermoplastic composite hybrid joints by means of a mandrel peel test," *Composites Part B: Engineering*, vol. 95, pp. 293–300, 2016.

[370] A. Endruweit, G. Y. Choong, S. Ghose, B. A. Johnson, D. R. Younkin, N. A. Warrior, and D. S. De Focatiis, "Characterisation of tack for uni-directional prepreg tape employing a continuous application-and-peel test method," *Composites Part A: Applied Science and Manufacturing*, vol. 114, pp. 295–306, 2018.

[371] G. Choong, A. Endruweit, and D. De Focatiis, "Analysis of contact area in a continuous application-and-peel test method for prepreg tack," *International Journal of Adhesion and Adhesives*, vol. 107, p. 102849, 2021.

[372] R. J. Crossley, P. J. Schubel, and D. S. De Focatiis, "Time–temperature equivalence in the tack and dynamic stiffness of polymer prepreg and its application to automated composites manufacturing," *Composites Part A: Applied Science and Manufacturing*, vol. 52, pp. 126–133, 2013.

[373] A. Endruweit, D. S. De Focatiis, S. Ghose, B. A. Johnson, D. R. Younkin, and N. A. Warrior, "Characterisation of prepreg tack on different surfaces to aid automated material placement," in *20th International Conference on Composite Materials, Copenhagen*, 2015.

[374] W. J. B. Grouve, L. Warnet, and R. Akkerman, "Critical assessment of the mandrel peel test for fiber reinforced thermoplastic laminates," *Engineering Fracture Mechanics*, vol. 101, pp. 96–108, 2013.

[375] F. Sacchetti, W. J. Grouve, L. L. Warnet, and I. F. Villegas, "Interlaminar fracture toughness of 5hs carbon/peek laminates. a comparison between DCB, ELS and mandrel peel tests," *Polymer Testing*, vol. 66, pp. 13–23, 2018.

[376] F. Daghia and C. Cluzel, "The climbing drum peel test: An alternative to the double cantilever beam for the determination of fracture toughness of monolithic laminates," *Composites Part A: Applied Science and Manufacturing*, vol. 78, pp. 70–83, 2015.

[377] S. Jain, K. M. Liechti, and R. T. Bonnecaze, "Cohesive zone models to understand the interface mechanics of thin film transfer printing," *Journal of Applied Physics*, vol. 125, no. 7, p. 075301, 2019.

[378] M. A. Meitl, Z.-T. Zhu, V. Kumar, K. J. Lee, X. Feng, Y. Y. Huang, I. Adesida, R. G. Nuzzo, and J. A. Rogers, "Transfer printing by kinetic control of adhesion to an elastomeric stamp," *Nature Materials*, vol. 5, no. 1, pp. 33–38, 2006.

[379] A. Carlson, A. M. Bowen, Y. Huang, R. G. Nuzzo, and J. A. Rogers, "Transfer printing techniques for materials assembly and micro/nanodevice fabrication," *Advanced Materials*, vol. 24, no. 39, pp. 5284–5318, 2012.

[380] A. Carlson, S. Wang, P. Elvikis, P. M. Ferreira, Y. Huang, and J. A. Rogers, "Active, programmable elastomeric surfaces with tunable adhesion for deterministic assembly by transfer printing," *Advanced Functional Materials*, vol. 22, p. 4476–4484, 6 2012.

[381] M. D. Swift, C. B. Haverkamp, C. J. Stabile, D. Hwang, R. H. Plaut, K. T. Turner, D. A. Dillard, and M. D. Bartlett, "Active membranes on rigidity tunable foundations for programmable, rapidly switchable adhesion," *Advanced Materials Technologies*, vol. 5, no. 11, p. 2000676, 2020.

[382] S. Song and M. Sitti, "Soft grippers using micro-fibrillar adhesives for transfer printing," *Advanced Materials*, vol. 26, no. 28, pp. 4901–4906, 2014.

[383] S. Kim, J. Wu, A. Carlson, S. H. Jin, A. Kovalsky, P. Glass, Z. Liu, N. Ahmed, S. L. Elgan, W. Chen, *et al.*, "Microstructured elastomeric surfaces with reversible adhesion and examples of their use in deterministic assembly by transfer printing," *Proceedings of the National Academy of Sciences*, vol. 107, no. 40, pp. 17095–17100, 2010.

[384] M. D. Bartlett and A. J. Crosby, "Material transfer controlled by elastomeric layer thickness," *Materials Horizons*, vol. 1, no. 5, pp. 507–512, 2014.

[385] D. R. Paretkar, M. D. Bartlett, R. McMeeking, A. J. Crosby, and E. Arzt, "Buckling of an adhesive polymeric micropillar," *The Journal of Adhesion*, vol. 89, no. 2, pp. 140–158, 2013.

[386] Y. Mengüç, S. Y. Yang, S. Kim, J. A. Rogers, and M. Sitti, "Gecko-Inspired Controllable Adhesive Structures Applied to Micromanipulation," *Advanced Functional Materials*, vol. 22, pp. 1246–1254, 1 2012.

[387] M. Zhou, Y. Tian, D. Sameoto, X. Zhang, Y. Meng, and S. Wen, "Controllable interfacial adhesion applied to transfer light and fragile objects by using gecko inspired mushroom-shaped pillar surface.," *ACS Applied Materials & Interfaces*, vol. 5, pp. 10137–44, 10 2013.

[388] C. Pang, S. M. Kim, Y. Rahmawan, and K.-Y. Suh, "Beetle-inspired bidirectional, asymmetric interlocking using geometry-tunable nanohairs," *ACS Applied Materials and Interfaces*, vol. 4, no. 8, pp. 4225–4230, 2012.

[389] H. Marvi, Y. Han, and M. Sitti, "Actively controlled fibrillar friction surfaces," *Applied Physics Letters*, vol. 051602, 2015.

[390] Z. Ye, G. Z. Lum, S. Song, S. Rich, and M. Sitti, "Phase change of gallium enables highly reversible and switchable adhesion," *Advanced Materials*, vol. 28, no. 25, pp. 5088–5092, 2016.

[391] J. D. Eisenhaure, T. Xie, S. Varghese, and S. Kim, "Microstructured shape memory polymer surfaces with reversible dry adhesion," *ACS Applied Materials & Interfaces*, vol. 5, no. 16, pp. 7714–7717, 2013.

[392] S. Y. Yang, A. Carlson, H. Cheng, Q. Yu, N. Ahmed, J. Wu, S. Kim, M. Sitti, P. M. Ferreira, Y. Huang, and J. Rogers, "Elastomer surfaces with directionally dependent adhesion strength and their use in transfer printing with continuous roll-to-roll applications," *Advanced Materials*, vol. 24, no. 16, pp. 2117–2122, 2012.

[393] J. Risan, A. B. Croll, and F. Azarmi, "Compliance switching for adhesion control," *Journal of Polymer Science Part B: Polymer Physics*, vol. 53, pp. 48–57, 2015.

[394] W. Wang, J. V. Timonen, A. Carlson, D.-M. Drotlef, C. T. Zhang, S. Kolle, A. Grinthal, T.-S. Wong, B. Hatton, S. H. Kang, *et al.*, "Multifunctional ferrofluid-infused surfaces with reconfigurable multiscale topography," *Nature*, vol. 559, no. 7712, pp. 77–82, 2018.

[395] D. M. Drotlef, P. Blümler, and A. Del Campo, "Magnetically actuated patterns for bioinspired reversible adhesion (dry and wet)," *Advanced Materials*, vol. 26, pp. 775–779, 2014.

[396] A. G. Gillies, J. Kwak, and R. S. Fearing, "Controllable particle adhesion with a magnetically actuated synthetic gecko adhesive," *Advanced Functional Materials*, vol. 23, p. 3256–3261, 2 2013.

[397] Z. Liu, Y. A. Huang, H. Liu, J. Chen, and Z. Yin, "Reliable peeling of ultrathin die with multineedle ejector," *IEEE Transactions on Components, Packaging and Manufacturing Technology*, vol. 4, no. 9, pp. 1545–1554, 2014.

[398] S. Bae, H. Kim, Y. Lee, X. Xu, J.-S. Park, Y. Zheng, J. Balakrishnan, T. Lei, H. R. Kim, Y. I. Song, *et al.*, "Roll-to-roll production of 30-inch graphene films for transparent electrodes," *Nature Nanotechnology*, vol. 5, no. 8, pp. 574–578, 2010.

[399] K. S. Novoselov, A. K. Geim, S. V. Morozov, D.-e. Jiang, Y. Zhang, S. V. Dubonos, I. V. Grigorieva, and A. A. Firsov, "Electric field effect in atomically thin carbon films," *Science*, vol. 306, no. 5696, pp. 666–669, 2004.

[400] D. Akinwande, C. J. Brennan, J. S. Bunch, P. Egberts, J. R. Felts, H. Gao, R. Huang, J.-S. Kim, T. Li, Y. Li, *et al.*, "A review on mechanics and mechanical properties of 2d materials—graphene and beyond," *Extreme Mechanics Letters*, vol. 13, pp. 42–77, 2017.

[401] Z. Cao, P. Wang, W. Gao, L. Tao, J. Suk, R. Ruoff, D. Akinwande, R. Huang, and K. Liechti, "A blister test for interfacial adhesion of large-scale transferred graphene," *Carbon*, vol. 69, pp. 390–400, 2014.

[402] Z. Cao, L. Tao, D. Akinwande, R. Huang, and K. M. Liechti, "Mixed-mode interactions between graphene and substrates by blister tests," *Journal of Applied Mechanics*, vol. 82, no. 8, 2015.

[403] S. Jain, T. Yang, M. Negley, S. R. Na, K. M. Liechti, and R. T. Bonnecaze, "A parametric cohesive zone beam theory analysis of mixed-mode graphene transfer," *International Journal of Adhesion and Adhesives*, vol. 89, pp. 129–138, 2019.

[404] R. H. Plaut, A. Borum, and D. A. Dillard, "Analysis of carbon nanotubes and graphene nanoribbons with folded racket shapes," *Journal of Engineering Materials and Technology*, vol. 134, no. 2, 2012.

[405] A. N. Gent, "Buckles in adhering elastic films and a test method for adhesion based on the elastica," *Journal of Adhesion Science and Technology*, vol. 8, no. 7, pp. 807–819, 1994.

[406] K. M. Barker, M. A. Poggi, L. Lizarraga, P. T. Lillehei, A. A. Ferri, and L. A. Bottomley, "Peeling of long, straight carbon nanotubes from surfaces," *Journal of Nanotechnology*, vol. 2014, 2014.

[407] C. Ke, M. Zheng, G. Zhou, W. Cui, N. Pugno, and R. N. Miles, "Mechanical peeling of free-standing single-walled carbon-nanotube bundles," *Small*, vol. 6, no. 3, pp. 438–445, 2010.

[408] Y. Li, Y. Xiong, Z. Zhou, B. Tang, Z. Yang, and J. Zhao, "The peeling behavior of nanowires and carbon nanotubes from a substrate using continuum modeling," *Journal of Applied Physics*, vol. 121, no. 5, p. 054303, 2017.

[409] X. Chen, M. Zheng, Q. Wei, S. Signetti, N. M. Pugno, and C. Ke, "Deformation of nanotubes in peeling contact with flat substrate: An in situ electron microscopy nanomechanical study," *Journal of Applied Physics*, vol. 119, no. 15, p. 154305, 2016.

[410] N. Khandoker, S. C. Hawkins, R. Ibrahim, and C. P. Huynh, "Peel test of spinnable carbon nanotube webs," *Physica E: Low-dimensional Systems and Nanostructures*, vol. 60, pp. 160–165, 2014.

[411] T.-H. Kim, K.-S. Cho, E. K. Lee, S. J. Lee, J. Chae, J. W. Kim, D. H. Kim, J.-Y. Kwon, G. Amaratunga, S. Y. Lee, *et al.*, "Full-colour quantum dot displays fabricated by transfer printing," *Nature Photonics*, vol. 5, no. 3, pp. 176–182, 2011.

[412] J. C. Love, L. A. Estroff, J. K. Kriebel, R. G. Nuzzo, and G. M. Whitesides, "Self-assembled monolayers of thiolates on metals as a form of nanotechnology," *Chemical Reviews*, vol. 105, no. 4, pp. 1103–1170, 2005.

[413] K. Felmet, Y.-L. Loo, and Y. Sun, "Patterning conductive copper by nanotransfer printing," *Applied Physics Letters*, vol. 85, no. 15, pp. 3316–3318, 2004.

[414] C. Kim, P. E. Burrows, and S. R. Forrest, "Micropatterning of organic electronic devices by cold-welding," *Science*, vol. 288, no. 5467, pp. 831–833, 2000.

[415] K.-H. Yim, Z. Zheng, Z. Liang, R. H. Friend, W. T. Huck, and J.-S. Kim, "Efficient conjugated-polymer optoelectronic devices fabricated by thin-film transfer-printing technique," *Advanced Functional Materials*, vol. 18, no. 7, pp. 1012–1019, 2008.

[416] J. P. Seymour, Y. M. Elkasabi, H.-Y. Chen, J. Lahann, and D. R. Kipke, "The insulation performance of reactive parylene films in implantable electronic devices," *Biomaterials*, vol. 30, no. 31, pp. 6158–6167, 2009.

[417] Q. Wei, K. Tajima, and K. Hashimoto, "Bilayer ambipolar organic thin-film transistors and inverters prepared by the contact-film-transfer method," *ACS Applied Materials & Interfaces*, vol. 1, no. 9, pp. 1865–1868, 2009.

[418] J. Gu, S. Miao, Z. Yan, and P. Yang, "Multiplex binding of amyloid-like protein nanofilm to different material surfaces," *Colloid and Interface Science Communications*, vol. 22, pp. 42–48, 2018.

[419] Z. Peng, S. Chen, and A. Soh, "Peeling behavior of a bio-inspired nano-film on a substrate," *International Journal of Solids and Structures*, vol. 47, no. 14-15, pp. 1952–1960, 2010.

[420] Z. Peng and S. Chen, "Effect of pre-tension on the peeling behavior of a bio-inspired nano-film and a hierarchical adhesive structure," *Applied Physics Letters*, vol. 101, no. 16, p. 163702, 2012.

[421] Z. Fan, J. C. Ho, T. Takahashi, R. Yerushalmi, K. Takei, A. C. Ford, Y.-L. Chueh, and A. Javey, "Toward the development of printable nanowire electronics and sensors," *Advanced Materials*, vol. 21, no. 37, pp. 3730–3743, 2009.

[422] D. Li and L. J. Guo, "Organic thin film transistors and polymer light-emitting diodes patterned by polymer inking and stamping," *Journal of Physics D: Applied Physics*, vol. 41, no. 10, p. 105115, 2008.

[423] D. Hines, A. Southard, A. Tunnell, V. Sangwan, T. Moore, J.-H. Chen, M. Fuhrer, and E. Williams, "Transfer printing as a method for fabricating hybrid devices on flexible substrates," in *Organic Field-Effect Transistors VI*, vol. 6658, pp. 141–151, SPIE, 2007.

[424] R. Qin, Y. Guo, H. Ren, Y. Liu, H. Su, X. Chu, Y. Jin, F. Lu, B. Wang, and P. Yang, "Instant adhesion of amyloid-like nanofilms with wet surfaces," *ACS Central Science*, vol. 8, pp. 705–717, 2022.

[425] W. Gao, Y. Zhang, D. Ramanujan, K. Ramani, Y. Chen, C. B. Williams, C. C. Wang, Y. C. Shin, S. Zhang, and P. D. Zavattieri, "The status, challenges, and future of additive manufacturing in engineering," *Computer-Aided Design*, vol. 69, pp. 65–89, 2015.

[426] J.-Y. Lee, J. An, and C. K. Chua, "Fundamentals and applications of 3D printing for novel materials," *Applied Materials Today*, vol. 7, pp. 120–133, 2017.

[427] Q. He, L. Ye, A. J. Kinloch, H. Wang, and B. Yin, "Characterisation of fusion bonding between filaments of thin 3D printed polyamide 6 using an essential work of fracture method," *Journal of Materials Science*, vol. 56, no. 3, pp. 2777–2794, 2021.

[428] Q. He, L. Ye, and A. J. Kinloch, "The essential work of fracture method for the characterisation of fusion bonding in 3d printed short carbon-fibre reinforced polyamide 6 thin films," *Composites Science and Technology*, p. 109361, 2022.

[429] I. Q. Vu, L. B. Bass, C. B. Williams, and D. A. Dillard, "Characterizing the effect of print orientation on interface integrity of multi-material jetting additive manufacturing," *Additive Manufacturing*, vol. 22, pp. 447–461, 2018.

[430] J. Butt, H. Mebrahtu, and H. Shirvani, "Peel and tensile test investigation of aluminium 1050 foil parts made with a new additive manufacturing process," *International Journal of Rapid Manufacturing*, vol. 5, no. 1, pp. 95–115, 2015.

[431] J. E. Seppala, S. H. Han, K. E. Hillgartner, C. S. Davis, and K. B. Migler, "Weld formation during material extrusion additive manufacturing," *Soft Matter*, vol. 13, no. 38, pp. 6761–6769, 2017.

[432] J. E. Seppala, K. E. Hillgartner, C. S. Davis, K. D. Migler, *et al.*, "Thermography and weld strength characterization of thermoplastic extrusion 3D printing," SPE ANTEC 2016, Indianapolis, IN, USA. 2016.

[433] C. S. Davis, K. E. Hillgartner, S. H. Han, and J. E. Seppala, "Mechanical strength of welding zones produced by polymer extrusion additive manufacturing," *Additive Manufacturing*, vol. 16, pp. 162–166, 2017.

[434] E. L. Gilmer, D. Anderegg, J. M. Gardner, G. Sauti, E. J. Siochi, S. H. McKnight, D. A. Dillard, C. McIlroy, and M. J. Bortner, "Temperature, diffusion, and stress modeling in filament extrusion additive manufacturing of polyetherimide: An examination of the influence of processing parameters and importance of modeling assumptions," *Additive Manufacturing*, vol. 48, p. 102412, 2021.

[435] P. Parandoush, L. Tucker, C. Zhou, and D. Lin, "Laser assisted additive manufacturing of continuous fiber reinforced thermoplastic composites," *Materials & Design*, vol. 131, pp. 186–195, 2017.

[436] S. Xia, L. Ponson, G. Ravichandran, and K. Bhattacharya, "Toughening and asymmetry in peeling of heterogeneous adhesives," *Physical Review Letters*, vol. 108, pp. 1–5, 5 2012.

[437] M. Kwak, H. Jeong, W. Bae, H. Jung, and K. Suh, "Anisotropic adhesion properties of triangular-tip-shaped micropillars," *Small*, vol. 7, pp. 2296–2300, 6 2011.

[438] W. G. Bae, D. Kim, M. K. Kwak, L. Ha, S. M. Kang, and K. Y. Suh, "Enhanced skin adhesive patch with modulus-tunable composite micropillars," *Advanced Healthcare Materials*, vol. 2, no. 1, pp. 109–113, 2013.

[439] S. Kim, M. Spenko, S. Trujillo, B. Heyneman, D. Santos, and M. R. Cutkosky, "Smooth vertical surface climbing with directional adhesion," *IEEE Transactions on Robotics*, vol. 24, no. 1, pp. 65–74, 2008.

[440] D. Sameoto, H. Sharif, J. P. Díaz Téllez, B. Ferguson, and C. Menon, "Nonangled anisotropic elastomeric dry adhesives with tailorable normal adhesion strength and high directionality," *Journal of Adhesion Science and Technology*, vol. 28, no. 3-4, pp. 354–366, 2014.

[441] S. A. Pendergraph, M. D. Bartlett, K. R. Carter, and A. J. Crosby, "Enhancing adhesion of elastomeric composites through facile patterning of surface discontinuities," *ACS Applied Materials & Interfaces*, vol. 6, no. 9, pp. 6845–6850, 2014.

[442] R. Zhao, S. Lin, H. Yuk, and X. Zhao, "Kirigami enhances film adhesion," *Soft Matter*, vol. 14, no. 13, pp. 2515–2525, 2018.

[443] V. Cacucciolo, H. Shea, and G. Carbone, "Peeling in electroadhesion soft grippers," *Extreme Mechanics Letters*, vol. 50, p. 101529, 2022.

[444] E. Kizilkan, J. Strueben, A. Staubitz, and S. N. Gorb, "Bioinspired photocontrollable microstructured transport device," *Science Robotics*, vol. 2, no. 2, p. eaak9454, 2017.

[445] D. J. Levine, G. M. Iyer, R. Daelan Roosa, K. T. Turner, and J. H. Pikul, "A mechanics-based approach to realize high–force capacity electroadhesives for robots," *Science Robotics*, vol. 7, no. 72, p. eabo2179, 2022.

[446] G. D. Anderson, *Long-term Durability Characterization and Prediction of a Urethane-based Adhesive*. PhD thesis, Virginia Tech, USA, 2020.

[447] K. Wan, "Adherence of an axisymmetric flat punch onto a clamped circular plate: transition from a rigid plate to a flexible membrane," *Journal of Applied Mechanics*, vol. 69, no. 2, pp. 110–116, 2002.

[448] S. Guo, K. T. Wan, and D. A. Dillard, "A bending-to-stretching analysis of the blister test in the presence of tensile residual stress," *International Journal of Solids and Structures*, vol. 42, no. 9-10, pp. 2771–2784, 2005.